Patcharanan Choto, MSc

Degenerate Electron Transfer Rates and Activation Parameters of Organic Redox Couples Measured in Debye and Non-Debye Solvents Using Dynamic ESR Spectroscopy

DOCTORAL THESIS

to achieve the university degree of

Doktorin der technischen Wissenschaften

submitted to

Graz University of Technology

Supervisor

O.Univ.-Prof. Dipl.-Ing. Dr.rer.nat. Günter Grampp

Physikalische und Theoretische Chemie

Optional field (second supervisor/name of the faculty, etc.)
max 2 lines

Graz, April 2015

AFFIDAVIT

I declare that I have authored this thesis independently, that I have not used other than the declared sources/resources, and that I have explicitly indicated all material which has been quoted either literally or by content from the sources used. The text document uploaded to TUGRAZonline is identical to the present doctoral thesis.

Date

Signature

I would like to thank:

Prof. Günter Grampp for giving me the chance to study in Graz. Under your guidance, I have gained a lot of experience with research and learned how to think like a scientist. Both are things that I plan to apply in the future.

Kenneth, my best friend and mentor, for teaching me what I needed to know about work and theory. You make me love what I am doing. Thank you for all the help, for understanding and believing in me and thanks for being patient instead of angry with me when I make mistakes. Thanks for being available for me when I need it.

Hilde and Ines, for your help in the lab preparing many solvents and compounds and Helmut for your help with all things technical. Marion for all your help with administrational necessities. Without the four of you I would not have finished my work in time.

Van, Hao and Yen, my Vietnamese colleagues for all your help and for taking care of me, and all my colleagues in the lab, who I have the pleasure of knowing.

Josua, who never hesitates to help me when I ask. Be it with measurements or German translations.

My Thai friends in Graz. Chanakan, who always helps, for all the nice times we have had together. Pornprapa, for taking good care of me and giving me advice on the necessities for living and studying in Graz. Thanks to all other Thai friends who I have the pleasure to know.

Nararak Leesakul, who gave me the idea of studying in Graz and introduced me to Prof. Grampp. Thanks to you I have seen a bigger world, know more people, and have had a great academic experience.

My Family. ขอบพระคุณคุณพ่อและคุณแม่ที่ให้กำเนิดและเลี้ยงดูลูกมาจนเติบใหญ่ ความรักและกำลังใจจากคุณพ่อคุณแม่ทำให้ลูกมีวันนี้ และขอบคุณน้องสาวและน้องชายที่อยู่เคียงข้างกันเสมอมา

Narong, who is right behind me, for always cheering me up. Your moral support and the laughs you give me are very important to me and they push me to achieve my goals.

Abstract

The electron self-exchange reactions of several redox couples have been studied from different points of view, using electron spin resonance (ESR) spectroscopy.

Solvent dynamic effects on the reactions of the exchange systems TCNE/$TCNE^{\bullet-}$ and DDQ/$DDQ^{\bullet-}$ (TCNE = tetracyanoethylene, DDQ = 2,3-dichloro-5,6-dicyano-1,4-benzoquinone) in non-Debye solvents, based on the application of different longitudinal relaxation times is the first subject of interest. Analyses of the experimental results using longitudinal relaxation times in the limits of low (τ_{L0}) and high ($\tau_{L\infty}$) frequencies are compared in order to decide which of these best describes the solvent dynamic effect observed in the reactions. The rate constants of the electron self-exchange reactions at room temperature are investigated by means of ESR line broadening experiments. The results are analysed within the framework of the Marcus Theory and the characteristic reorganization energy, λ, is determined. Both systems clearly indicate an adiabatic behaviour controlled by the longitudinal relaxation time, τ_L of the solvents, where the TCNE/$TCNE^{\bullet-}$ system is fully adiabatic (α=1), and the DDQ/$DDQ^{\bullet-}$ couple shows a small diabatic contribution to the effect (α=0.85). Furthermore, both redox couples indicate that the best results are obtained when using the high frequency limiting $\tau_{L\infty}$.

The second part of this work deals with the study of the self-exchange couples $Th^{\bullet+}$/Th and $MTh^{\bullet+}$/MTh (Th = thianthrene, MTh = 2,3,7,8-tetramethoxythianthrene) in organic solvents. The large structural difference between the radical cations of the thianthrenes and their neutral parent molecules can possibly affect their electron self-exchange reactions. Before this can be investigated experimentally, however, it is necessary to first understand the influence of the solvent on such electron transfer reactions. ESR line-broadening experiments at room temperature show the presence of an adiabatic solvent dynamic effect for both thianthrene couples. The very small values of the activation energies, obtained from the experiments at varied temperature for both couples, indicate that the structural changes seem to not play a significant role on the electron transfer reactions.

Zusammenfassung

Elektronenselbstaustausch-Reaktionen verschiedener Redox-Paare wurden mittels Elektronenspinresonanz (ESR) Spektroskopie untersucht. Die Arbeit fokussiert sich auf zwei unterschiedliche Aspekte und ist deshalb zweigeteilt.

Der erste Teil befasst sich mit dynamischen Lösungsmitteleffekten von TCNE/$TCNE^{\bullet-}$ und DDQ/$DDQ^{\bullet-}$ (TCNE = Tetracyanoethylen, DDQ = 2,3-Dichlor-5,6-dicyano-1,4-benzoquinon) in nicht-Debye Lösungsmitteln. Die Geschwindigkeitskonstanten des Elektronenselbstaustausches wurden mittels ESR-Linienverbreiterung bei Raumtemperatur in unterschiedlichen Lösungsmitteln bestimmt. Die experimentellen Ergebnisse wurden jeweils mittels der unterschiedlichen longitudinalen Relaxationszeiten im niedrig- (τ_{L0}) und hochfrequenten ($\tau_{L\infty}$) Bereich analysiert, um aus dem direkten Vergleich die bessere Beschreibung des dynamischen Lösungsmitteleffekts zu ermitteln. Zudem konnte mit einer Analyse basierend auf der Marcus Theorie der charakteristische Reorganisationsparameter λ berechnet werden. Beide Systeme zeigten von τ_L bestimmtes adiabatisches Verhalten, wobei für TCNE/$TCNE^{\bullet-}$ dieses voll ausgeprägt ist, (α=1) bei DDQ/$DDQ^{\bullet-}$ jedoch ein kleiner diabatischer Beitrag zum Effekt festgestellt wurde. (α=0,85) Zudem wurden für beide Redox-Paare bessere Ergebnisse unter Verwendung von $\tau_{L\infty}$ erhalten.

Im zweiten Teil wurde $Th^{\bullet+}$/Th und $MTh^{\bullet+}$/MTh (Th = Thianthren, MTh = 2,3,7,8-Teramethoxythianthren) in organischen Lösungsmitteln untersucht, da sich hier Radikal und Neutralspezies sehr ausgeprägt in ihrer Struktur unterscheiden, was möglicherweise einen signifikanten Einfluss auf den Elektronentransfer hat. Um diese Vermutung experimentell zu beweisen, ist es jedoch notwendig den Einfluss des Lösungsmittels selbst zu verstehen. Mittels ESR-Linienverbreiterung bei Raumtemperatur wurde ein adiabatischer Lösungsmitteleffekt für beide Redox-Paare festgestellt. Aus Daten bei weiteren Temperaturen wurden Aktivierungsenergien bestimmt, die in ihren Beträgen so klein waren, dass die Strukturänderung scheinbar keinen signifikanten Einfluss auf den Elektronentransfer hat.

Table of Contents

1 Introduction

The electron self-exchange between a neutral molecule and its radical anion or cation is one of the simplest electron transfer reactions imaginable. Because of this, such reactions are often used as models when exploring specific details of electron transfer theories, such as the Marcus Theory.[1,2] This particular theory is widely used in many branches of chemistry, Physics, and biochemistry and that it has been expanded on by many authors since Marcus originally published it.[3,4,5]. The reaction between donor and acceptor molecules does not form or break any chemical bonds. Nevertheless, the mechanism of the electron transfer process, which is connected to the energies of the reactant molecules themselves and of the surrounding environment, is of interest to researchers. The ESR line broadening method[6] is almost as old as the Marcus Theory and that it is very well suited for measuring the electron transfer rate constants of organic and inorganic self-exchange couples. Since these couples involve a redox pair, one of the two partners must be paramagnetic, and as shall be seen later, the ESR spectrum of the radical is sensitive to the self-exchange reaction.[7,6,8] One of the main topics that has been extensively studied in many organic systems involves the dielectric properties of the solvent in terms of solvent dynamics,[9] which can strongly affect the electron transfer reaction. For example, the $TEMPO^{+}/TEMPO^{\bullet}$ couple[10] ($TEMPO^{\bullet}$ = 2,2,6,6-tetramethyl-1-piperidinyloxy radical) in acetonitrile, benzonitrile, deuterium oxide, propylene carbonate, tetrahydrofuran and water measured by ESR line broadening[6] shows a solvent dynamic friction effect strongly controlled by the longitudinal relaxation time, τ_L of the solvents, and this behavior corresponds to the so-called the adiabatic solvent dynamic effect. The same behavior has been published for $DDQ/DDQ^{\bullet-}$ [11] (DDQ = 2,3-dicyano-5,6-dichloro-*p*-benzoquinone) in solvents of different polarity like chloroform, dichloromethane, acetonitrile, benzonitrile and acetone. Furthermore, seven organic π-systems in 18 aprotic solvents[4] of a wide range of τ_L ($0.2 < \tau_L$ /ps < 10), and polarity, expressed by the Pekar factor, γ, ($0.05 < \gamma < 0.53$) have been revealed and adiabatic dynamics were found for the electron self-exchange of $TCNQ/TCNQ^{\bullet-}$ (TCNQ = tetracyanoquinodimethane), $TTF^{\bullet+}/TTF$ (TTF = tetrathiafulvalene) and $TCNE/TCNE^{\bullet-}$ (TCNE=tetracyanoethylene), whereas four substituted *p*-phenylenediamines showed a diabatic solvent dynamic effect which is independent of solvent relaxation.

As mentioned above, the dielectric relaxation in terms of τ_L can govern the electron transfer reactions significantly. The solvent dynamics for systems in Debye solvents with a single relaxation process can be determined straightforwardly, however, this is not the case for non-Debye solvents showing multiple relaxation processes, where they exhibit different frequency limits of τ_L. The low- and high-frequency limits for τ_L were described by Fawcett[12] and are denoted as τ_{L0} and $\tau_{L\infty}$, respectively. The problem is that it is not clear which of these limits of τ_L will influence the electron transfer most. This can depend on both the class of solvent and the system. In order to gain insight into this question, the electron self-exchange of the well-described systems TCNE/$TCNE^{\bullet-}$ and DDQ/$DDQ^{\bullet-}$ has been investigated by ESR line broadening experiments in different non-Debye solvents at room temperature. Analyses of the data based on τ_{L0} and $\tau_{L\infty}$ have been compared in order to obtain the best fitting description of such reactions.

In addition to the study above, the solvent dynamic effects on the electron transfer reaction of $Th^{\bullet+}$/Th (Th = thianthrene) and $MTh^{\bullet+}$/MTh (MTh = 2,3,7,8-tetramethoxythianthrene) have been observed with another purpose in mind. The notion behind this is connected to the large difference between the structures of the neutral thianthrenes and their radical cations. For example, the thianthrene (Th) neutral molecule is bent with dihedral angles of 128°,[13] whereas the radical cation ($Th^{\bullet+}$) is almost planar[14]. Therefore a large change in geometry in the couple can be expected, when it undergoes electron transfer, and the corresponding rate constant would be expected to be relatively small. However, before investigating the role of the structural changes, that of the solvent must first be looked into. As mentioned above, solvent dynamic effects in systems of neutral molecules and the corresponding radical ions, studied by ESR line broadening, have been published. However, none of those systems involve a large difference in their structures. In contrast, the self-exchange of cyclooctatetraene (COT) and its radical anion, where the neutral molecule transforms from a tub-shaped to a planar conformation, has been studied.[15] ESR line broadening experiments show that the extraordinarily high inner-sphere reorganization energy of 158 kJ mol^{-1} at 298 K causes the slow rate constant of k_{et} = 5±3 × 10^5 M^{-1} s^{-1} in acetonitrile, which is three orders of magnitude lower than those of the systems mentioned above. Unfortunately, this rate constant is close to the limit detectable by ESR and for this reason it has not been possible to determine if a solvent dynamic effect is present for the COT/$COT^{\bullet-}$ couple.

Recently, the interactions of the trimeric $(Th)_3^{2+}$ ion were determined in molecular crystals of $[Th]_3[Al_2Cl_7]_2$ and the average S···S distance between neighbouring molecules in the stacked Th trimer was reported as 3.167 Å.[16] Also, the bonding mechanism of charged stacks of thianthrene radical cations was studied using quantum-chemical methods,[14] reporting the bending angles of thianthrene as 127.9° which is in agreement with experimental results.[13] This geometric data illustrates the changes which the molecules must undergo during the electron transfer reaction, and can be used to estimate the reaction distance of the couples investigated in this work.

In the present work we discuss the homogeneous electron self-exchange of $Th^{\bullet+}$/Th and $MTh^{\bullet+}$/MTh investigated by ESR line broadening.[17] The extent to which the relatively large structural changes in the thianthrene redox couples affect the rate constants of electron self-exchange reactions is probed. The influence of solvent dynamics on the reactions needs to be investigated first to properly distinguish between the two effects, and have been observed at room temperature. To study the role of the geometric changes in the reactions, the activation energies must be determined, which will be discussed using the results obtained from the temperature dependence experiments.

2 Theory of Outer-Sphere Electron Transfer

2.1 The Electron Transfer Mechanism

The theory of the outer-sphere electron transfer reaction in chemical systems was contributed by Rudolph A. Marcus, who won the Nobel Prize in chemistry 1992 for his work. The general mechanism of outer-sphere electron transfer can be described by equation 2.1 as a series of three steps; association, electron transfer and dissociation. First, the molecules of the redox pair form the so-called precursor complex (P) with the corresponding association constant, $K_A = k_d/k_{-d}$. After that, the electron transfer takes place, with the rate constant k_{ex}, leading to the successor complex (S). This in turn undergoes fast dissociation with the rate constant k_{diss}. Note that it has been assumed that no back electron transfer occurs.

$$D^- + A \underset{k_{-d}}{\overset{k_d}{\rightleftharpoons}} \underbrace{[D^- \cdots A]}_{\text{precursor complex (P)}} \xrightarrow{k_{ex}} \underbrace{[D \cdots A^-]}_{\text{successor complex (S)}} \xrightarrow{k_{diss}} D + A^- \qquad (2.1)$$

The figure below depicts the general aspects of the electron transfer reaction taking place in a polar solvent. The structural changes in reactants and the solvent polarization allow the electron transfer. This determines the free energy of activation and thus the reaction rate, and will be described in detail later.

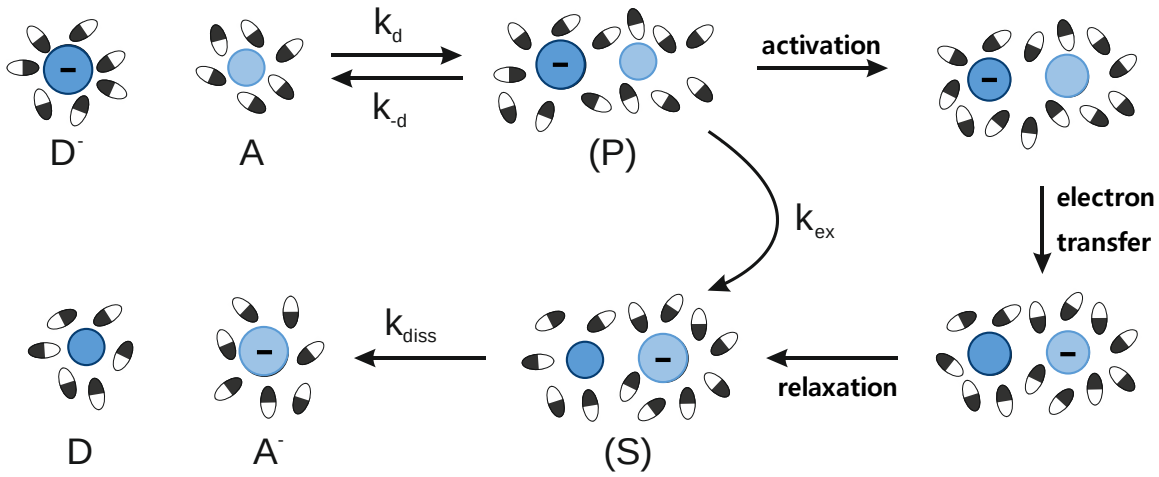

Figure 1. Scheme of the electron transfer reaction

One of the simplest electron transfer reactions imaginable is the so-called electron self-exchange reaction, which describes the ET between the two partners in a redox couple. Often this consists of a neutral molecule and its radical anion or cation, and only this type of reaction was studied in this work. The reaction scheme of such a reaction is illustrated in equation 2.2 with the slight difference to the general one above that back electron transfer between the successor and precursor complexes must be taken into account. For the part of dissociation, the process is still expressed by an irreversible reaction, instead of an equilibrium. On a sub-atomic level the reactants and products are different and thus the reaction can be observed using techniques which are sensitive to changes on this level. For example, Marcus used radioactive isotopes[2] and Weissman used ESR,[7] which detects differences in nuclear spins. From that point of view, the 'back-dissociation' would be considered the start of a new electron transfer reaction.

$$A + A^{\bullet}{}^{-/+} \underset{k_d}{\overset{k_d}{\rightleftharpoons}} \left[A \cdots A^{\bullet}{}^{-/+} \right] \underset{k_{-ex}}{\overset{k_{ex}}{\rightleftharpoons}} \left[A^{\bullet}{}^{-/+} \cdots A \right] \xrightarrow{k_{diss}} A^{\bullet}{}^{-/+} + A \qquad (2.2)$$

Several terms related to the electron transfer mechanism, both in general and for self-exchange, are described in the following.

The association constant, K_A, determines the preequilibrium forming the precursor complex (P) and is given by:

$$K_A = K_0 \exp(-w(d)/RT) \qquad (2.3)$$

where $w(d)$ is the electrostatic energy as a function of the intermolecular distance, *d*, between the reactants.

Eigen and Fuoss[18] described K_0 for spherical molecules with a reaction distance *d*:

$$K_0 = \frac{4\pi}{3} N_A d^3 \qquad (2.4)$$

A reaction zone, δd, within the distance *d* around a centre[19] is used in a second model:

$$K_0 = 4\pi N_A d^2 \delta d \qquad (2.5)$$

Here, N_A is Avogadro's constant and $\delta d \approx 0.8$ Å is the approximation usually used.[20]

The diffusion rate constant, k_d is given by the Smoluchowski equation as shown below. This is merely the diffusion rate constant associated with the Brownian motion of donor and acceptor molecules:

$$k_d = 4\pi N_A(D_A + D_D)(r_A + r_D) \tag{2.6}$$

with r_A and r_D being the radii of acceptor and donor where the molecules are assumed to be spheres. D_A and D_D represent the respective diffusion coefficients according to the Stokes-Einstein equation:

$$D_i = \frac{k_B T}{6\pi r_i \eta} \tag{2.7}$$

where η describes the viscosity of the solvent and k_B is the Boltzmann constant.

The simplified equation 2.8 is usually used when the size of donor and acceptor are approximately the same, as is the case for many self-exchange reactions. However, equation 2.9 is used instead when similar radii of the reactants cannot be assumed:

$$k_d = \frac{8RT}{3\eta} \tag{2.8}$$

$$k_d = \frac{2RT}{3\eta}\left(\frac{1}{r_A} + \frac{1}{r_D}\right)(r_A + r_D) \tag{2.9}$$

The overall electron transfer rate constant, k_{et}, can be determined as follows:

$$k_{et} = K_A k_{ex} \tag{2.10}$$

where k_{ex} is given by;

$$k_{ex} = Z exp\left(-\frac{\Delta G^*}{RT}\right) \tag{2.11}$$

with ΔG^* being the activation energy. The pre-exponential factor is given as $Z = \kappa_{el}\nu_n$, where κ_{el} denotes the transmission coefficient and ν_n expresses the nuclear barrier frequency.

k_{obs} is defined as the overall measurable rate constant and can be determined, by applying the steady-state assumption to both the precursor and successor complexes, as the following expression:

$$k_{obs} = \frac{k_d k_{ex}}{k_{-d} + k_{ex}} \tag{2.12}$$

Using equation 2.10 leads to the simplified expression for *the general electron transfer reaction*, as given by:

$$\frac{1}{k_{obs}} = \frac{1}{k_{et}} + \frac{1}{k_d} \tag{2.13}$$

For the *electron self-exchange reaction*, k_{obs} must be changed to the following expression because of the added back-electron transfer step:

$$\frac{1}{k_{obs}} = \frac{1}{k_d} + \frac{1}{K_A k_{ex}}\left(1 + \frac{k_{-ex}}{k_{diss}}\right) \tag{2.14}$$

Due to the symmetry of the reaction scheme, one may use the substitution of k_{ex} for k_{-ex} and k_{-d} for k_{diss}. Hence, the rate constant must be the following term below:

$$\frac{1}{k_{obs}} = \frac{1}{k_{et}} + \frac{2}{k_d} \tag{2.15}$$

2.2 The Marcus Model

The Marcus model[1,2] describes the distortion of the reactants, products, and solvent from their equilibrium using identical parabolas which are shifted relatively to each other according to the driving force of the reaction, $-\Delta G^o$. Figure 2 illustrates energy surfaces of precursor and successor complexes representing the energy as a parabolic function of the reaction coordinate. The electronic transition occurs in the electron transfer process, once the top of the activation barrier is reached. The activation energy, ΔG^*, can be estimated by the Marcus equation:

$$\Delta G^* = W + \frac{\lambda}{4}\left(1 + \frac{\Delta G^o}{\lambda}\right)^2 - V_{PS} \tag{2.16}$$

where λ represents the reorganization energy defined as the energy for the vertical electron transfer without replacement of the nuclear frame, and will be explained in detail later. W describes the Coulombic work, and V_{PS} is the resonance splitting energy.

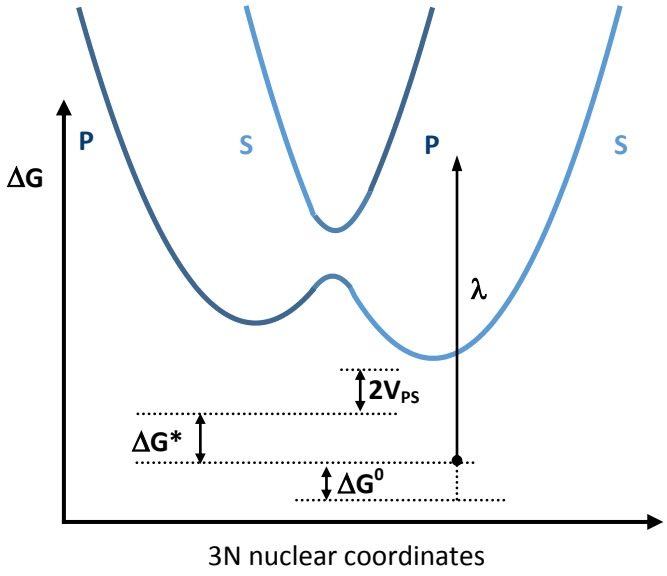

Figure 2. Energy diagram of the electron transfer reaction

ΔG^o, represented in equation 2.16, may be defined using the reduction potentials, $E^o(A/A^-)$ and $E^o(D/D^-)$ of the reactants:

$$\Delta G^o = -F\left(E^o(A/A^-) - E^o(D/D^-)\right) \tag{2.17}$$

with F being the Faraday constant.

The work term, W, accounts for the electrostatic energy, or Coulombic work, which is required to bring the two spherical reactants from an infinite distance to the reaction distance, d, between the centres, forming the donor-acceptor association complex:

$$W = \frac{z_A z_D e_o^2 N_A}{4\pi\varepsilon_o\varepsilon_s d} \tag{2.18}$$

where z_A and z_D represents the charge of the electron acceptor and donor, respectively, e_o the electronic charge, ε_s the static dielectric constant of the medium, and ε_0 the permittivity of vacuum.

The resonance splitting energy, V_{PS}, is a quantum mechanical quantity, caused by the rule of non-crossing.[21,22,23]

The strength of the electronic coupling, which causes the avoided crossing, determines whether a reaction is *diabatic*, for a small V_{PS}, or *adiabatic*, for a large V_{PS}. If V_{PS} is small, there is a chance that when the reaction reaches the would-be crossing point, it continues on the precursor curve instead of switching to the successor curve. This corresponds to the geometry changing without the electron being transferred. Marcus Theory uses the electronic transmission factor, κ_{el}, to describe this. For a purely diabatic reaction, κ_{el} is much less than one and for an adiabatic reaction, $\kappa_{el} \approx 1$, corresponding to the limit for large V_{PS}.

Determination of the activation energy is less complex in case of electron self-exchange reaction since there is no driving force involved, $\Delta G^o = 0$, and the work term can be neglected because the reaction involves neutral molecules. The energy diagram of such a reaction then becomes as given in figure 3. Consequently, the activation energy, ΔG^*, can be simplified as the following expression:

$$\Delta G^* = \frac{\lambda}{4} - V_{PS} \tag{2.19}$$

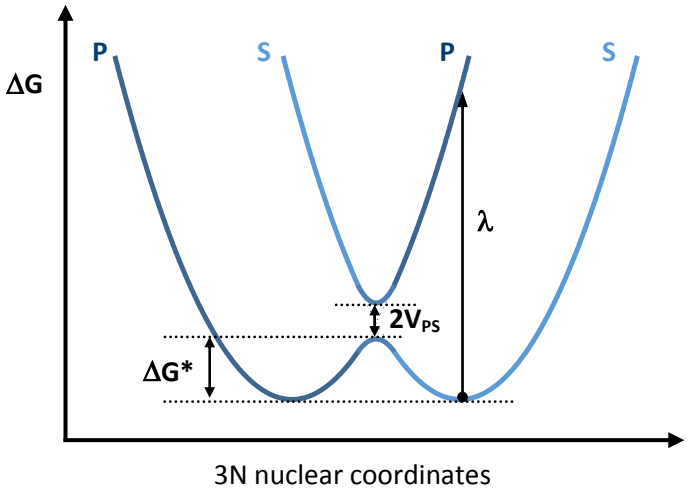

Figure 3. Energy diagram of the electron self-exchange reaction.

2.3 The Reorganization Energy

The reorganization energy, λ, is described as the energy necessary to force the reactants to have the same nuclear configuration as the products meaning the energy it would take to reorganize reactant bonds and surrounding solvent molecules. In the following, this energy involving the inner-sphere reorganization energy, λ_i, and the outer-sphere reorganization energy, λ_o, shall be explained in detail.

2.3.1 The Inner Reorganization Energy

The inner-sphere reorganization energy, λ_i, describes the changes in bond lengths and bond angles which occur during the electron transfer reaction, often approximated by the classic high temperature limit, where all vibration frequencies fulfil $\nu_n \ll k_B T/h$. The reactants are treated as system of as many independent harmonic oscillators as bonds. During the reaction, the j'th bond length is changed by Δq_j, and has the associated force constants of the precursor and successor being f_R^j and f_P^j, respectively. λ_i may be calculated as:

$$\lambda_i^{\infty} = \sum_j \frac{f_P^j \cdot f_S^j}{f_P^j + f_S^j} (\Delta q_j)^2 \tag{2.20}$$

The expression above is not always valid, especially when the reaction occurs at high temperature. This means that a correction for quantum-mechanical tunnelling should be included.[20,24,25,26] For the π-systems of organic molecules, the relevant vibrational frequencies are only partially excited at room temperature. A calculation of the temperature dependence of λ_i was proposed by Holstein[24]:

$$\lambda_i(T) = \lambda_i^{\infty} \frac{4k_B T}{h\overline{\nu}} tanh\left(\frac{h\overline{\nu}}{4k_B T}\right) \tag{2.21}$$

where $\overline{\nu} \approx 5 \cdot 10^{13}\ s^{-1}$ is used as the mean vibrational frequency for an organic redox pair.

Another approach for the determination of λ_i is the so-called Nelsen method[27], based on the combination of the different energies of the acceptor and the donor compounds with and without relaxation, corresponding to the vertical ionization potential and the vertical electron affinity[28] (see figure 4).

Quantum mechanical calculations can be performed as a method to determine the energies of the reactants and products in their most stable geometry. λ_i can be calculated as the sum of λ_A and λ_D. The expression then becomes:

$$\lambda_i^{\infty} = [E(A,D) + E(D,A)] - [E(A,A) + E(D,D)] \tag{2.22}$$

Here $E(A,D)$ is the energy of the acceptor molecule in the stable geometric configuration of the donor. Similarly, $E(D,A)$ is the energy of the donor molecule in the stable geometry of the acceptor. $E(A,A)$ and $E(D,D)$ correspond to the energies of the acceptor and donor molecules in their most stable geometry, respectively.

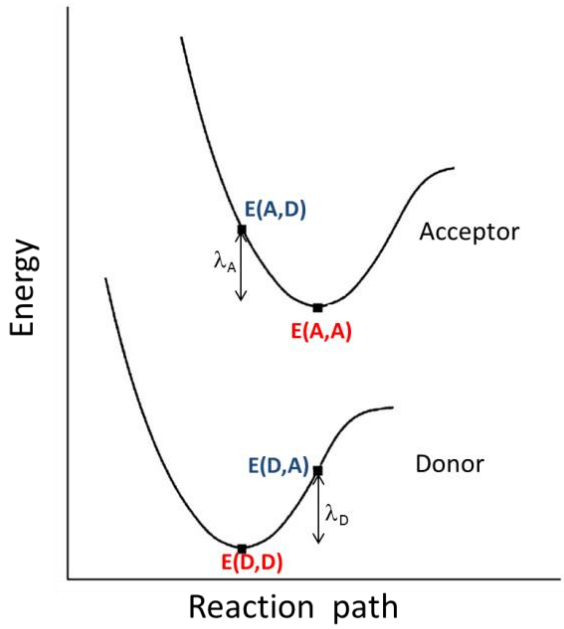

Figure 4. The potential energy curves of the electron transfer

2.3.2 The Outer Reorganization Energy

The outer-sphere reorganization energy, λ_o, describes the changes taking place in the surrounding solvent molecules. Assuming the reactants as spheres, λ_o is calculated using an equation based on the Born continuum model. The expression obtained by Marcus for λ_o is given by:

$$\lambda_0 = \frac{e_0^2 N_A}{4\pi\varepsilon_0} g(r,d) \cdot \gamma \tag{2.23}$$

Here, γ is the Pekar factor, which is the solvent dependent contribution given by:

$$\gamma = \frac{1}{\varepsilon_\infty} - \frac{1}{\varepsilon_s} \approx \frac{1}{n^2} - \frac{1}{\varepsilon_s} \tag{2.24}$$

ε_s and ε_∞ are the static and optical dielectric constants, respectively. Since it is difficult to obtain precise experimental values of ε_∞, usually an approximation expressed by the refractive index, *n*: $\varepsilon_\infty \approx n_D^2$ is applied.

The term $g(r,d)$ is a function of the effective molecular radius r and the reaction distance d. This term can be defined using a spherical model as the simplest form, in which case it is given by:

$$g(r,d) = \frac{1}{r} - \frac{1}{d} \tag{2.25}$$

Normally d is taken as closest contact, $d = r_A + r_B$ and often it is assumed that the radii of the reactants are identical, making d=2r. When the reactants are organic molecules, the ellipsoid model is used instead for proper approximation. Therefore, r is replaced by the mean elliptical radius, $\overline{r}$ with semiaxes $a > b > c$:

$$\overline{r} \approx \frac{(a^2 - b^2)^{1/2}}{F(\varphi, \alpha)} \tag{2.26}$$

$F(\varphi, \alpha)$ indicates ellipsoid integrals of the first kind, $\varphi = arcsin\left[(a^2 - c^2)^{1/2}/a\right]$ and $\alpha = \arcsin[(a^2 - b^2)/(a^2 - c^2)]^{1/2}$. A good approximation is: $\overline{r} \approx \frac{1}{3}(a + b + c)$. Because of the shape of the ellipsoids, the reaction distance in the precursor complex can be less than the sum of mean elliptical radii. A better estimate is provided by d',[29,30] which is given as:

$$\frac{1}{d'} = \frac{1}{d}\left[1 + \frac{2c^2 - a^2 - b^2}{3d^2} + \frac{abc}{d^3} + \frac{4(8c^4 + 3(a^4 + b^4) - 8c^2(a^2 + b^2) + 2a^2b^2}{15d^4}\right] \tag{2.27}$$

2.4 The Inverted Region

According to the Marcus equation 2.16, the activation energy decreases as long as the reactions are endergonic and slightly to moderately exergonic, meaning that the reaction rates increase, with positive to slightly negative driving force. However, the reaction can reach *the Marcus inverted region* when it becomes strongly exergonic. This means that the activation energy must increase again when ΔG^o continues to become more negative and its absolute value is much larger than that of reorganization energy.

The variation in logarithm of the rate constant with the driving force for the electron transfer reaction can be seen in figure 5. In the normal Marcus region, $-\Delta G^o < \lambda$, log k_{et} increases if $-\Delta G^o$ decreases. The reaction is barrierless when $-\Delta G^o = \lambda$. In the region where $-\Delta G^o > \lambda$, log k_{et} decreases with increasing driving force.[31]

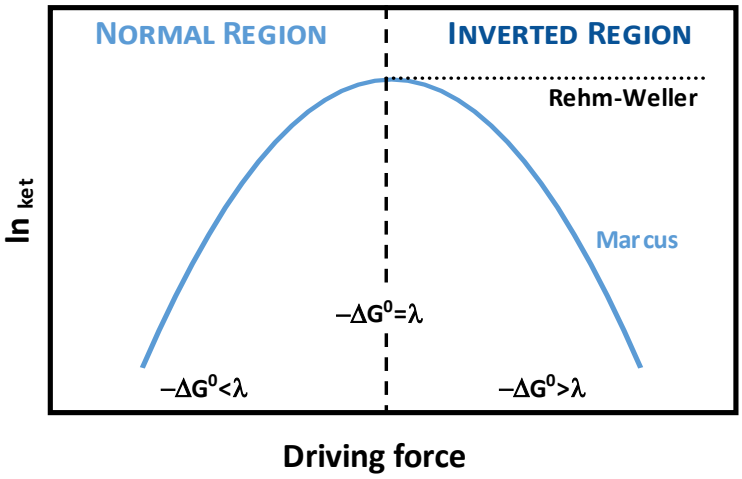

Figure 5. Illustration of Marcus' inverted region.

It is, however, very difficult to prove the existence of the inverted region by experimental evidence. For most exergonic reactions observed rate constants have been reported to increase until a certain point, after which they remained unchanged. This led to the development of several empirical extensions of the Marcus equation, for instance, the equation introduced by Rehm and Weller[32]:

$$\Delta G^* = \frac{\Delta G^o}{2} + \sqrt{\left(\frac{\lambda}{4}\right)^2 + \left(\frac{\Delta G^o}{2}\right)^2} \qquad (2.28)$$

According to the problem described above, Marcus suggested[33] the explanation that the electron transfer may occur at a reaction distance greater than closest contact. This leads to an increasing outer reorganization energy and the inverted region is then shifted toward even higher exergonicity. The inverted region will become more difficult to reach experimentally if the reaction distance keeps increasing. Nevertheless, experimental evidence of the inverted region, investigated by observing charge recombination in photochemically generated radical ion pairs, have been published by Gould and co-workers.[34,35] In this case, donor and acceptor are generated at close contact, as the reaction distance controlled by the absence of diffusion. Another way to have a controlled reaction distance is to observe an intramolecular reaction. This was

first done by Closs and Miller[36] in their investigations on intramolecular electron transfer in steroids. Further experimental evidence of the inverted region was reported by Grampp and Hetz[37] who studied the photoinduced back electron transfer reactions within geminate radical pairs containing triplet-thionine and one of various aromatic donors.

2.5 Solvent Dynamic Effects

It is known that the properties of the solvent can also have a big influence on the electron transfer rate constant, for example through the so-called solvent dynamic effect (friction).[9] This effect is manifested in the pre-exponential factor, $Z = \kappa_{el}\nu_n$. This means that the expression for Z depends on whether a solvent dynamic effect, being either diabatic or adiabatic, or no solvent friction is present.

The Marcus model describes ν_n using a simple gas-phase collision model[1], with which the following expression can be made:

$$\nu_n = d^2 N_A \left(\frac{16\pi RT}{M}\right)^{1/2} \tag{2.29}$$

with M being the molar mass.

The formation of the precursor complex can be controlled by the solvent dynamics. For rapid dielectric relaxation in the solvent, the total frequency factor can be determined as a combination of the frequencies of the solvent, ν_o, and the reactants, ν_i, weighted by the respective reorganization energy, as is given by[20]:

$$\nu_n = \left(\frac{\nu_i^2\lambda_i + \nu_o^2\lambda_o}{\lambda}\right)^{1/2} \tag{2.30}$$

For slow dielectric relaxation, as first pointed out by Zusman[38], the longitudinal relaxation time, τ_L, is necessary for the description of such electron transfer reactions. τ_L is interrelated to the transverse or Debye relaxation time, τ_D, by the relation:

$$\tau_L = \frac{\varepsilon_\infty}{\varepsilon_s}\tau_D \tag{2.31}$$

This follows from the Debye equations of dielectric relaxation.[39,40] Under the condition of constant charge during the reaction, τ_L is associated with the relaxation of the electric

field E after a jump in the electric displacement D, while τ_D is associated with the relaxation of D after an E field jump. ε_∞ denotes the dielectric constant for high frequencies ($\omega \rightarrow \infty$), whereas ε_s is the static dielectric constant (ω=0) of the solvent.

Under the condition that $\lambda_i << \lambda_o$, the resulting pre-exponential factor is:

$$Z_{adiab} = \nu_n = \frac{1}{\tau_L}\left(\frac{\lambda_o}{4\pi RT}\right)^{1/2} \tag{2.32}$$

Note that for the *adiabatic* electron transfer reaction, the transmission factor, κ_{el}, is one, which is why it has been omitted in equation 2.32.

For the *diabatic* reaction, the pre-exponential factor is given by[38,4,41]:

$$Z_{diab} = \kappa_{el}\nu_n = \frac{2\pi V^2}{\hbar N_A (4\pi\lambda_o RT)^{1/2}} \tag{2.33}$$

The experimental value, Z_{obs}, can be investigated using simple mathematical treatment of equation 2.11, as suggested by Weaver[9]:

$$Z_{obs} = k_{et,obs} K_A^{-1} exp\left(\frac{\Delta G^*_{calc}}{RT}\right) \tag{2.34}$$

Here the calculated activation energy, ΔG^*_{calc} can be calculated using equation 2.16, and $k_{et,obs}$ is the experimentally determined rate constant.

It is possible to test which theoretical case fits the experiment best by comparing Z_{obs} with the respective Z_{theory}. In principle, if the assumed theory corresponds to the experiment, the plot between theoretical ln Z_{theory} and observed ln Z_{obs} must provide a line with slope of unity. This is known as a *Weaver plot* and can be seen in figure 6 and in the expression below:

$$ln\, Z_{obs} = lnZ_{theory} + a \tag{2.35}$$

Since it is the adiabatic reaction which applies to all reactions studied in the present work, this will be used as an example:

$$lnZ_{obs} = ln\left(\gamma^{1/2}\tau_L^{-1}\right) + b \tag{2.36}$$

with a and b being constants. Similarly, the plots corresponding to the diabatic and the absence of solvent friction case can also be made using the same method with different expressions of Z_{theory}.

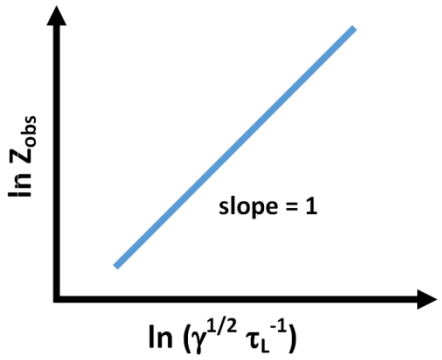

Figure 6. Weaver plot showing the slope of unity.

According to an adiabatic behavior as just described above, combining the equations 2.10, 2.11 and 2.32 provides the resulting equation:

$$k_{et} = K_A \tau_L^{-1} (\lambda_o / 4\pi RT)^{\frac{1}{2}} \exp(\frac{-\Delta G^*}{RT}) \quad (2.37)$$

The equation above can be linearized as follows:

$$ln(k_{et}\tau_L \gamma^{1/2}) = c - m\gamma \quad (2.38)$$

with *c* being a different constant, defined as in the equations above. An illustration of a plot following this expression can be seen in figure 7.

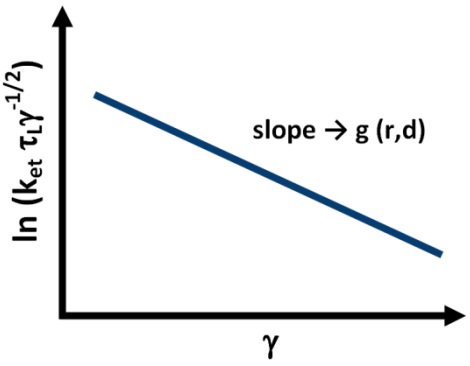

Figure 7. Dependence of $ln(k_{et}\tau_L\gamma^{1/2})$ on the solvent parameter γ which the slope provides d'_{exp}.

Note that the plots of all three cases of reaction determine an identical slope *m* which can be expressed as in equation 39. The experimental reaction distance, $d'_{exp,}$ can, therefore, be determined from slope of such lines:

$$m = \frac{e_0^2 N_A}{16\pi\varepsilon_0 RT} g(r_A, r_D, d') \tag{2.39}$$

The Weaver plot works well for the three distinct cases described above. However, the method tends to fail and become very sensitive to poor theoretical data in situations where the reaction behavior is rather described as partly adiabatic or diabatic. This leads to an alternative method, the so-called *Fawcett method,* which initiates with Marcus and Sumi[42], and has been extensively applied by Fawcett.[43,44] The possibility of different degrees of adiabaticity is included in the expression of the electron transfer rate constant, as given by:

$$k_{ex} = A\tau_L^{-\alpha} exp\left(\frac{-\Delta G^*}{RT}\right) \tag{2.40}$$

Here α is a constant, $0 \leq \alpha \leq 1$, with the value 0 for diabatic and 1 for adiabatic. *A* describes the solvent independent part of the pre-exponential factor, but must depend on γ. Even though γ is a solvent parameter, its influence is still significantly less than that of τ_L. The expression is actually similar to that from the Weaver method where α is 0 and 1. Equation 2.41 illustrates adiabatic reaction, described as the function $Y(k_{et},\gamma)$ and the value of α can then be determined from the slope of a plot of this function vs. $ln\ \tau_L$,:

$$Y(k_{et}, \gamma) = lnk_{et} - \frac{1}{2} ln\gamma + \frac{\Delta G^*}{RT} = const - \alpha ln\tau_L \tag{2.41}$$

2.6 Temperature Dependence of the Electron Transfer Reaction

The dependence of a reaction rate constant, k_{ex}, on temperature is described by the Arrhenius equation. However, in the case of Marcus theory, the temperature dependence must be present not only in the denominator of the exponential term of k_{ex} but also in the activation energy, via γ, and the pre-exponential factor. Since τ_L can vary significantly with temperature, it therefore has a strong influence on the temperature dependence of *Z* for the adiabatic reaction. Some of the electron transfer reactions in this work have been studied under temperature dependence, and will be discussed in more detail later.

$$k_{ex}(T) = Z(T) exp\left(\frac{-\Delta G^*(T)}{RT}\right) \tag{2.42}$$

2.7 Dielectric Relaxation

As mentioned above, the longitudinal relaxation time is an integral parameter in the analysis of solvent dynamic effects and obtaining the right value of τ_L is not always straightforward. Therefore, some of the concepts in dielectric relaxation and how to use them to determine τ_L are given in the following.

When polar solvent molecules experience a changing electrical field, their dipole vectors must be reoriented in order to remain at minimum energy. However, the intermolecular forces do not allow the process to be infinitely fast. The properties of the medium control the time scale, which is often in the order of 1-100 ps.[12] Dielectric relaxation experiments, such as dielectric relaxation spectroscopy, is a very useful tool to provide information about molecular motion in polar liquids, and also helps in understanding the way solvent molecules respond to changing electrical conditions.

According to the Debye model, dielectric relaxation in a polar solvent is associated with the static permittivity ε_s, the Debye relaxation time τ_D, and the high-frequency permittivity ε_∞. The frequency dependence of the permittivity ε can be described by two components, i.e. the dispersion spectrum curve $\varepsilon'(\omega)$ and the dielectric loss spectrum curve $\varepsilon''(\omega)$, as given in the following equations:

$$\varepsilon'(\omega) = \epsilon_\infty + \frac{\varepsilon_s - \varepsilon_\infty}{1 + \omega^2 \tau_D^2} \tag{2.43}$$

$$\varepsilon''(\omega) = \frac{\omega \tau_D (\varepsilon_S - \varepsilon_\infty)}{1 + \omega^2 \tau_D^2} \tag{2.44}$$

According to equation 2.43, $\varepsilon'(\omega)$ is equal to ε_s at very low frequency ($\omega \rightarrow 0$), whereas it is equal to ε_∞ at the very high frequency limit ($\omega \rightarrow \infty$). $\varepsilon'(\omega)$ will drop rapidly from ε_s to ε_∞ when the frequency is close to $1/\tau_D$, and it will reach $(\varepsilon_s + \varepsilon_\infty)/2$ when the value of $\omega\tau_D$ is equal to one.

Considering $\varepsilon''(\omega)$ in equation 2.44, it is zero in the limits of very low and high frequencies. Its maximum value is equal to $(\varepsilon_s - \varepsilon_\infty)/2$ when $\omega\tau_D$ is one. Plots of $\varepsilon'(\omega)$ and $\varepsilon''(\omega)$, corresponding to a hypothetical solvent, as a function of the logarithm of the frequency illustrates the behaviour described in equations 2.43 and 2.44, as seen in

figure 8. The parameters assumed in the generation of the plots are $\varepsilon_s = 50$, $\varepsilon_\infty = 2$, and $\tau_D = 20$ ps.

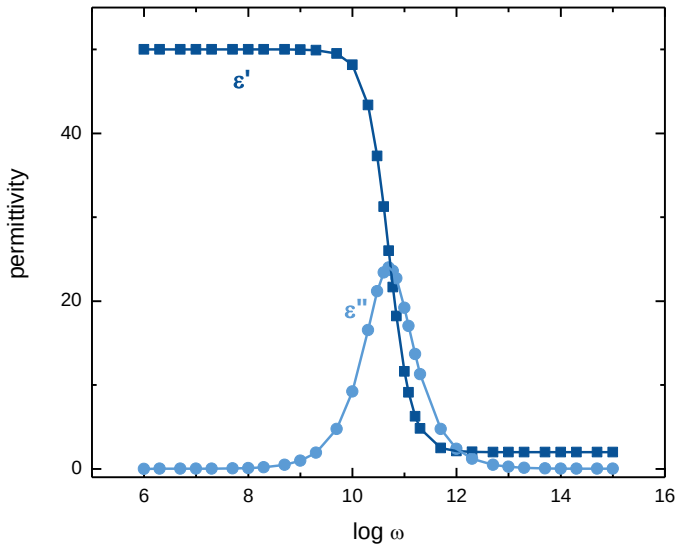

Figure 8. Plot of the ε'(ω) and ε''(ω) components of the dielectric permittivity of a hypothetical Debye solvent against the logarithm of frequency.

An alternative plot which can be obtained from the previous two equations is the so-called *Cole-Cole plot*, as shown in figure 9. This plot provides the value of τ_D from the maximum point of the dielectric loss $\varepsilon''(\omega)$, and those of ε_S and ε_∞ are obtained from the limits $\omega \rightarrow 0$ and $\omega \rightarrow \infty$.

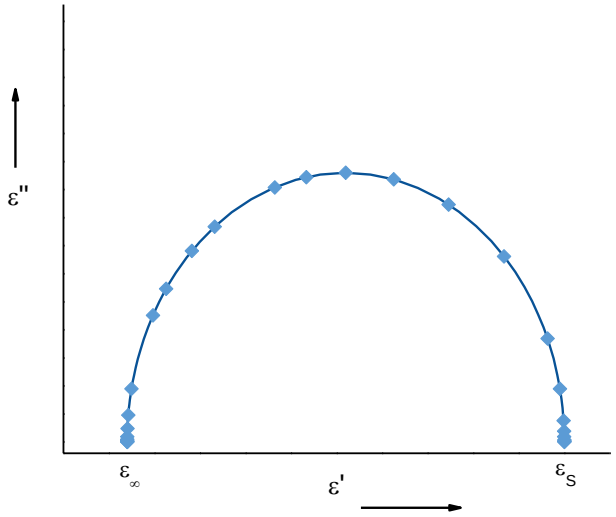

Figure 9. A Cole-Cole plot obtained from a hypothetical Debye solvent.

Dielectric relaxation experiments in electrolyte solutions may involve several relaxation processes. For example, three relaxation processes take place in a 0.08 M Mg_2SO_4 solution[45,46] as seen in figure 10. The first process belongs to the ion pair, with a relaxation time of 181 ps, and the permittivity between 82.9 and 75.2. The second, involves the slow reorientation of water clusters, with the relaxation time of 8.4 ps, and the permittivity between 75.2 and 8.4. The last is the high-frequency process, and is attributed to the formation and breaking of hydrogen bonds, which occurs with a relaxation time of 1.5 ps, and the permittivity between 8.4 and 4.6.

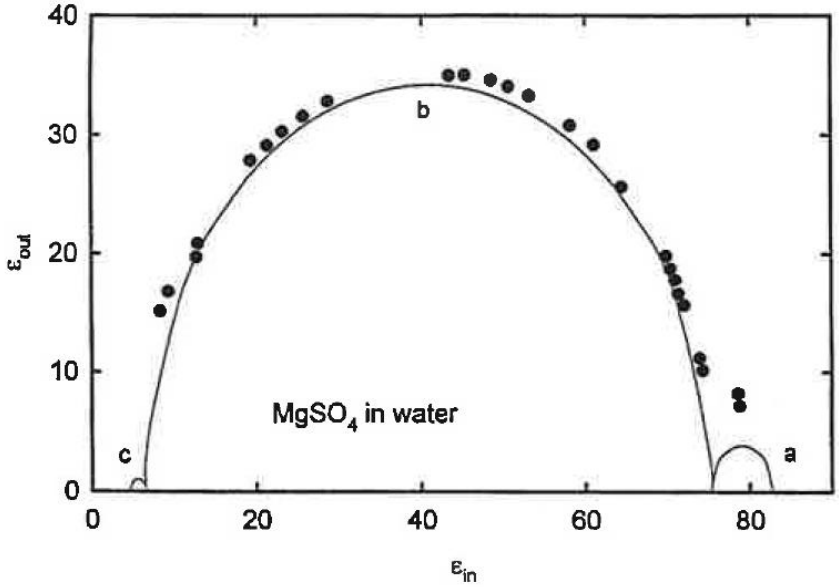

Figure 10. Cole-Cole plot for dielectric relaxation data obtained with 0.08 M Mg_2SO_4 in water. The semicircles show the resolved Debye relaxation process for (a) the ion-pair; (b) the slow reorientation of water clusters; (c) the fast process in water. [From ref 12]

The three important parameters for Debye relaxation described above are useful for estimation of the longitudinal relaxation time τ_L, as mentioned earlier in equation 2.31, which is applicable for Debye solvents with a single relaxation process. For solvents with multiple relaxation processes, τ_L can be determined using different expressions, which were introduced by Hynes[47] and Fawcett.[12,48] Some examples of non-Debye solvents with their dielectric relaxation parameters are shown in table 1.

In the case that two relaxation processes are present, the low-frequency limit for τ_L may be expressed as:

$$\tau_{L0} = \frac{\varepsilon_\infty}{\varepsilon_s}(f_1\tau_{D1} + f_2\tau_{D2}) \tag{2.45}$$

where

$$f_i = \frac{\varepsilon_{io} - \varepsilon_{i\infty}}{\varepsilon_s - \varepsilon_\infty} \tag{2.46}$$

At the high-frequency limit, the value of τ_L is

$$\tau_{L\infty} = \frac{\varepsilon_\infty}{\varepsilon_s}\left(\frac{f_1}{\tau_{D1}} + \frac{f_2}{\tau_{D2}}\right)^{-1} \tag{2.47}$$

Using similar expressions, for a solvent with three relaxation processes, the expressions for τ_L become:

$$\tau_{L0} = \frac{\varepsilon_\infty}{\varepsilon_s}(f_1\tau_{D1} + f_2\tau_{D2} + f_3\tau_{D3}) \tag{2.48}$$

and

$$\tau_{L\infty} = \frac{\varepsilon_\infty}{\varepsilon_s}\left(\frac{f_1}{\tau_{D1}} + \frac{f_2}{\tau_{D2}} + \frac{f_3}{\tau_{D3}}\right)^{-1} \tag{2.49}$$

Table 1. Dielectric relaxation parameters for some organic solvents having multiple relaxation processes.

Solvents	$\varepsilon_s = \varepsilon_{10}$	τ_1 / ps	$\varepsilon_{1\infty} = \varepsilon_{20}$	τ_2 / ps	$\varepsilon_{2\infty} = \varepsilon_{30}$	τ_3 / ps	ε_∞
Propylene carbonate[49]	64.97	43	4.47	0.57	-	-	2.42
Benzonitrile[49]	25.17	34.1	3.8	2.61	-	-	2.93
Methanol[50]	32.5	51.49	5.91	7.09	4.9	1.12	2.79
Ethanol[51]	24.47	164.9	4.53	10.4	3.79	1.69	2.6
Iso-propanol[52]	19.34	354.6	3.66	23.4	3.11	2.12	2.48

3 Elementary Theory of Electron Spin Resonance

The technique of Electron Spin Resonance (ESR) spectroscopy has been widely used as an effective tool for qualitative and quantitative analyses in free radical studies. One of the main applications which has received much attention involves the line width. This is useful as it helps the understanding of the electron distributions in paramagnetic species, ion pair interactions, molecular motions in different environments, and also the rate of chemical reactions. Such an ESR line width method, investigating the electron transfer reaction of organic compounds is one example which has been applied in this work. The elementary concepts of line broadening thus shall be described after the basics of ESR have been introduced.

3.1 Spin and Magnetic Moment of the Electron

Spin is an intrinsic form of orbital angular momentum in quantum mechanics. The direction of each electron in an orbital can be described by a spin quantum number, S = ½. The magnetic spin quantum number, M_s = +½, -½ will be effective when a strong external magnetic field, $\vec{B}$, is present. Consider the electron spin as a vector $\vec{S}$ precessing about $\vec{B}$ in the z direction as it is illustrated in figure 11. The magnitude of this vector is given in equation 3.1. The component S_z in the z direction is defined as $\hbar M_s = +\hbar/2$ or $-\hbar/2$ with the positive value being parallel to the z direction and denoted as α, while the negative is antiparallel to that and β is used for its symbol.

$$\left|\vec{S}\right| = \hbar\sqrt{S(S+1)} = \hbar\frac{\sqrt{3}}{2} \tag{3.1}$$

Here $\hbar = h/2\pi$, and h = 6.6262×10^{34} J·s is Planck's constant.

According to classical physics, the magnetic moment, $\vec{\mu}_e$, is associated with the electron spin, i.e. it is proportional to $\vec{S}$:

$$\vec{\mu}_e = -\left(\frac{g_e\mu_B}{\hbar}\right)\vec{S} \tag{3.2}$$

where $\mu_B = e_0\hbar/2m_e$ = 5.79×10^{-4} eV·T^{-1} is the Bohr magneton, with e_0 being the elementary charge, and m_e = 9.1096×10^{-31} kg the mass of the electron. g_e = 2.0023

represents the so-called g_e factor of the free electron. Following the equation above, the negative charge of the electron gives rise to opposite directions of $\vec{\mu}_e$ and $\vec{S}$, as is shown in figure 11.

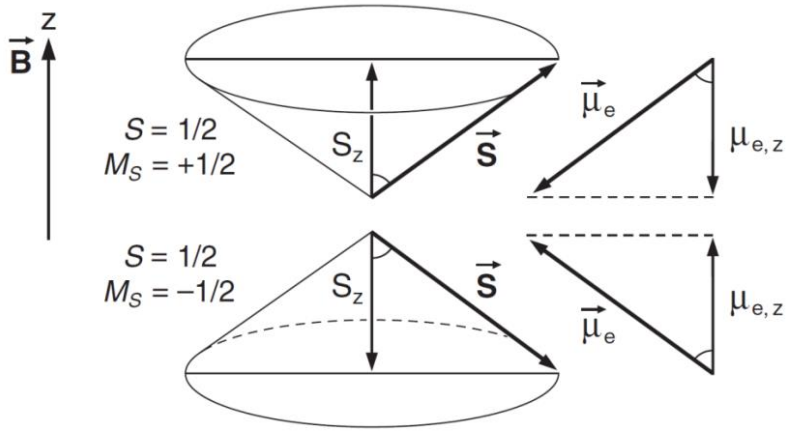

Figure 11. Precession of the spin vector $\vec{S}$ about the magnetic field $\vec{B}$ in the *z* direction. [From ref 53]

3.2 Zeeman Splitting and Resonance Condition

In the presence of the external magnetic field, $\vec{B}$, the magnetic moment, $\vec{\mu}_e$, associated with the electron spin results in an energy:

$$E = -\vec{\mu}_e \vec{B} = g_e \mu_B M_s B \tag{3.3}$$

with *B* being the magnetic field strength. The two sorts of electron spin, oriented either parallel or antiparallel to the magnetic field vector, give rise to a difference in energy as illustrated in figure 12:

$$E_+ = +\left({}^1/_2\right) g_e \mu_B B \ , \ E_- = -\left({}^1/_2\right) g_e \mu_B B \tag{3.4}$$

The energy difference between the two energy states, $E_+ - E_-$, is the so-called *electron-Zeeman splitting*, and is proportional to the magnetic field strength, *B*, (figure 12). The transition between the energy levels takes place when the resonance condition is fulfilled, and hence results in the absorption of energy. This can be achieved by application an electromagnetic radiation *hv*, such as radio or microwave radiation. An oscillating field will then be induced and allow spin inversion, complying with the selection rule $\Delta M_s = \pm 1$. According to the *z* direction of the external magnetic field $\vec{B}$

(figure 11), the direction of the magnetic field associated with this radiation lies in the *xy*-plane, meaning it is perpendicular to that of $\vec{B}$. *The resonance condition* is fulfilled when the energy of the radiation is equal to that of the Zeeman splitting:

$$h\nu = E_+ - E_- = g_e \mu_B B \tag{3.5}$$

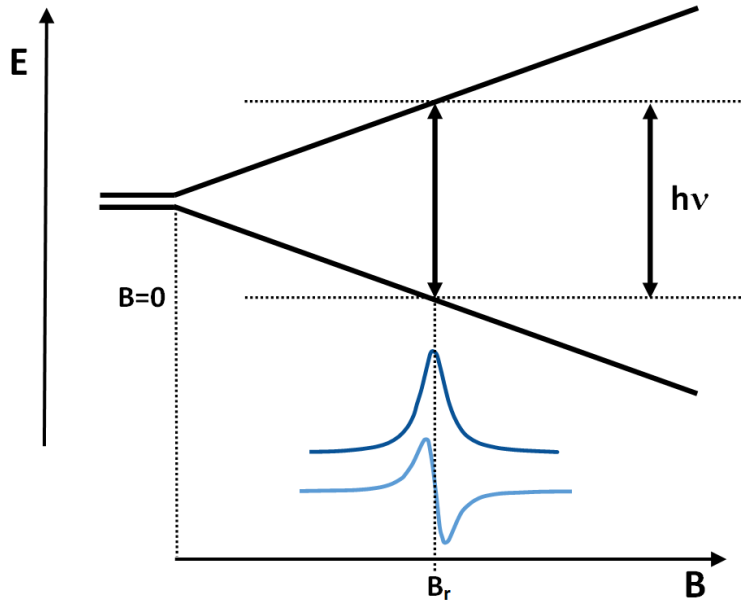

Figure 12. Illustration of the Electron-Zeeman splitting as a function of the strength, *B*, of the magnetic field and the resonance condition.

The angular frequency with which the spin $\vec{S}$ precesses about $\vec{B}$ is known as the Larmor frequency, ω_L:

$$\omega_L = g_e(\mu_B/\hbar)B = 2\pi\gamma_e B \tag{3.6}$$

where $\omega_L = 2\pi\nu$, and ν is the frequency of the electromagnetic radiation. γ_e denotes the *gyromagnetic* ratio of the electron, $\gamma_e = \nu/B = g_e\mu_B/h = 2.8024\times10^6$ $s^{-1}G^{-1}$.

To satisfy the resonance condition applied to ESR spectroscopy, it is easier to keep the frequency ν constant and vary the field strength *B*. The most used frequency is the microwave X band with ν of ca. 9.5 GHz, which requires a field strength of ca. 3400 G ($g_e = 2$).

3.3 The ESR Line Width

According to the Boltzmann distribution, it is more favourable for the population of electrons to reside at the lower energy level, E_-, than at that of the higher state, E_+. The ratio between the populations, n_- and n_+, of the two Zeeman levels is given by:

$$\frac{n_+}{n_-} = exp\left[\frac{-(E_+ - E_-)}{k_B T}\right] = exp\left[\frac{-(g_e \mu_B B)}{k_B T}\right] \quad (3.7)$$

with k_B = 1.3806×10^{-23} J·K^{-1} being the Boltzmann constant, and T the absolute temperature in K. Therefore, after the absorption resulting from the resonance condition occurs, a number of electrons situated at E_+ must be converted into E_- via a *relaxation* process, as illustrated in figure 13.

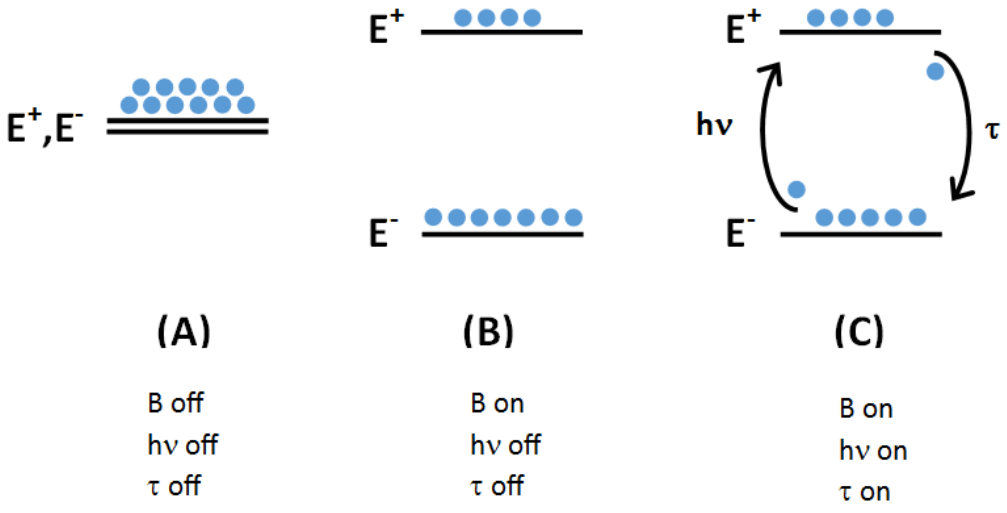

Figure 13. The populations of electrons in the Zeeman levels: (A) without external magnetic field, (B) with applied external magnetic field, (C) the conversion giving rise to the absorption and relaxation processes.

The electron spin in the excited state can be considered as a "hot" spin system. Its excess energy must be related to the surrounding, thus leading to a "cooling" process. This can be described as an exponential decay:

$$\delta E = \delta E_0 exp\left(-\frac{t - t_0}{\tau}\right) \quad (3.8)$$

Here δE and δE_0 denote the excess energy absorbed by the system, at a given time t and at the time t_0, respectively. τ is the lifetime of a spin state.

The process, which requires the transfer of energy from the spin ensemble to the surroundings (or lattice), such as solvent molecules, via thermal vibrations, is the so-

called *spin-lattice relaxation*, and can be characterized by the *spin-lattice relaxation time*, τ_1. This relaxation time is also referred to as the *longitudinal relaxation time*, since it is defined empirically as the characteristic relaxation time of processes in the direction (longitudinal) of the magnetic field. There are other pathways of relaxation, such as interaction with neighbouring spins, i.e. *spin-spin relaxation* or relaxation induced by chemical reactions. Considering the former relaxation, it is characterized by the *spin-spin relaxation time*, τ_2. This is the relaxation time of processes orthogonal (transverse) to the field, and it is therefore also known as the *transverse relaxation time.* The importance of the relaxation times described above shall become apparent later.

Applying the Heisenberg uncertainty principle, the relaxation process can be related to the line width:

$$\delta E = h\delta\nu = h\gamma_e \delta B \geq \frac{\hbar}{\tau} \tag{3.9}$$

where δE is the uncertainty of the energy of the system, which is related to the lifetime (in s) of a spin state, τ. δE can be expressed in terms of a $\delta\nu$ (in Hz) or δB (in G) via the resonance condition. δB provides the width of the ESR signal.

As seen, the ESR line width is connected to the lifetime, and the latter can be approximated using the relaxation times τ_1 and τ_2:

$$\frac{1}{\tau} \approx \frac{1}{\tau_1} + \frac{1}{\tau_2} \tag{3.10}$$

For most organic radicals, τ_2 is much shorter (10^{-5} to 10^{-7} s) than τ_1 (10^{-3} to 10^{-1} s),[53] and for this reason, τ_1 in equation 3.10 is often neglected.

3.4 The g_e Factor

The ESR absorption spectrum recorded at a constant microwave frequency, ν, and variable field strength B, provides the position of the ESR signal characterized by the g_e factor (or g_e-value) of the paramagnetic species. The g_e-value reveals structural information about paramagnetic species, especially compounds containing heavy atoms, such as transition metal complexes with organic ligands. It is seen in Figure 14 the g_e-values of compounds with an unpaired d-electron that they can appear anywhere in the spectrum. For organic radicals in the absence of heavy atoms, however, the g_e factor is

close to 2, or slightly above than that of the free electron (2.0023). Most organic radicals have g_e-values in the narrow range of 2.00-2.01[53] and for identification purposes it is cumbersome to determine them with sufficient precision, see below. Therefore g_e factors of organic radicals are rarely specified in reported ESR studies. The spin-orbit coupling, which influences an orbital admixture to the spin magnetism, is strong and particularly effective in heavy atoms. Therefore, deviations of g_e in the narrow range of 2.00-2.01 from 2.0023 (free electron) occur when heteroatoms are present. High π-spin population of heavier heteroatoms such as P and S will lead to the largest deviations.

The g_e factor can be determined either directly or indirectly. The former needs very precise measurement of the microwave frequency and the field strength, i.e. many significant digits are needed, and thus, in practice it can be difficult to achieve. Nevertheless, the g_e-value can be calculated using the resonance condition, as given by:

$$g_e = \frac{h}{\mu_B}\left(\frac{\nu}{B}\right) = 7.144775 \times 10^{-2}\left(\frac{\nu}{B}\right) \qquad (3.11)$$

More practically, an indirect method is usually used, comparing with a standard compound with a known g_e-value,[53] such as 2.0036 of 2,2-diphenyl-1-picrylhydrazyl (DPPH), or 2.00550±0.00005 of $(NO^{\bullet})(SO_3^{-})_2 2K^{+}$ (*Frémy's salt)* in saturated Na_2CO_3 solution, or 2.00258±0.000006 of the perylene radical in conc. H_2SO_4, as illustrated in figure 14.

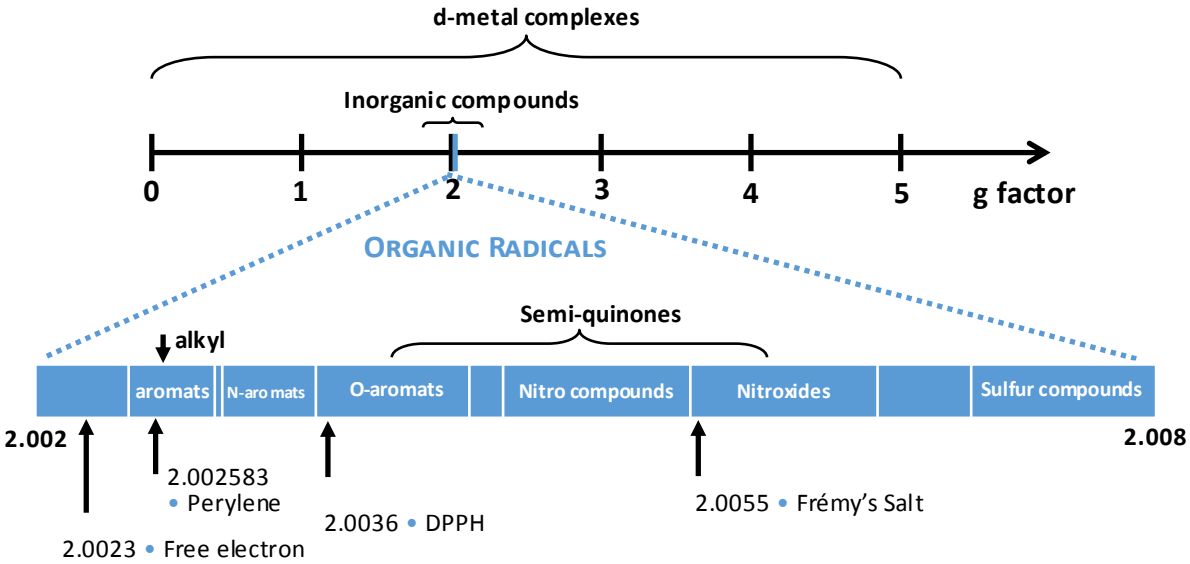

Figure 14. g_e factors of various paramagnetic species.

3.5 Hyperfine Interactions

For organic radicals in a magnetic field $\vec{B}$ upon irradiation, interactions between the spins of unpaired electrons and magnetic nuclei give rise to *hyperfine splitting* (hfs) in the ESR spectra. This phenomenon provides the most important structural information about organic radicals. The energy of the hyperfine interaction, E_{hf}, is the sum of a dipolar term, E_{dip}, and the so-called Fermi-contact term, E_{FC}:

$$E_{hf} = E_{dip} + E_{FC} \tag{3.12}$$

The classical term of dipolar energy, E_{dip}, describes the direct magnetic dipole-dipole interaction between electron and nucleus, which can be determined as is given by:

$$E_{dip} = \frac{\mu_0}{4\pi}\left[\frac{\vec{\mu}_e \cdot \vec{\mu}_n}{|\vec{r}|^3} - 3\frac{(\vec{\mu}_e \cdot \vec{r})(\vec{\mu}_n \cdot \vec{r})}{|\vec{r}|^5}\right] \tag{3.13}$$

with μ_0 being the vacuum permeability and $\vec{r}$, the vector joining the magnetic moments of electron and nucleus, $\vec{\mu}_e$ and $\vec{\mu}_n$, Being a function of $\vec{r}$, E_{dip} is strongly anisotropic, however, it is generally averaged out to zero by the Brownian motion of molecules in fluid solution.

The quantum mechanical term of E_{FC} presented in equation 3.12 is isotropic, and can be expressed as:

$$E_{FC} = -\frac{2\mu_0}{3}(\vec{\mu}_e \cdot \vec{\mu}_n)\rho_s(0) \tag{3.14}$$

Here $\rho_s(0)$ is the spin density $\rho_s(x, y, z)$ at the nucleus ($x = y = z = 0$), where it is in 'contact' with the unpaired electron. The expression above can be transformed into:

$$E_{FC} = [(2/3)\mu_o g_e g_n \mu_B \mu_N \rho_s(0)] M_S M_I \tag{3.15}$$

where, μ_N is the nuclear magneton. The sign of E_{FC} is determined by those of g_N of nucleus X, $\rho_s(0)$ and $M_S M_I$. Assuming that the first two are positive, a negative sign of $M_S M_I$ describes the hyperfine interaction as a stabilization of the electron-Zeeman level. On the other hand, its destabilization is indicated when the sign of $M_S M_I$ is positive.

The hyperfine splitting of the electron-Zeeman level by a nucleus with $I \neq 0$ for a radical in a magnetic field $\vec{B}$, can usually be observed in ESR spectra. Transitions are allowed corresponding to the ESR selection rules $\Delta M_S = \pm 1$ and $\Delta M_I = 0$. Two transitions occur for a single nucleus with $I = ½$, and thus leads to two absorption lines, while three

transition are allowed for in the case of I = 1 (see figure 15). The ESR lines are separated by the absolute value of the hyperfine splitting constant a_x, which means that the sign of this value cannot be directly measured from the ESR spectrum. Basically, a_x infers the interaction between nucleus X and the unpaired electron in a given radical, where it depends on the electron density. a_x is expressed in the magnetic field unit, G, and is given equation 3.16:

$$a_x = (2/3\,\mu_o \mu_N g_n)\rho_s(0) \tag{3.16}$$

An empirical equivalent of this is the well-known McConnell equation:

$$a_x = Q\rho_s(0) \tag{3.17}$$

where, Q is a constant that depends on the type of compound studied.

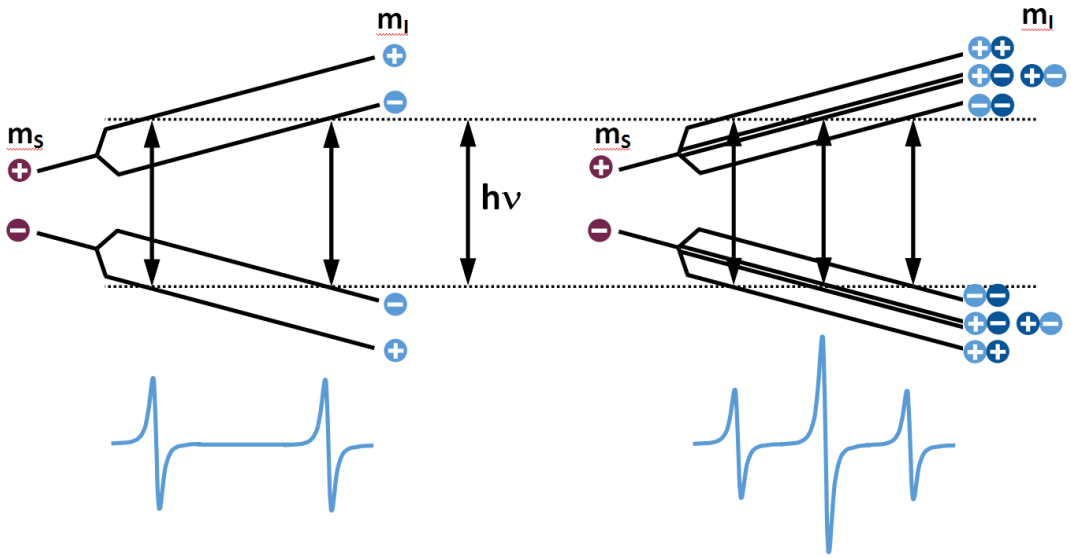

Figure 15. Hyperfine splitting of the electron-Zeeman level and ESR signals for one nucleus with either $I = 1/2$ (left) or 1 (right).

The number of hyperfine components represented as ESR lines depends on the number n of magnetic nuclei. For nonequivalent nuclei, each nucleus X splits every line into $2I$+1 lines, while n equivalent nuclei give rise to $2nI$+1 lines because these must all have the same a_x, and thus some ESR lines coincide. As a consequence, in the case in the latter, all lines in the spectrum cannot have the same intensity but tend to follow

patterns as illustrated in figure 16. The example of the hyperfine splitting caused by two equivalent nuclei X with either I = *1/2* or 1 is also shown in figure 17.

The total number of lines for a given radical, containing *k* sets of nuclei, each with a given number (n_j) and spin (I_j), is given by:

$$(2n_1I_1 + 1)(2n_2I_2 + 1)(2n_3I_3 + 1) \dots (2n_kI_k + 1) \qquad (3.18)$$

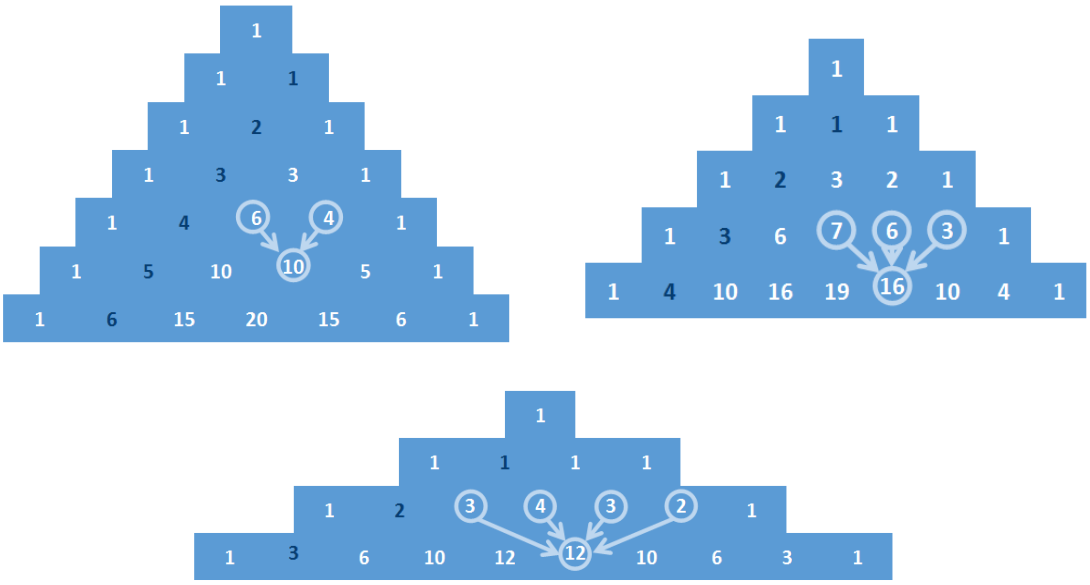

Figure 16. The distribution of intensities for *n* equivalent nuclei with *I* = 1/2, 1 and 3/2. Dark coloured numbers indicate *n* and the relative intensities are given in the corresponding row.

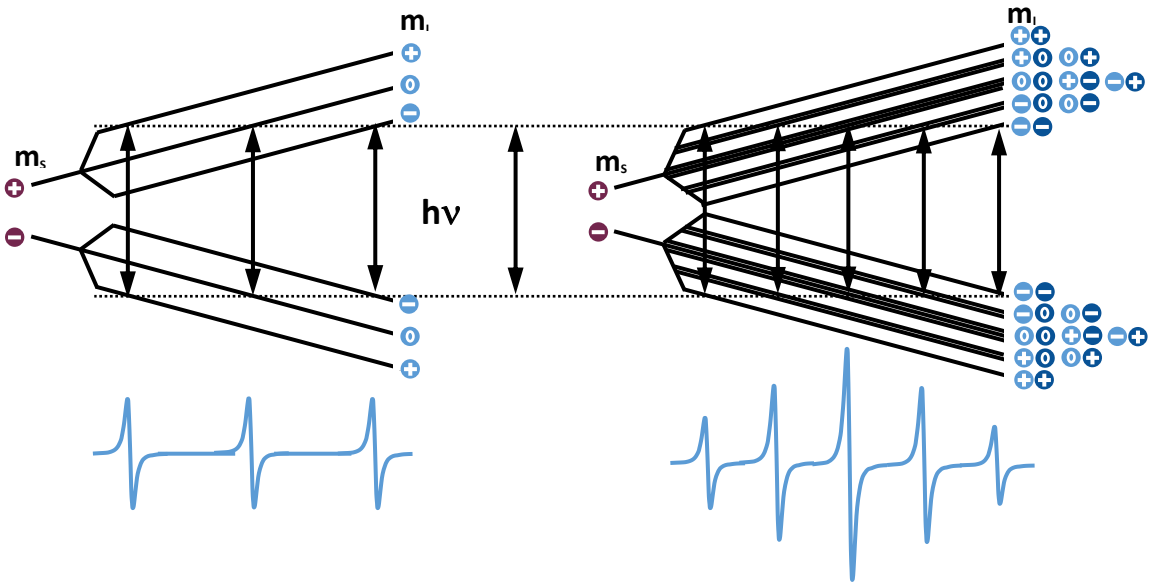

Figure 17. Hyperfine splitting of the electron-Zeeman level and ESR signals for two equivalent nuclei with either *I* = 1/2 (left) or 1 (right).

3.6 The Bloch Model

For a sample containing an ensemble of spins, the spin relaxation can be probed by considering the total spin magnetization vector. This notion was introduced in the *Bloch equations* by Felix Bloch, which describe a set of equations of motion. The Bloch model is applied in both ESR and NMR spectroscopy. The model is suitable for the understanding of the line broadening effects, which is the main subject in this work. The assumption made is only valid for low densities of electron spins, i.e. when the treatment of the spin-spin coupling from spins that are close together can be neglected.

The magnetization, $\vec{M}$, describes the total magnetic moment of an ensemble, and is defined as the sum of all magnetic moment vectors, $\vec{\mu}_i$, divided by the volume, *V*:

$$\vec{M} = \frac{1}{V}\sum_{i=1}^{n}\vec{\mu}_i \tag{3.19}$$

In the case of electrons, the expression above can be connected to the applied magnetic field via the *rationalized volume magnetic susceptibility*, χ_m, yielding the following expression:

$$\vec{M} = \frac{\chi_m}{\kappa_m \mu_o}\vec{B} \tag{3.20}$$

Here κ_m is a dimensional constant owing to the medium in question.

The base equation of motion for the angular momentum or the magnetic moment is given as:

$$\frac{d\vec{\mu}}{dt} = \gamma\vec{\mu} \times \vec{B} \tag{3.21}$$

The time dependence of $\vec{M}$, i. e. the differentation of $\vec{M}$ by time represents the change in the overall orientation of spins caused by the various processes that take place. This can be viewed in a simple way using a vector model. From equation 3.21, the magnetization varies with the magnetic moment, and the expression then becomes:

$$\frac{d\vec{M}}{dt} = \gamma_e\vec{M} \times \vec{B} \tag{3.22}$$

with $\vec{B}$ along the *z*-direction. The vector product of the above equation are obtained by the computation, obtaining as *x*-, *y*-components (transverse direction), and *z*-component (longitudinal direction):

$$\begin{aligned} \frac{dM_x}{dt} &= \gamma_e B M_y \\ \frac{dM_y}{dt} &= -\gamma_e B M_x \\ \frac{dM_z}{dt} &= 0 \end{aligned} \tag{3.23}$$

with solutions

$$\begin{aligned} M_x &= M_\perp^o \cos\ (\omega_L t) \\ M_y &= M_\perp^o \sin\ (\omega_L t) \\ M_z &= M_z^o \end{aligned} \tag{3.24}$$

$M_\perp^o$ and M_z^o denote the magnitudes of the magnetization perpendicular and parallel to $\vec{B}$. In the case of $M_\perp^o \neq 0$, the magnetization vector precesses about the *z*-axis with the Larmor frequency, ω_L.

In solution, before the external magnetic field is applied, the magnitude of $\vec{M}$ is assumed to be zero since the spin magnetic moments are oriented randomly in every direction. A change in magnetization can be observed when the magnetic field is turned on. The spins then align parallel to the field direction, leading to an exponential rise of the *z*-component of magnetization vector, as shown in figure 18.

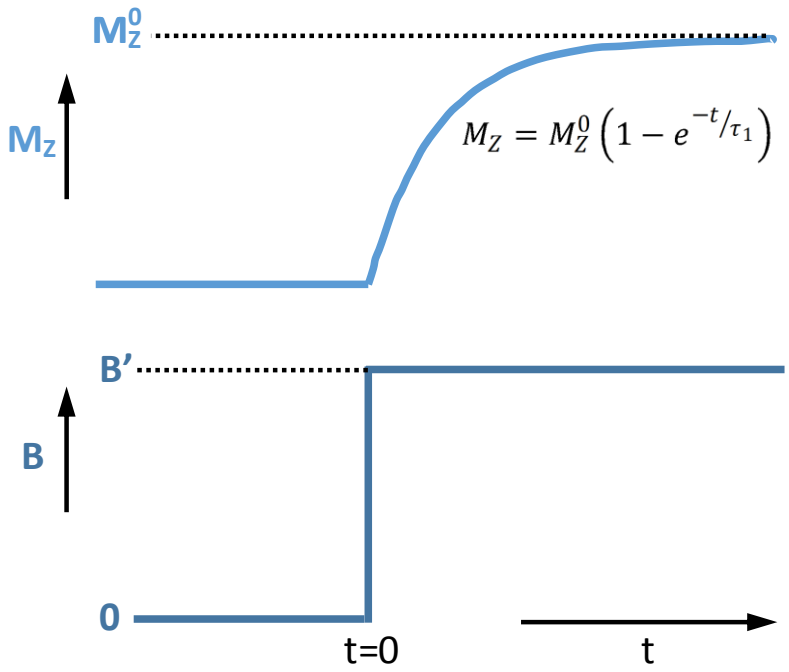

Figure 18. Behaviour of the magnetization when a constant magnetic field, *B'*, is applied

Two relaxation rates depending on the longitudinal relaxation time (τ_1) and transverse relaxation time (τ_2) are now introduced, resulting in the equation below. The relaxation of M_x and M_y gives rise to the same rate constant, which characterized by τ_2:

$$\begin{aligned} \frac{dM_x}{dt} &= \gamma_e B M_y - \frac{M_x}{\tau_2} \\ \frac{dM_y}{dt} &= \gamma_e B M_x - \frac{M_y}{\tau_2} \\ \frac{dM_z}{dt} &= \frac{M_z^o - M_z}{\tau_1} \end{aligned} \tag{3.25}$$

Relaxation can only take place after the application of electromagnetic radiation, meaning the microwave irradiation perpendicular to the magnetic field for ESR. Only the magnetic part, $\vec{B}_1$, of this wave with the oscillation frequency, ω, is considered, as given by the following components:

$$\begin{aligned} B_{1,x} &= B_1 \cos(\omega\, t) \\ B_{1,y} &= B_1 \sin(\omega\, t) \\ B_{1,z} &= 0 \end{aligned} \tag{3.26}$$

Inserting this into equation 3.23, in the absence of relaxation, the cross product becomes:

$$\frac{d\vec{M}}{dt} = \gamma_e \vec{M} \times (\vec{B} + \vec{B}_1) \tag{3.27}$$

and with the addition of relaxation, the Bloch equations can now be expressed as follows:

$$\begin{aligned} \frac{dM_x}{dt} &= \gamma_e\left(BM_y - B_1 \sin\omega t \; M_z\right) - \frac{M_x}{\tau_2} \\ \frac{dM_y}{dt} &= \gamma_e(B_1 \cos\omega t \; M_z - BM_x) - \frac{M_y}{\tau_2} \\ \frac{dM_z}{dt} &= \gamma_e B_1\left(\sin\omega t \; M_{zx} - \cos\omega t \; M_y\right) - \frac{M_z - M_z^o}{\tau_1} \end{aligned} \tag{3.28}$$

The solutions to Bloch equations will lead to a description of the measured signal or absorption. To solve such differential equations, it is convenient to transform them to a new coordinate frame, where the *x*-axis always aligns with the direction of $\vec{B}_1$, through a rotation by the angle φ between the new and old *x*-axis, and which rotates at an angular frequency of ω (figure 19). The Bloch equations now form a set of coupled differential equations with the coordinates $M_{x\phi}$, $M_{y\phi}$, and M_z of the magnetization, together with the Larmor frequency, $\omega_B = -\gamma_e B$, as given in equation 3.29.

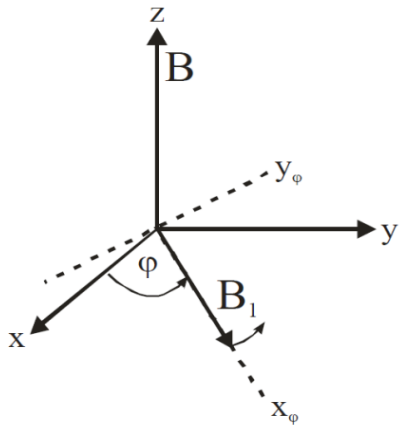

Figure 19. The rotating coordinate frame shown relatively to that of the old one

$$\frac{dM_{x\varphi}}{dt} = -(\omega_B - \omega)M_{y\varphi} - \frac{M_{x\varphi}}{\tau_2}$$
$$\frac{dM_{y\varphi}}{dt} = (\omega_B - \omega)M_{x\varphi} + \gamma_e B_1 M_z - \frac{M_{y\varphi}}{\tau_2} \qquad (3.29)$$
$$\frac{dM_{z\varphi}}{dt} = -\gamma_e B_1 M_{y\varphi} - \frac{M_z - M_z^o}{\tau_1}$$

The appropriate set of steady-state solutions are shown in the following equation:

$$M_{x\varphi} = -M_z^o \frac{\gamma_e\, B_1\, (\omega_B - \omega)\, \tau_2^2}{1 + (\omega_B - \omega)^2\, \tau_2^2 + \gamma_e^2\, B_1^2 \tau_1 \tau_2}$$
$$M_{y\varphi} = M_z^o \frac{\gamma_e\, B_1 \tau_2}{1 + (\omega_B - \omega)^2\, \tau_2^2 + \gamma_e^2\, B_1^2 \tau_1 \tau_2} \qquad (3.30)$$
$$M_z = M_z^o \frac{1 + \ (\omega_B - \omega)\, \tau_2^2}{1 + (\omega_B - \omega)^2\, \tau_2^2 + \gamma_e^2\, B_1^2 \tau_1 \tau_2}$$

Note that the last term in the denominators in equation 3.30 including the quadratic dependence on B_1, is sometimes called the *(power-)saturation term*, and can be neglected if B_1 is small, as it is often the case for ESR spectroscopy.

In ESR experiments, the $\vec{B}_1$ field is usually applied linearly in the *x*-direction. The *x*-component of $\vec{B}_1$ is given in equation 3.31, whereas *y*- and *z*-components are equal to zero:

$$B_{1,x} = 2B_1 \cos\ (\omega\, t) \qquad (3.31)$$

The sum of two fields with equal magnitude and rotating in opposite directions is used to express $\vec{B}_1$, as is given in equation 3.31. This leads to a simpler way of using the solutions shown in equation 3.29.

$$\vec{B}_1 = \vec{B}_{1,+} + \vec{B}_{1,-} \qquad (3.32)$$

where

$$\vec{B}_{1,+} = \begin{pmatrix} B_1 \cos\ (\omega t \\ B_1 \sin\ (\omega t \\ 0 \end{pmatrix} \quad \text{and} \quad \vec{B}_{1,-} = \begin{pmatrix} B_1 \cos\ (\omega t \\ -B_1 \sin\ (\omega t \\ 0 \end{pmatrix} \qquad (3.33)$$

The effects of $\vec{B}_1$ on the magnetization can also be described in terms of the magnetic susceptibilities:

$$\chi^o = \frac{\kappa \mu_o M_z^o}{B}$$
$$\chi' = \frac{\kappa \mu_o M_{x\varphi}}{B_1} \tag{3.34}$$
$$\chi'' = -\frac{\kappa \mu_o M_{y\varphi}}{B_1}$$

Here $M_{x\varphi}$ and $M_{y\varphi}$ define the coordinate frame of magnetization and χ^o is the static magnetic susceptibility. χ' and χ'' are two dynamic susceptibilities, with the former representing the dispersion, while the latter represents the power absorption, P_a. These terms are also known as the *Bloch susceptibilities*, which can be further derived as given in equation 3.25.

$$\chi' = \chi^o \frac{\omega_B(\omega_B - \omega)\tau_2^2}{1 + (\omega_B - \omega)^2 \tau_2^2 + \gamma_e^2 B_1^2 \tau_1 \tau_2}$$
$$\chi'' = \chi^o \frac{\omega_B \tau_2}{1 + (\omega_B - \omega)^2 \tau_2^2 + \gamma_e^2 B_1^2 \tau_1 \tau_2} \tag{3.35}$$

χ'' which is related to $M_{y\varphi}$ (equation 3.34) is the important part of the solution of the Bloch equations, as it contains the ESR absorption line. It can be rewritten to an expression using the half-width at half-height, Γ, as given in the following form:

$$\chi'' = \chi^o B_r \frac{1}{\Gamma^2 + (\omega - \omega_B)^2} \tag{3.36}$$

with B_r being the resonant magnetic field, and

$$\Gamma = \frac{1}{\tau_2}(1 + \gamma_e^2 \, B_1^2 \, \tau_1 \, \tau_2)^{1/2} \tag{3.37}$$

Equation 3.36 can be further rewritten to yield equation 3.39 by using a normalized Lorentz function, *Y*:

$$Y(\omega - \omega_B) = \frac{1}{\pi} \frac{\Gamma}{\Gamma^2 + (\omega + \omega_B)^2} \tag{3.38}$$

$$\chi'' = \frac{\pi \chi^o B_r}{(1 + \gamma_e^2 \, B_1^2 \, \tau_1 \, \tau_2)} Y(\omega - \omega_B) \tag{3.39}$$

As just mentioned χ'' is connected to the power absorption, P_a, which is given in the following expression:

$$P_a = \frac{\omega B_1^2 \chi''}{\mu_o} \tag{3.40}$$

Expressing the absorbed power in term of a Lorentz function yields:

$$P_a = \frac{\omega B_1^2}{\mu_o} \frac{\pi \chi^o B_r}{(1 + \gamma_e^2 B_1^2 \tau_1 \tau_2)} Y(\omega - \omega_B) \tag{3.41}$$

From the discussion above, it thus becomes clear that the ESR absorption line contains a Lorentzian shape with a maximum value at $\omega = \omega_B$ and a line width of Γ in the unit of frequency. The line width when dealing with unit of magnetic field can be obtained using the relation $\Gamma = \gamma_e \, \Delta B$, i.e. Γ in equation 3.37 is divided by the gyromagnetic ratio:

$$\Delta B = \frac{1}{|\gamma_e| \tau_2} (1 + \gamma_e^2 \, B_1^2 \, \tau_1 \, \tau_2)^{1/2} \tag{3.42}$$

For non-saturated conditions, which is usually performed with ESR, the Lorentzian line width is simplified to the expression given in equation 3.43.

$$\Delta B = \frac{1}{|\gamma_e| \tau_2} \tag{3.43}$$

The Bloch model with Lorentzian function works well for samples of liquid solutions. It is, however, inapplicable to the samples of solid states, due to their more complicated spin relaxation. A Gaussian function is the alternative for this situation, in which the line width can be defined by the following expression:

$$\Delta B = \frac{1}{(\pi \ln 2)^2 |\gamma_e| \tau_2} \tag{3.44}$$

The shape of Lorentzian and Gaussian functions, and of their first derivatives are illustrated in figure 20.[54]

In principle, when the sample is placed in a homogeneous magnetic field and when the system presents resolved hyperfine structure, all lines in the ESR spectrum have the same width, determined by *the homogenous line width*, ΔB^o:

$$\Delta B^o = \frac{1}{|\gamma_e|} \left(\frac{1}{2\tau_1} + \frac{1}{\tau_2} (1 + \gamma_e^2 B_1^2 \tau_1 \tau_2)^{1/2} \right) \tag{3.45}$$

As mentioned before in equation 3.10, τ_1 is not important for the ESR spectra of solutions, since $\tau_1 \gg \tau_2$. The expression of the line width thus normally reduces to equation 3.43.

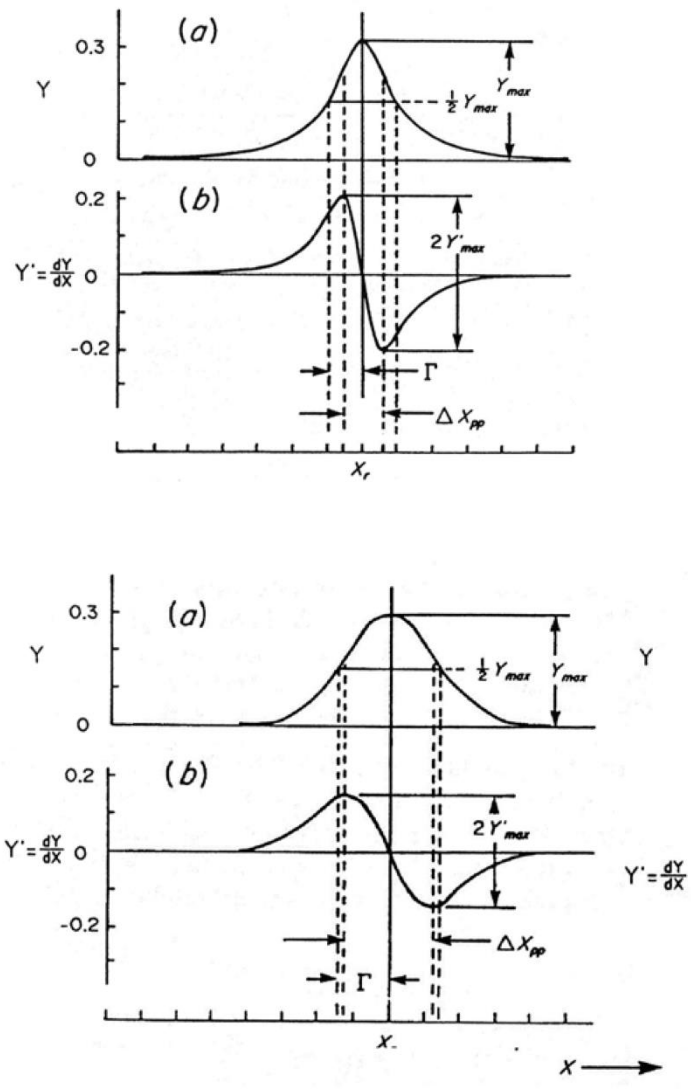

Figure 20. The shape of Lorentzian (top) and Gaussian (bottom) functions (a), with their first derivatives (b). [Adapted from ref 54.]

3.7 ESR Line Broadening and Dynamic Line Shape Effects

Line broadening experiments can be performed using the concentration dependence of reactions, such as Heisenberg exchange, electron self-exchange, and proton or counter ion transfer. However, only the general concept in terms of electron self-exchange is discussed in this work. The kinetics of such exchange is determined by the observed

rate constant, as given in equation 2.15, of which an abbreviation is shown below, where *a* and *b* represent molecules having different nuclear spin configurations:

$$A_{(a)} + A^{\bullet -}_{(b)} \xrightarrow{k_{obs}} A^{\bullet -}_{(a)} + A_{(b)} \tag{3.46}$$

The dynamic effects can be described since the change in lifetime gives rise to line shape effects. In the *slow exchange region*, where well separated lines are the outcome, the line width is shown in the following equation:

$$\Delta B = \Delta B^{o} + \frac{1 - p_j}{|\gamma_e \tau|} \tag{3.47}$$

where p_j is the probability of both reactants having the same nuclear spin configuration, corresponding to the *j*'th ESR line.

Assuming the concentration of diamagnetic species is constant, the reaction can hence be expressed using the relationship between lifetime and first order rate constant given in equation 3.48,[54] further taking the combination with equation 3.47 and the first derivative Lorentzian form of the ESR signal, leads to the association of the line broadening with the rate constant shown in equation 3.49.

$$\tau = \frac{1}{k_{obs}[A]} \tag{3.48}$$

$$\Delta B_{pp} - \Delta B^{o}_{pp} = \left(\frac{\left(1 - p_j\right) k_{obs}}{\sqrt{3}\pi |\gamma_e|} \right) [A] \tag{3.49}$$

Here ΔB^{o}_{pp} and ΔB_{pp} denote the peak-to-peak widths of the first derivative line in the absence and presence of the self-exchange reaction.

Large increases in [A] can take the exchange system into the *fast exchange region*. The lifetimes in this region are short as very rapid reactions take place, resulting in the spectrum collapsing to one single line, which narrows with increasing concentration. This can also be expressed in the terms of the rate constant:

$$\Delta B_{pp} - \Delta B^{o}_{pp} = \left(\frac{4\pi |\gamma_e| \nabla_2}{3 k_{obs}} \right) \frac{1}{[A]} \tag{3.50}$$

with ∇_2 being the second moment of ESR spectrum:

$$\nabla_2 = \sum_j p_j \left(\bar{B} - B_j\right)^2 \tag{3.51}$$

Here $\bar{B}$ represents the centre field of the spectrum and B_j the resonant magnetic field strength of the *j*'th ESR line.

The line broadening owing to equation 3.50 is not always valid with every single-line ESR spectrum since it is possible that the reactions are still in the intermediate region, where the outer lines shift towards to the centre. A way to determine if the fast exchange region is reached, is given in equation 3.52, which uses the parameter *X*, i.e. if $X \leq 0.2$, the reaction is admitted to be in the fast exchange region.

$$X = \frac{\sqrt{3}}{2} \frac{\left(\Delta B_{pp} - \Delta B_{pp}^{o}\right)}{\sqrt{\nabla_2}} \leq 0.2 \tag{3.52}$$

It is simple to transform equations 3.49 and 3.50 into linear expressions, describing ΔB_{pp} as function of [A] for slow exchange or 1/[A] for fast exchange. This provides a very convenient way to determine k_{obs} from the slopes of plots like the ones illustrated in figure 21. The advantage of using line widths instead of broadening is that, from an experimental point of view, ΔB_{pp}^{o} needs not be known precisely.

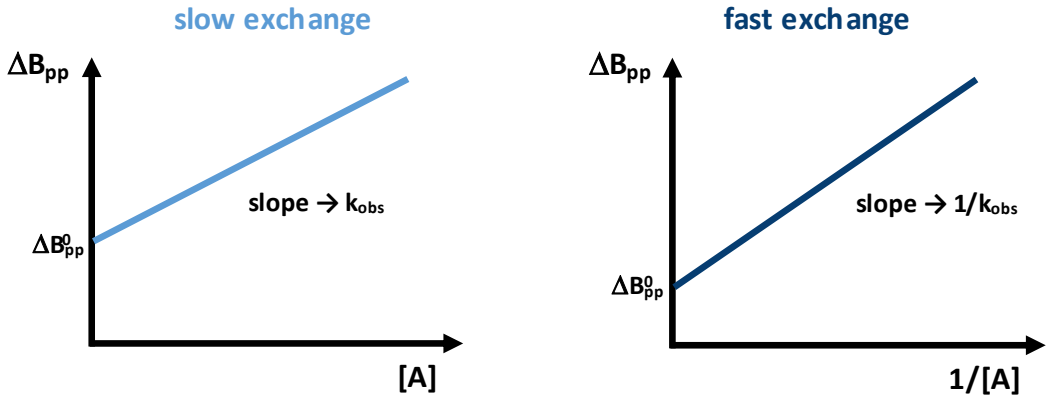

Figure 21. k_{obs} determined from the line broadening of slow exchange (left) and fast exchange (right) regions.

Systems in the intermediate region are more complicated, and it is not possible to obtain simple equations for k_{obs}. Computer simulations, however, are often used to investigate such dynamic regions, as shall be described further in the experimental part. Note that

most simulation programs usually also cover the slow and fast exchange regions and that knowledge of ΔB_{pp}^{o} is usually required.

Below, the self-exchange line broadening of 2,3-dichloro-5,6-dicyano-1,4-benzoquinone (DDQ) and its radical anion is used as an example of the dynamic line shape effects, which is shown in figure 22.

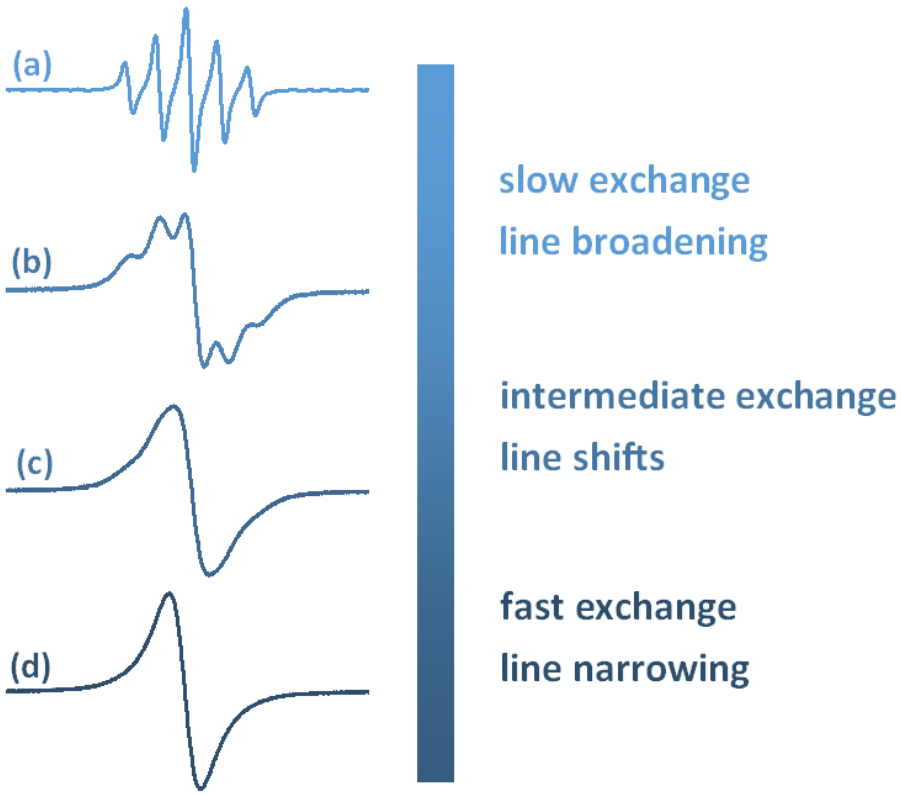

Figure 22. Experimental line broadening effects seen in the self-exchange reaction containing various concentrations of 2,3-Dichloro-5,6-dicyano-1,4-benzoquinone [DDQ] at a constant concentration, 0.5 mM of its radical anion [$DDQ^{\bullet -}$]; (a) [DDQ] = 0 mM, (b) [DDQ] = 2.3 mM, (c) [DDQ] = 3.9 mM, (d) [DDQ] = 10 mM

4 Experimental

In this thesis, the homogeneous electron self-exchange of four systems in various organic solvents, which are presented in table 2, is discussed. The radicals related to this work are shown in figure 23, and consist of the thianthrene radical cation ($Th^{\bullet+}$), the 2,3,7,8-tetramethoxythianthrene radical cation ($MTh^{\bullet+}$), together with the anion radicals of 2,3-dichloro-5,6-dicyano-1,4-benzoquinone ($DDQ^{\bullet-}$), and tetracyanoethylene ($TCNE^{\bullet-}$).

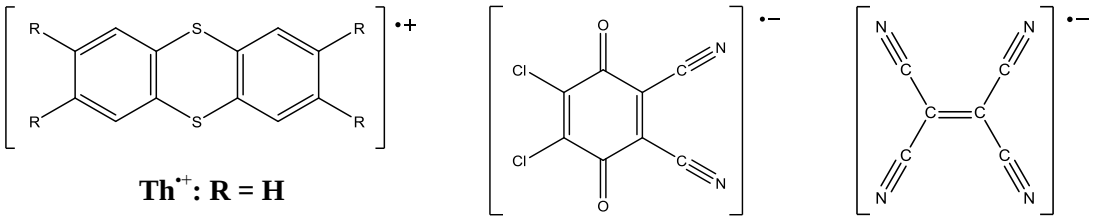

$Th^{\bullet+}$: R = H

$MTh^{\bullet+}$: R = OCH_3

$DDQ^{\bullet-}$

$TCNE^{\bullet-}$

Figure 23. Paramagnetic species involved in the electron self-exchange reactions in this work; Thianthrene radical cation (**$Th^{\bullet+}$**), 2,3,7,8-tetramethoxythianthrene radical cation (**$MTh^{\bullet+}$**), 2,3-Dichloro-5,6-dicyano-1,4-benzoquinone radical anion (**$DDQ^{\bullet-}$**), Tetracyanoethylene radical anion (**$TCNE^{\bullet-}$**).

The main interests in the present study are divided into two subjects. The first concerns the two thianthrene redox couples, which are investigated according to the influence of the large structural difference between the radical cations and their parent molecules on their electron self-exchange reactions, as described earlier in the introduction. In order to obtain further useful information, the systems of ($Th^{\bullet+}$/Th) and ($MTh^{\bullet+}$/MTh) have been investigated under temperature dependence as well. The second interest involves the remaining two systems, DDQ/$DDQ^{\bullet-}$ and TCNE/$TCNE^{\bullet-}$, which were investigated only in non-Debye solvents showing more than one relaxation time. In this case, the multiple Debye equation given in equation 2.45-2.49 may be taken into account for calculation of the longitudinal relaxation time. For both systems, it is sufficient to observe the solvent dependence at room temperature. Returning to the reactions of ($Th^{\bullet+}$/Th) and ($MTh^{\bullet+}$/MTh), it is noted that both of these have also been investigated in a non-Debye solvent, which is propylene carbonate (PC).

In the following, the methodology including the chemicals, starting materials and sample preparation, instrumentation, and interpretation of ESR spectra, shall be described in detail.

Table 2. Self-exchange reaction systems in different solvents.

System	Solvent	Condition
$Th^{\bullet+}$/Th	ACN DCM *PC DCB	Temperature
$MTh^{\bullet+}$/MTh	ACN DCM *PC	dependence
DDQ/$DDQ^{\bullet-}$	*DMA *EtOH * iPrOH *MeOH *PC *FA	Room temperature
TCNE/$TCNE^{\bullet-}$	*DMA *EtOH * iPrOH *DMF *BN	

*Non-Debye solvents
ACN = Acetonitrile, DCM = Dichloromethane, PC = Propylene carbonate, DCB = 1,2-Dichlorobenzene, MeOH = Methanol, EtOH = Ethanol, iPrOH = Isopropanol, DMA = Dimethylacetamide, DMF = Dimethylformamide, BN = Benzonitrile, FA = Formamide

4.1 Chemicals

The radical cations of Th and MTh were found to be either instable or insoluble in many organic solvents and therefore successful measurements were only possible in ACN, DCM, PC and DCB. Th was purchased from Aldrich, whereas MTh has been prepared as reported in the literature,[55] described later. Also, the preparation of dark purple and green solids of ($Th^{\bullet+}BF_4^-$) and ($MTh^{\bullet+}BF_4^-$) is given. All solutions of both thianthrene couples contained 1×10^{-4} M of the radicals and various concentrations of the neutral compounds up to 2.5×10^{-2} M. The concentration of radicals was chosen to be low enough to avoid dimerization, which is a known issue at low temperatures. For example, in ACN, dimerization constants of 4×10^6 M^{-1} (233 K) and 1.1×10^4 M^{-1} (256 K) have been reported[56] and using this data, an equilibrium constant of approximately 6 M^{-1} can be estimated for 293 K. This corresponds to a conversion of 0.02% of the radical to dimer at this temperature.

For the reactions of DDQ/$DDQ^{\bullet-}$ and TCNE/$TCNE^{\bullet-}$, numerous studies in various organic solvents, mostly being Debye solvents, have been reported.[11,4] The selected solvents for both systems here, are non-Debye solvents with two or three relaxation times. The radicals in samples of both systems were fixed at 2×10^{-4} M, whereas their

parent molecules were varied up to about 3×10^{-2} M. DDQ and TCNE were purchased from Aldrich and Fluka, respectively. Their radical anions were formed by reduction with tetrabutylammonium iodide (TBAI), which will be described in detail below.

The solvents for all reactions were of analytical grade (p.a.), dynamically dried over molecular sieves, 3 Å or 4 Å as appropriate, and distilled before use. In order to keep the solvents dry and oxygen free, they were kept and used under argon or nitrogen gas.

4.1.1 Preparation of 2,3,7,8-tetramethoxythianthrene (MTh)

7.5 ml (12.2 g, 118 mmol) of SCl_2 in 50 ml ACN was slowly added drop-wise to 10 ml (10.8 g, 78 mmol) of 1,2-dimethoxybenzene in 100 ml ACN under stirring. After that, the mixture was stirred further for 1.5 h, and a dark green precipitate was formed during the reaction. The filtered off precipitate was washed with ACN, suspended in $MeOH/H_2O$ and allowed to react with $SnCl_2$ until it was light yellow. Subsequently, this precipitate was extracted by acetone and was dried under vacuum using a reflux evaporator. 71% (9.3 g, 27.6 mmol) of product, with melting point 456-457 K, was obtained after recrystallization with EtOH.

4.1.2 Preparation of Thianthrene tetrafluoroborate ($Th^{\bullet+}BF_4^-$) and 2,3,7,8-Tetramethoxythianthrene tetrafluoroborate ($MTh^{\bullet+}BF_4^-$)

($Th^{\bullet+}BF_4^-$) and ($MTh^{\bullet+}BF_4^-$) were prepared under the same conditions, the only difference being that a suspension of 2,3,7,8-tetramethoxythianthrene (MTh) was used instead of that of thianthrene (Th) for the latter. Therefore only the preparation regarding to the former, which was applied from the literature, [57] shall be discussed here.

A suspension of 20 mmol (4.32 g) of thianthrene in 70 ml dry ACN was prepared and cooled to 233 K using liquid nitrogen. Under rigorous stirring, 20 mmol (2.34 g) $NOBF_4$ was gradually added. Subsequently, in order to remove nitrose gases, the mixture was stirred for 1 h under nitrogen gas, as shown in figure 24a. The solution was brought to room temperature and approximately 50 ml was drawn off. By addition of 100 ml dried diethylether, the salt of the radical cation formed a precipitate that was

filtered off using a frit (figure 24b). After drying this salt in high vacuum, the product was weighed under inert atmosphere, providing a yield of 83% (5.03 g, 16.6 mmol).

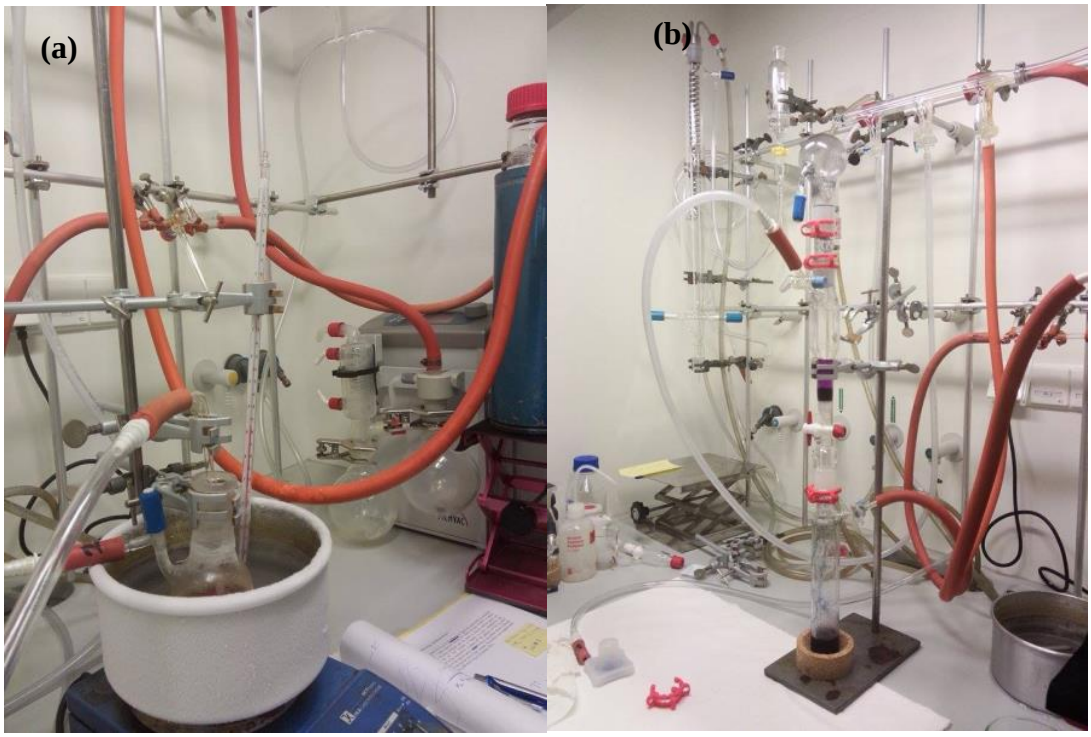

Figure 24. Preparation of ($Th^{\bullet+}BF_4^-$); (a) a mixture of Th and $NOBF_4$ in dry ACN, cooled to 233 K, stirring for 1h under nitrogen gas, (b) filtering off the dark purple precipitate of ($Th^{\bullet+}BF_4^-$).

4.2 Sample Preparation

As mentioned earlier, the used solutions contain a constant amount of radicals, and the self-exchange was investigated by varying the amount of the neutral compounds. Since the solutions of both radical cations, $Th^{\bullet+}$ and $MTh^{\bullet+}$, are very sensitive to water and oxygen, the preparation and measurement must be done under purified nitrogen gas, and the solvents used need to be dried and have any present oxygen removed. The samples of both couples were made in similar ways, by adding solvent to the solid mixture of radical cations and the appropriate parent compounds. Oxygen was removed from the glass flask before the stating materials were added, by performing several cycles of first evacuating the glass flask and subsequently filling it with nitrogen gas. The reactions yielded purple solutions for $Th^{\bullet+}$/Th (figure 25) and green solutions for $MTh^{\bullet+}$/MTh.

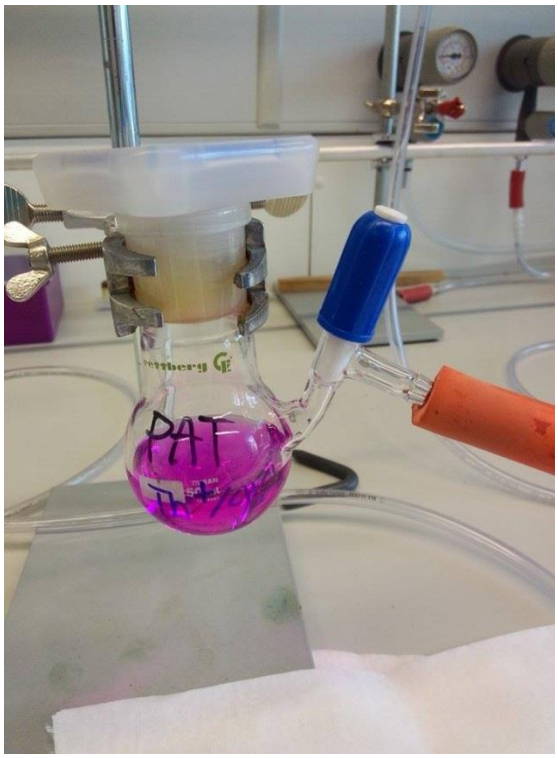

Figure 25. Solution of $Th^{\bullet+}$/Th in DCM prepared under nitrogen gas.

In case of the DDQ/$DDQ^{\bullet-}$ and TCNE/$TCNE^{\bullet-}$, 2×10^{-4} M stock solutions of tetrabutylammonium iodide (TBAI) in the solvents given in table 2 were made, and varying amounts of DDQ or TCNE were added depending on the desired concentration of the samples. The radical anions were formed, according to reactions 4.1 and 4.2, yielding reddish purple and yellow solutions of DDQ/$DDQ^{\bullet-}$ and TCNE/$TCNE^{\bullet-}$, respectively.

$$DDQ + (n-Bu)_4N^+I^- \longrightarrow DDQ^{\bullet-} + (n-Bu)_4N^+ + \frac{1}{2}I_2 \qquad (4.1)$$

$$TCNE + (n-Bu)_4N^+I^- \longrightarrow TCNE^{\bullet-} + (n-Bu)_4N^+ + \tfrac{1}{2}I_2 \qquad (4.2)$$

4.3 Instrumentation

ESR spectra of the $Th^{\bullet+}$/Th and the $MTh^{\bullet+}$/MTh systems were recorded at room temperature with a Varian E-9 ESR spectrometer (figure 28). Temperature dependent measurements of $Th^{\bullet+}$/Th and $MTh^{\bullet+}$/MTh as well as room temperature experiments of

DDQ/DDQ$^{\bullet-}$ and TCNE/TCNE$^{\bullet-}$ reactions were acquired using a Bruker ELEXSYS E-500 series spectrometer (figure 27). Both spectrometers operate at X-band with a modulation frequency of 100 kHz, and additionally a flow-through capillary system was connected to the ESR resonator (figure 26). All samples were bubbled in the glass reservoir under nitrogen gas for 15 min before use.

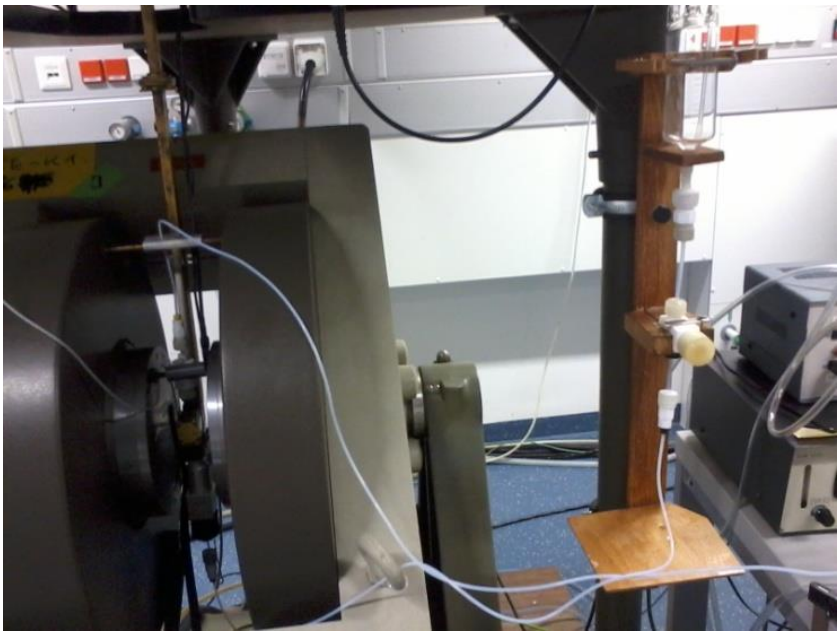

Figure 26. Varian E-9 ESR spectrometer with the flow-through system attached to the ESR resonator placed in the cavity.

4.3.1 Bruker ELEXSYS E-500

There are four important parts of the spectrometer shown in figure 27, consisting of the microwave bridge (1), the magnet (2), the resonator (3), and finally the acquisition server (4). During the ESR measurement, the sample under study is situated in the cavity or resonator and is subjected to a magnetic field B originating from the ESR magnet. The microwave bridge is where the X-band microwaves with energy $h\nu$ are generated. All needed setup parameters can be adjusted by a computer, which is connected to the acquisition server recording the spectrum. The spectrometer is equipped with a Bruker variable temperature controller (ER 4131VT) (5), which keeps the temperature stable within 0.2 K of the desired value.

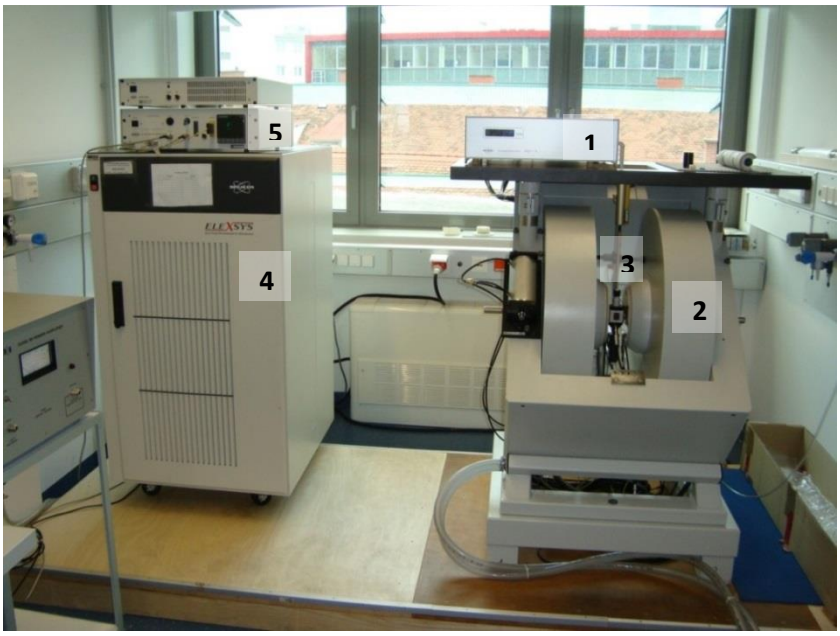

Figure 27. The Bruker ELEXSYS E-500 series spectrometer.

4.3.2 Varian E-9

This spectrometer system from Varian is shown in figure 28, and also consists of the microwave bridge (1), magnet (2) and resonator (3). The recording is controlled by the console (4) where the setup parameters need to be selected. In order to measure the power and frequency of the microwave, as well as the field, a power meter (5), a frequency counter (7) and a Gauss/Tesla-meter (6) are used. Furthermore, the console is connected to a computer which stores a digital versions of the recorded spectra.

Figure 28. The Varian E-9 spectrometer.

4.4 Interpretation of ESR Spectra

The rates of the electron self-exchange were obtained from individual spectra using a non-commercial simulation software based on the density matrix formalism.[58] The simulation provided the optimum values of the line width and the hyperfine splitting constant of the no-exchange ESR spectra. Subsequently, these parameters were fixed for the self-exchange spectra and the simulation then determined the rates of reaction, which were further used to obtain the observed rate constants, as shall be described in greater detail in the following chapters.

5 Results and Discussion: The TCNE/TCNE$^{\bullet-}$ and DDQ/DDQ$^{\bullet-}$ Couples

5.1 Electron Self-Exchange at Room Temperature

When studying solvent dynamic effects, the longitudinal relaxation time, τ_L of the solvents may strongly control the reactions. For reactions in non-Debye solvents, which possess multiple relaxation processes, the way of analysing the data may become more complicated than when dealing with Debye solvents possessing only a single relaxation time. In this study, the reactions of the TCNE/TCNE$^{\bullet-}$ and DDQ/DDQ$^{\bullet-}$ couples in non-Debye solvents have been observed. The limiting relaxation times τ_{L0} and $\tau_{L\infty}$ have been applied to the studied reactions in order to compare both models, investigating which of them may provide a better fit to the experimental systems, as shall be discussed in detail later.

5.1.1 ESR Measurements

Simulation of ESR spectra of no-exchange for TCNE/TCNE$^{\bullet-}$, measured at room temperature in all used solvents, provided nine lines belonging to four nitrogen atoms, with a hfs constant in the range of 1.57-1.60 G and a line width of 0.04-0.05 G, depending on the solvent. Figure 29 is given as an example of the ESR line broadening for this system investigated in BN, showing experimental spectra together with their simulations.

Similarly to the system above, the ESR line broadening of DDQ/DDQ$^{\bullet-}$ in MeOH is shown in figure 30. For no-exchange of the DDQ/DDQ$^{\bullet-}$ system in different solvents at room temperature (e.g. figure 2a), the ESR spectra contain 5 lines owing to two nitrogen atoms, with a hfs constant of 0.56-0.60 G, which is in a good agreement with the literature.[11] The line widths are in the range of 0.059-0.087 G.

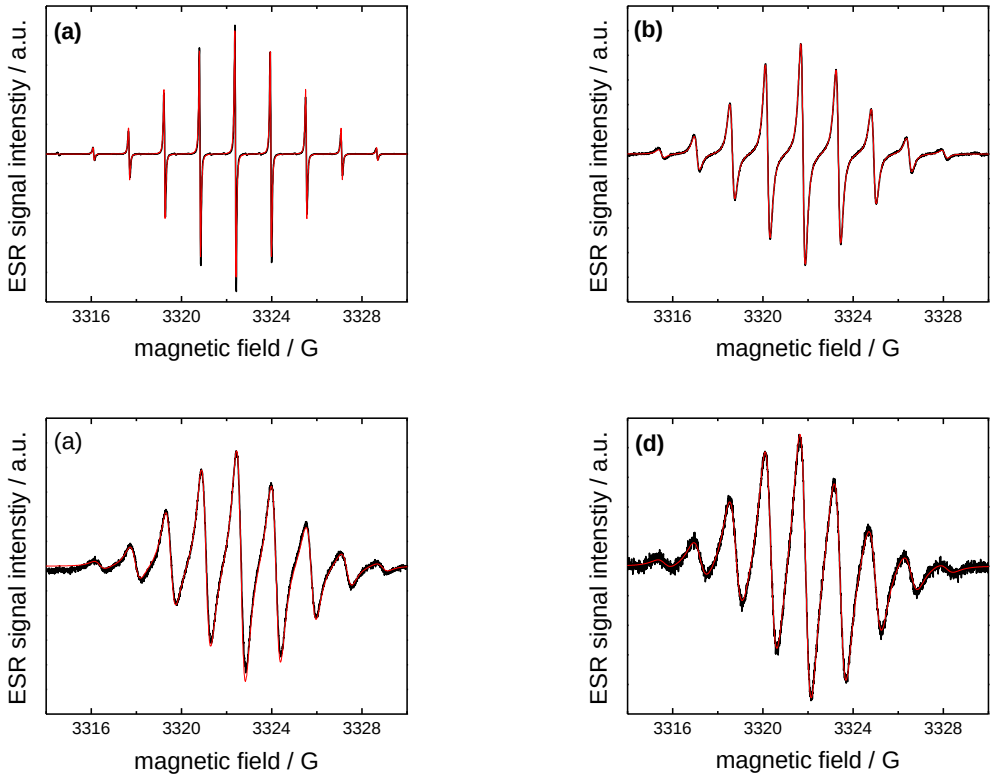

Figure 29. ESR spectra of TCNE/TCNE$^{\bullet-}$ in BN at room temperature. [TCNE$^{\bullet-}$] is kept as 2×10^{-4} M; (a) [TCNE] = 0 mM, (b) [TCNE] = 3.3×10^{-3} M, (c) [TCNE] = 6.6×10^{-3} M, (d) [TCNE] = 9.7×10^{-3} M.

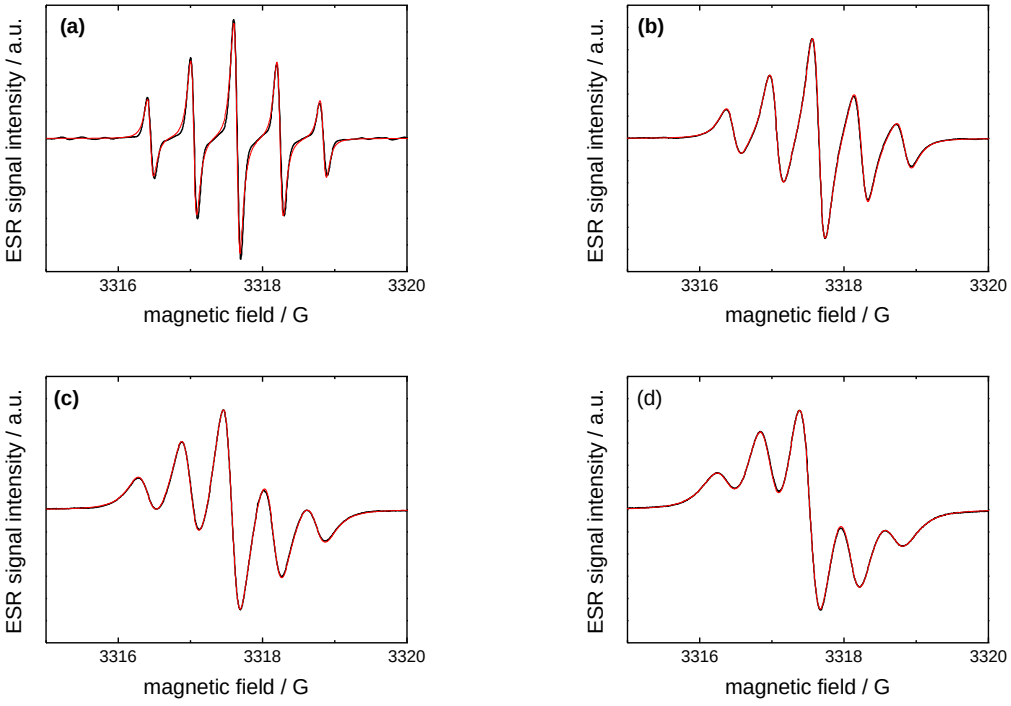

Figure 30. ESR spectra of DDQ/DDQ$^{\bullet-}$ in DMA at room temperature. [DDQ$^{\bullet-}$] is kept as 2×10^{-4} M; (a) [DDQ] = 0 mM, (b) [DDQ] = 1.4×10^{-2} M, (c) [DDQ] = 2.2×10^{-2} M, (d) [DDQ] = 3.1×10^{-2} M.

5.1.2 Rate Constants of Electron Self-Exchange Reactions

As mentioned in the experimental part, the observed rate constants k_{obs} have been determined from the exchange rates of the reaction k_{dyn}, which were obtained from the simulations. The concentration dependence of k_{dyn} for DDQ/DDQ$^{\bullet-}$ and TCNE/TCNE$^{\bullet-}$ in various solvents provided the values of k_{obs} directly from the slopes, as shown in figures 31 and 32. Only for TCNE/TCNE$^{\bullet-}$ in DMF and DMA the k_{obs} were obtained in the slow exchange region, from the peak-to-peak line width ΔB_{pp}, which were determined from observing solely the central ESR line. The reason for this is that the systems of TCNE/TCNE$^{\bullet-}$ in these solvents are not stable. Therefore, performing a much quicker scan of just the central line was an alternative. The plots of ΔB_{pp} against various concentrations of TCNE in DMF and DMA are shown in figure 33. Their k_{obs} were investigated from the slopes corresponding to the expression given in equation 3.49. All values of k_{obs} together with k_d and consequently k_{et} of the DDQ/DDQ$^{\bullet-}$ and TCNE/TCNE$^{\bullet-}$ systems are shown in table 3.

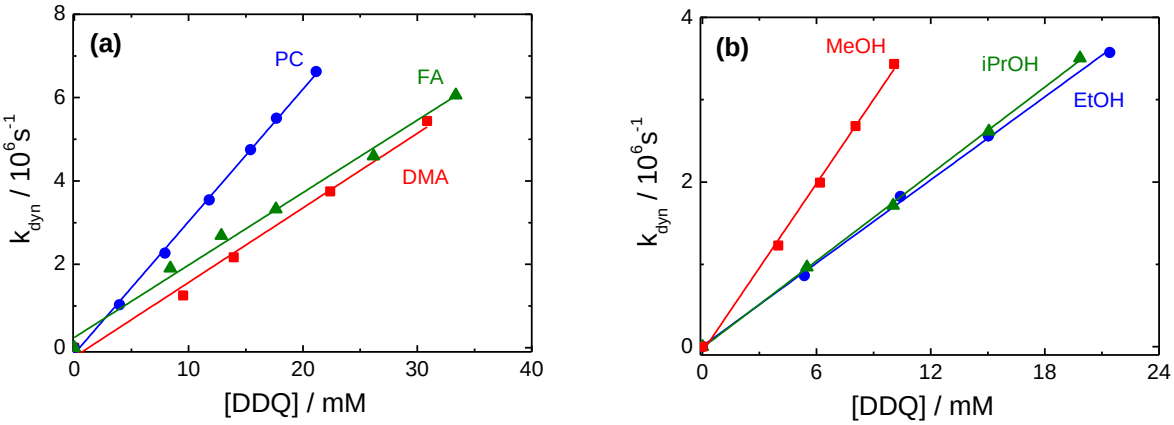

Figure 31. Concentration dependence of the exchange rate of the reaction, k_{dyn}, of DDQ/DDQ$^{\bullet-}$ in (a) solvents with two relaxation processes, (b) alcohol solvents with three relaxation processes.

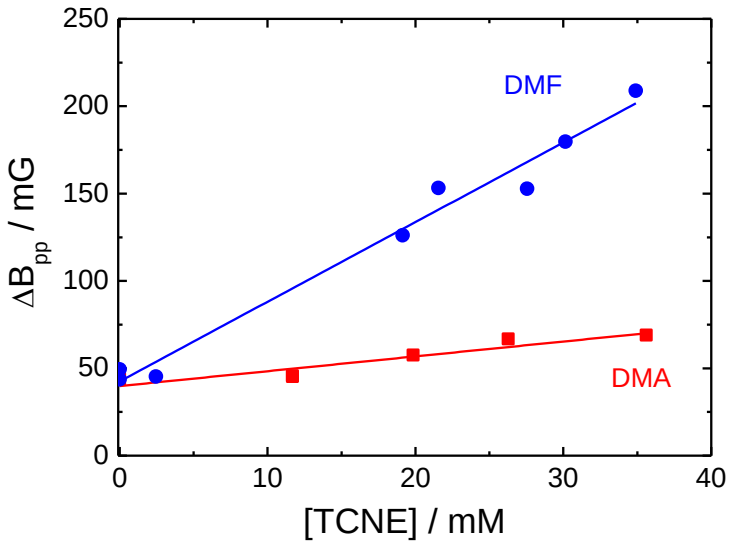

Figure 33. Concentration dependence of the peak-to-peak line width, ΔB_{pp}, of TCNE/TCNE$^{\bullet-}$ in DMF and DMA.

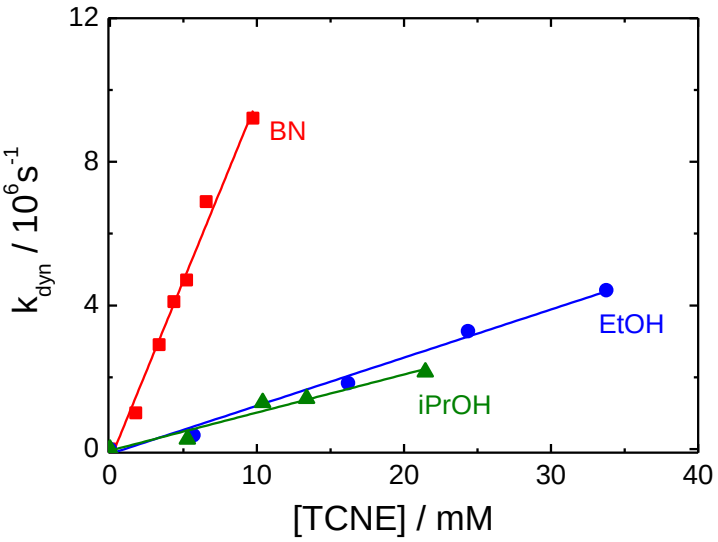

Figure 32. Concentration dependence of the exchange rate of the reaction, k_{dyn}, of TCNE/TCNE$^{\bullet-}$ in BN, EtOH and iPrOH.

Table 3 Rate constants for TCNE/TCNE$^{\bullet-}$ and DDQ/DDQ$^{\bullet-}$ in the given solvents at room temperature.

Solvent	k_{obs} (10^8 $M^{-1}s^{-1}$)	k_d[(a)] (10^8 $M^{-1}s^{-1}$)	k_{et}[(b)] (10^8 $M^{-1}s^{-1}$)
TCNE/TCNE$^{\bullet-}$			
DMF	1.04±0.06	71.5	1.07±0.06
DMA	0.19±0.04	70.0	0.20±0.04
BN	9.7±0.4	53.3	15.3±0.6
EtOH	1.37±0.08	54.3	1.44±0.08
iPrOH	1.1±0.1	27.7	1.2±0.1
DDQ/DDQ$^{\bullet-}$			
DMA	1.79±0.09	70.0	1.89±0.09
PC	3.18±0.05	24.0	4.32±0.07
FA	1.74±0.05	20.5	2.09±0.08
MeOH	1.68±0.09	54.3	1.8±0.1
EtOH	1.76±0.03	27.7	2.02±0.03
iPrOH	3.41±0.02	113.2	3.63±0.02

(a) from equation 2.8, (b) from equation 2.15

The values of k_{et} for TCNE/TCNE$^{\bullet-}$ in DMF and DMA may be unreliable because of the instability of these solutions and especially the k_{et} in DMA is very small when compared to the systems in the other solvents (table 4). Even speeding up the acquisition of data, by measuring only the central ESR line, may not help provide reliable results for these solvents. The system in BN provides the largest value of k_{et} with $9.7\pm0.4 \times 10^8$ $M^{-1}s^{-1}$, and this is in good agreement with the reported values from other Debye and non-Debye solvents. The k_{et} from the two alcohol solvents are substantially smaller than those of BN and the literature data, excluding the reactions in DMF and DMA. However, unlike in the amide solvents, the systems in the alcohols were stable.

For the reactions of DDQ/DDQ$^{\bullet-}$, the values of k_{et} are in the range of $1.89\pm0.09 \times 10^8$ $M^{-1}s^{-1}$ to $4.32\pm0.07 \times 10^8$ $M^{-1}s^{-1}$. They are smaller by approximately a factor of ten (table 4) than those from the literature. However, as shall be seen shortly, this does not indicate a poor correlation with the literature data.

5.1.3 Calculation of Activation Energies and Pre-Exponential Factors

Considering equation 2.34, the observed pre-exponential factor, Z_{obs}, can be estimated if the rate constant and the activation energy, ΔG^*, are known. One may calculate the latter parameter using the framework of Marcus theory, i.e. equation 2.19. This means that the data related to the geometry, *g(r,d)*, as well as the reorganization energy, λ, and the resonance splitting energy, V_{PS}, of the molecules are needed. Several reports on these parameters have been given for TCNE[4,59] and DDQ.[11,60,61] In this work, the parameters taken from the literature were chosen on the base of the latest reports using the most reliable methods.

For TCNE, the experimental value of the radius, *r*, and the reaction distance, *d*, have been reported as 3.10 Å[4] and 2.87 Å[59], respectively. The parameters used for the calculation of ΔG^* are λ_o/γ = 133.38 kJ mol^{-1},[4] λ_i^{∞} = 27.1 kJ mol^{-1},[59] and V_{PS} = 9.45 kJ mol^{-1}.[59]

For DDQ, the experimental values of d = 2.9 Å, λ = 89.5 kJ mol^{-1} and V_{PS} = 13.4 kJ mol^{-1} have been reported by Kochi.[60] From these, using λ_i^{∞} = 40.9 kJ mol^{-1},[61] a value of λ_o/γ = 132 kJ mol^{-1} was calculated and together with the above mentioned value of V_{PS}, ΔG^* has been determined. Also using the reported data, a radius of 2.3 Å was calculated.

According to the parameters above, the calculated activation energies, ΔG^*_{cal}, and their corresponding observed pre-exponential factors, Z_{obs}, of both redox systems determined for the measurements of this work, as well as those in the literature, are summarized in table 4.

Table 4. Calculated activation energies, ΔG^*_{cal}, observed pre-exponential factors, Z_{obs}, and rate constants k_{et}, for TCNE/TCNE$^{\bullet-}$ and DDQ/DDQ$^{\bullet-}$ in Non-Debye solvents compared with those from the literature.

	TCNE/TCNE$^{\bullet-}$			**DDQ/DDQ$^{\bullet-}$**		
solvent	**k_{et}** (10^8 $M^{-1}s^{-1}$)	**ΔG^*_{cal}[(a)]** (kJ mol^{-1})	**ln Z_{obs}[(b)]**	**k_{et}** (10^8 $M^{-1}s^{-1}$)	**ΔG^*_{cal}[(a)]** (kJ mol^{-1})	**ln Z_{obs}[(b)]**
DMF	1.07±0.06	9.84	22.5	-	-	-
DMA	0.20±0.04	9.11	20.5	1.89±0.09	6.58	21.7
BN	15.3±0.6	6.80	23.9	-	-	-
MeOH	-	-	-	1.8±0.1	9.18	23.4
EtOH	1.44±0.08	10.4	23.0	2.02±0.03	7.90	22.2
iPrOH	1.2±0.1	9.67	22.5	3.63±0.02	7.14	22.0
FA	-	-	-	2.09±0.08	6.91	21.9
PC	-	-	-	4.32±0.07	7.30	22.8
Data from the literature						
DCM	61.7[4]	6.54	25.2	72.5[11]	4.03	24.3
ACN	25.8[4]	11.3	26.2	33.7[11]	8.74	25.5
*$CHCl_3$**	50.1[4]	2.80	23.4	47.8[11]	0.34	22.4
BN	-	-	-	13.4[11]	4.28	22.7
PC	31.7[4]	9.84	23.5	-	-	-
*AC**	-	-	-	16.7[11]	7.75	24.4
*PhBr**	31.1[4]	1.47	22.5	-	-	-

(a) From equation 2.19, (b) from equation 2.34.
*$CHCl_3$ = Chloroform, AC = Acetone, PhBr = Bromobenzene.
Italic letters represent the Debye-solvents.

5.1.4 Solvent Dynamics

Following equation 2.36 which is applied for adiabatic reactions, Weaver plots have been made for every system studied. Here, the systems of TCNE/TCNE$^{\bullet-}$ and DDQ/DDQ$^{\bullet-}$ in non-Debye solvents have been compared with the systems from the literature, which have been investigated in other Debye and non-Debye solvents. For TCNE/TCNE$^{\bullet-}$, Weaver plots taking different values of τ_{L0} and $\tau_{L\infty}$ into account are shown in figure 34. Similarly for DDQ/DDQ$^{\bullet-}$, such plots are given in figure 35. The

relevant solvent parameters, including their single and multiple longitudinal relaxation times, are provided in table 5.

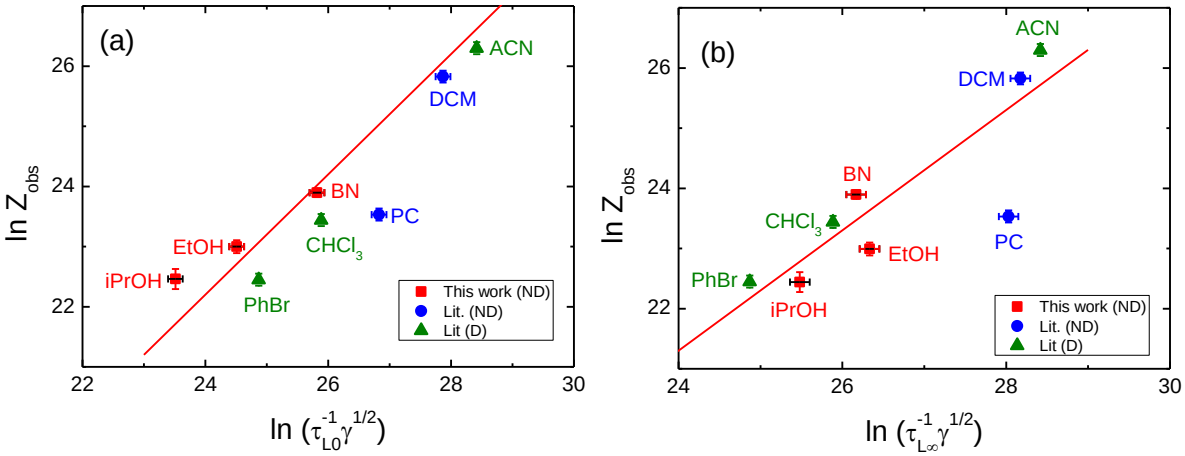

Figure 34. Weaver plots of (a) ln Z_{obs} *vs.* $\ln\left(\tau_{L0}^{-1}\gamma^{1/2}\right)$, (b) ln Z_{obs} *vs.* $\ln\left(\tau_{L\infty}^{-1}\gamma^{1/2}\right)$, of TCNE/TCNE$^{\bullet-}$ in different solvents at room temperature.

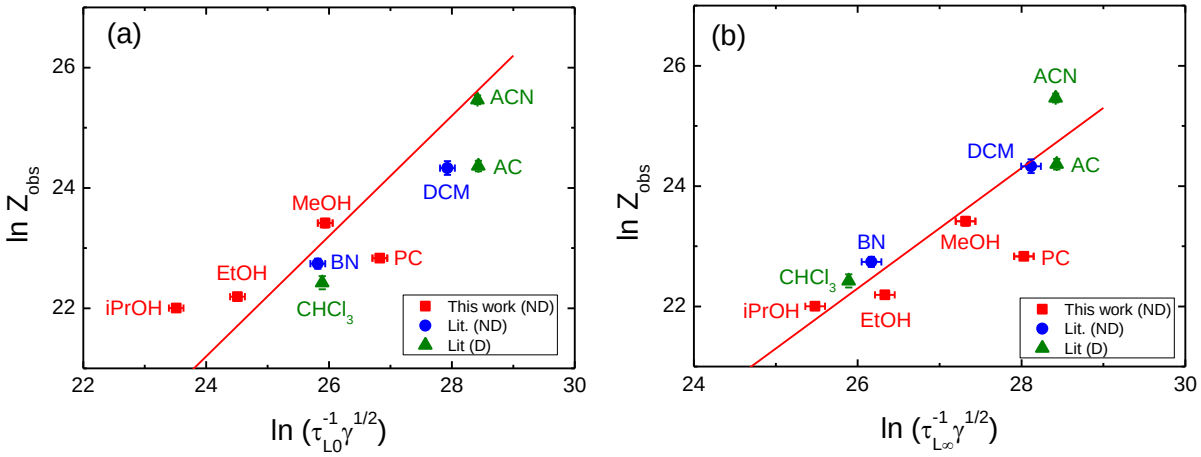

Figure 35. Weaver plots of (a) ln Z_{obs} *vs.* $\ln\left(\tau_{L0}^{-1}\gamma^{1/2}\right)$, (b) ln Z_{obs} *vs.* $\ln\left(\tau_{L\infty}^{-1}\gamma^{1/2}\right)$, of DDQ/DDQ$^{\bullet-}$ in different solvents at room temperature.

Table 5. Viscosities and dielectric parameters of given organic solvents.

Solvent	$\eta^{(a)}$ (cP)	γ	$n_D^{2\,(a)}$	ε_{s1}	ε_{s2}	ε_{s3}	ε_{∞}	τ_1 (ps)	τ_2 (ps)	τ_3 (ps)	$\tau_{L0}^{(b)}$ (ps)	$\tau_{L\infty}^{(c)}$ (ps)
ACN	0.341	0.525	1.806	35.84[62]	-	-	3.51[62]	3.37[62]	-	-	0.33*	-
AC	0.32	0.494	1.846	20.9[4]	-	-	1.9[4]	3.3[4]	-	-	0.316*	-
$CHCl_3$	0.57	0.270	2.091	4.8[4]	-	-	2.22[4]	6.4[4]	-	-	2.98*	-
PhBr	1.13	0.23	2.424	5.45[4]	-	-	2.58[4]	16.4[4]	-	-	7.6*	-
DCM	0.43	0.382	2.019	8.83[63]	3.77[63]	-	2.36[63]	2.17[63]	0.57[63]	-	0.487	0.359
PC	2.76	0.481	2.015	64.97[49]	4.47[49]	-	2.42[49]	43[49]	0.57[49]	-	1.55	0.466
DMF	0.924	0.462	2.046	37.31[64]	4.48[64]	-	3.02[64]	10.4[64]	0.85[64]	-	0.809	0.569
DMA	0.945	0.460	2.061	38.25[64]	3.97[64]	-	2.98[64]	15.8[64]	0.95[64]	-	1.120	0.856
BN	1.24	0.390	2.328	25.17[49]	3.8[49]	-	2.93[49]	34.1[49]	2.61[49]	-	3.83	2.70
FA	3.23	0.469	2.093	109.5[64]	7.08[64]	-	4.48[64]	37.3[64]	1.16[64]	-	1.49	0.862
MeOH	0.584	0.537	1.76	32.5[50]	5.91[50]	4.9[50]	2.79[50]	51.49[50]	7.09[50]	1.12[50]	3.98	1.00
EtOH	1.218	0.50	1.848	24.47[51]	4.53[51]	3.79[51]	2.6[51]	164.9[51]	10.4[51]	1.69[51]	16.0	2.59
iPrOH	2.388	0.476	1.897	19.34[52]	3.66[52]	3.11[52]	2.48[52]	354.6[52]	23.4[52]	2.12[52]	42.4	5.92

* τ_L for Debye-solvents calculated from 2.31, (a) from ref 65, (b) from equation 2.45 and 2.48, (c) from equation 2.47 and 2.49

The literature values for the physical properties of the solvents can differ depending on the source. The numbers given in Table 5 represent what is believed to be the most reliable data. Errors on γ and τ_L were estimated based on reported values of the relevant physical properties[4,65,66,63,67,62] and for γ, an error of 2% was found, whereas for τ_L it was 10%. Note that a non-Debye behaviour has been reported for DCM,[63] but it is more complex than for the other non-Debye solvents mentioned earlier. Therefore only τ_1 can be determined accurately, whereas τ_2 must be estimated.

Apart from the Weaver plots given above, the DDQ/DDQ$^{\bullet-}$ system has also been treated using a different model. This was done because the reactions of DDQ/DDQ$^{\bullet-}$ have been reported as weakly diabatic with α = 0.85[68] which is corresponding to equation 3.1. Therefore, Weaver plots taking this α into account have been compared with the ones in figure 35, and are shown in figure 36.

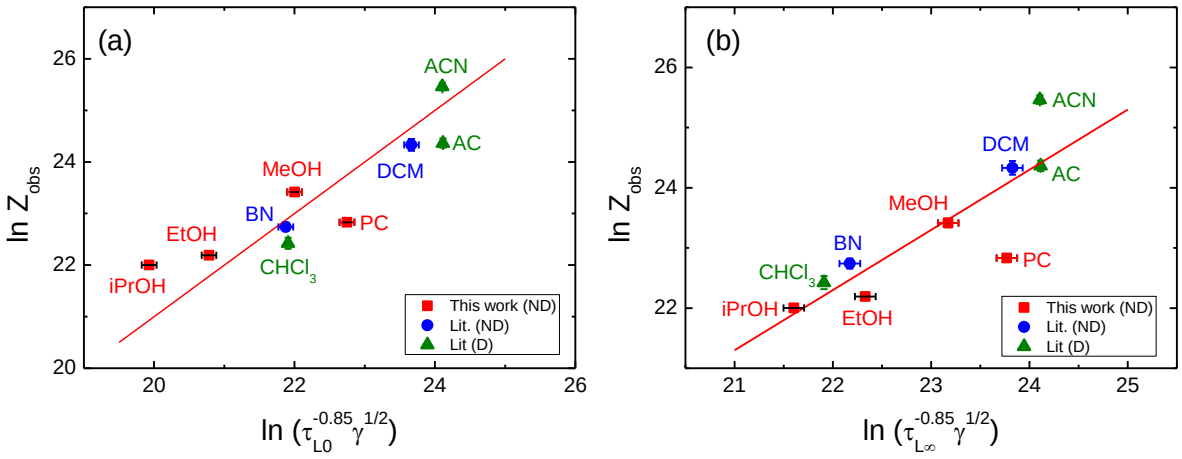

Figure 36. Weaver plots of (a) ln Z_{obs} *vs.* $\ln\left(\tau_{L0}^{-0.85}\gamma^{1/2}\right)$, (b) ln Z_{obs} *vs.* $\ln\left(\tau_{L\infty}^{-0.85}\gamma^{1/2}\right)$, of DDQ/DDQ$^{\bullet-}$ in different solvents at room temperature.

Considering all Weaver plots given above, there seems to be no difference between the Debye and non-Debye solvents. For the TCNE/TCNE$^{\bullet-}$ systems, due to the instability of the reactions in DMF and DMA as just described, their results have not been included in the plots in figure 34. All data points using $\tau_{L\infty}$ give a better fit to the slope of unity than those of τ_{L0}. A similar behaviour is seen for DDQ/DDQ$^{\bullet-}$ in figure 35, with the results on the basis of $\tau_{L\infty}$ being more promising than those of the τ_{L0}. Note that data points

from the reactions in FA and DMA place far from the other systems, which is possibly caused by an instability of the reactions, and therefore they have been omitted for all cases of DDQ/DDQ$^{\bullet-}$. Considering the system of DDQ/DDQ$^{\bullet-}$ corresponding to the weakly diabatic behaviour with α = 0.85 (figure 36), the data points for each plot fit the line with the slope of one even better than those of the completely adiabatic reaction, and also here, the best result is obtained from those of $\tau_{L\infty}$.

As seen, in all cases, the plots using the limiting values of $\tau_{L\infty}$ give better fitting results with those in the literature compared with τ_{L0}. This observation is in good agreement with previous observations by Fawcett and Foss.[69] These authors investigated the electrode reduction of the cobaltocenium cation as well as the oxidation of p-phenylenediamine, in non-Debye solvents, and noticed a better correlation when τ_L is estimated on the basis of the high-frequency value $\tau_{L\infty}$.

Due to the adiabatic reaction behaviour controlled by τ_L, plots of the dependence of ln $(k_{et}\tau_{L0}\gamma^{-1/2})$ and ln $(k_{et}\tau_{L\infty}\gamma^{-1/2})$ on the solvent parameter $\gamma = \left(\frac{1}{n^2} - \frac{1}{\varepsilon_s}\right)$ have been made, as shown as figure 37 for TCNE/TCNE$^{\bullet-}$. The plots for DDQ/DDQ$^{\bullet-}$ are presented using two values of α like above, i.e. as ln $(k_{et}\tau_L\gamma^{-1/2})$ *vs* γ and ln $(k_{et}\tau_L^{0.85}\gamma^{-1/2})$ *vs* γ. The former is illustrated in figure 38, the latter in figure 39.

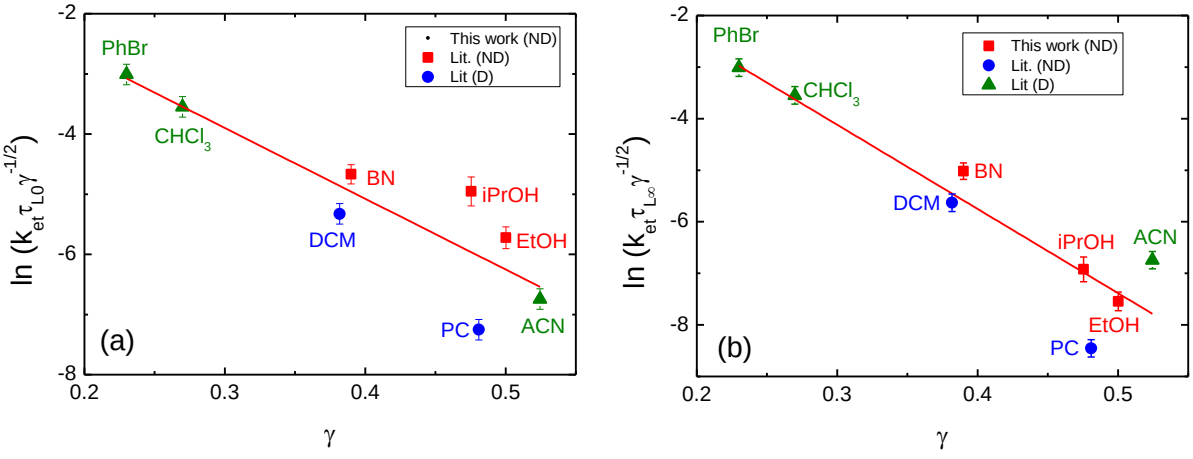

Figure 37. The dependence of (a) ln$\left(k_{et}\tau_{L0}\gamma^{-1/2}\right)$, (b) ln$\left(k_{et}\tau_{L\infty}\gamma^{-1/2}\right)$, on the solvent parameter γ of TCNE/TCNE$^{\bullet-}$ in different solvents at room temperature.

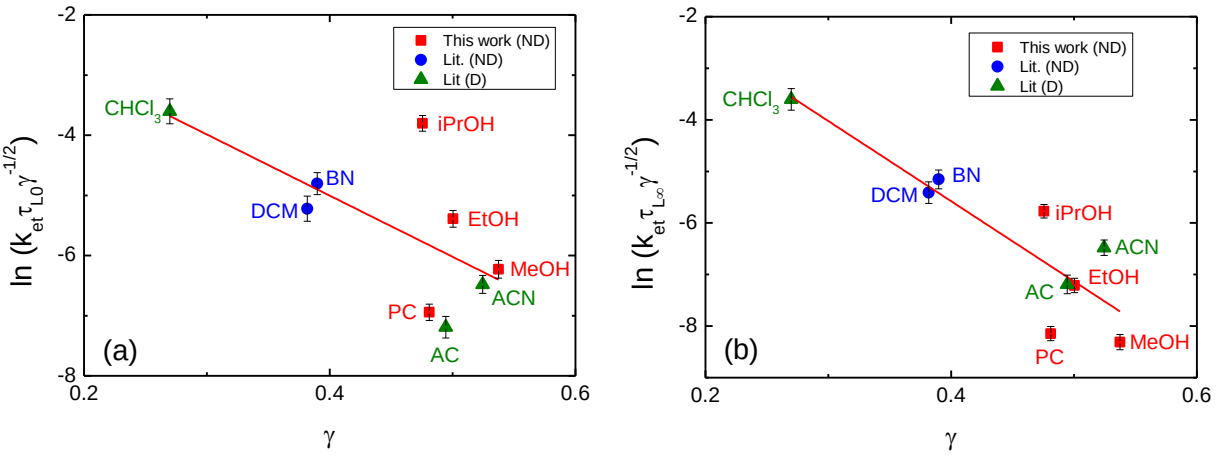

Figure 38. The dependence of (a) . $\ln\left(k_{et}\tau_{L0}\gamma^{-1/2}\right)$, (b) $\ln\left(k_{et}\tau_{L\infty}\gamma^{-1/2}\right)$, on the solvent parameter γ of $DDQ^{\bullet-}$/DDQ in different solvents at room temperature.

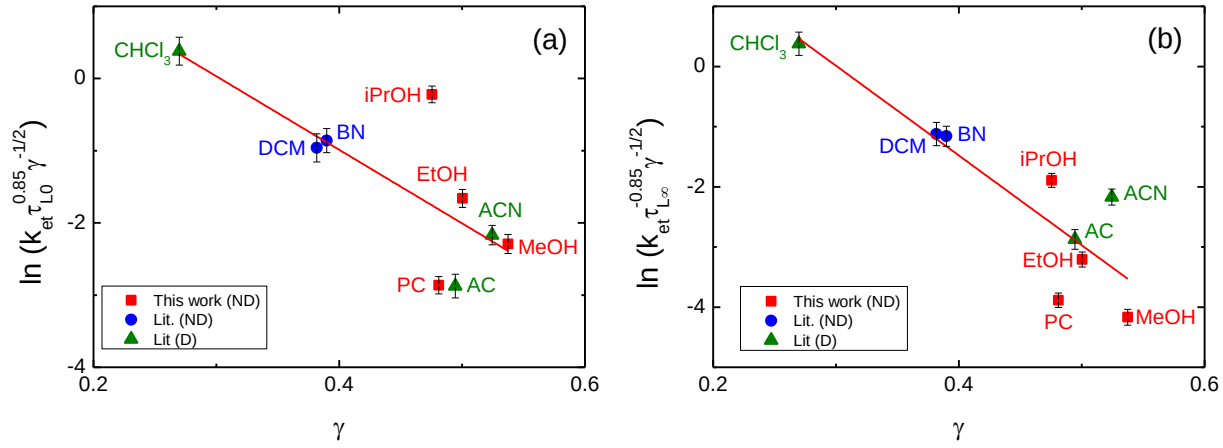

Figure 39. The dependence of (a) $\mathbf{\ln\left(k_{et}\tau_{L0}^{0.85}\gamma^{-1/2}\right)}$, (b) $\mathbf{\ln\left(k_{et}\tau_{L\infty}^{0.85}\gamma^{-1/2}\right)}$, on the solvent parameter γ of DDQ/$DDQ^{\bullet-}$ in different solvents at room temperature.

From the plots in figures 37, 38 and 39, it is seen that the results of this work based on $\tau_{L\infty}$ fit the literature data better than those using τ_{L0}, which is in accordance with the results from the Weaver plot described above. The slopes of the calculated regression lines provide the value of $g(r,d')_{exp}$, and, in turn, the value of d'_{exp} if the r_e of molecule is known.

For TCNE/$TCNE^{\bullet-}$, this results in the values of $g(r,d')_{exp}$, listed in table 6. The values of $g(r,d')_{exp}$ based on τ_{L0} and $\tau_{L\infty}$ are equal to 8.39×10^8 m^{-1} and 11.6×10^8 m^{-1}, which are in good agreement with $g(r,d')_{exp} = 9.6 \times 10^8$ m^{-1} reported by Grampp et al.[4] By using the radius 3.10 Å[4] of a TCNE molecule with the values of $g(r,d')_{exp}$ mentioned above,

the d'_{exp} are found to be 4.19 Å and 4.85 Å for the results based on τ_{L0} and $\tau_{L\infty}$, which are both still close to the 4.44 Å obtained from the literature.[4]

Table 6. The values of the slopes obtained from the plots in figure 37, and their consequent values of $g(r,d')$ and $d'_{exp.}$

$TCNE^{\bullet-}$/TCNE	**$\ln(k_{et}\tau_{L0}\gamma^{-1/2})$ vs γ**	**$\ln(k_{et}\tau_{L\infty}\gamma^{-1/2})$ vs γ**
Slope	-11.76	-16.33
r_e / (Å)[(a)]	3.10	3.10
$g(r,d')$ / (10^8 m^{-1})[(b)]	8.39	11.6
d'_{exp} / (Å)[c)]	4.19	4.85

* (a) from ref 4, (b) from equation 2.39, (c) from equation 2.25

For $DDQ/DDQ^{\bullet-}$, the reported value of $g(r,d')_{exp}$ is equal to 10.0×10^8 m^{-1},[11] which is almost identical with the $g(r,d') = 10.6 \times 10^8$ m^{-1} (table 7) of the result based on $\tau_{L\infty}^{0.85}$ as shown in figure 39b. For comparison, the result based on $\tau_{L\infty}$ as shown in figure 38b, provides $g(r,d') = 11.1 \times 10^8$ m^{-1} which is still close to those two values. The radius of a DDQ molecule of 2.3 Å was used to determine d'_{exp} for each approach, which are listed in table 7. The d'_{exp} investigated from the plots in figure 38b and 39b are equal to 3.09 Å and 3.05 Å, which are very close to d'_{exp} = 2.9 Å determined from the literature.[60]

Table 7. The values of the slopes obtained from the plots in figure 38 and 39, and their consequent values of $g(r,d')$and $d'_{exp.}$

$DDQ/DDQ^{\bullet-}$	**$\ln(k_{et}\tau_{L0}\gamma^{-1/2})$ vs γ**	**$\ln(k_{et}\tau_{L\infty}\gamma^{-1/2})$ vs γ**
Slope	-10.17	-15.55
r_e / (Å)[(a)]	2.3	2.3
$g(r,d')$ / (10^8 m^{-1})[(b)]	7.25	11.1
d'_{exp} / (Å)[c)]	2.76	3.09
$DDQ/DDQ^{\bullet-}$	**$\ln(k_{et}\tau_{L0}^{0.85}\gamma^{-1/2})$ vs γ**	**$\ln(k_{et}\tau_{L\infty}^{0.85}\gamma^{-1/2})$ vs γ**
Slope	-10.19	-14.92
r_e / (Å)[(a)]	2.3	2.3
$g(r,d')$ / (10^8 m^{-1})[(b)]	7.15	10.6
d'_{exp} / (Å)[c)]	2.75	3.05

* (a) calculated from ref 60 (b) from equation 2.39, (c) from equation 2.25

In summary, the results obtained from Weaver plots and those of ln ($k_{et}\tau_L\gamma^{-1/2}$) *vs.* γ for $TCNE^{\bullet-}$/TCNE and DDQ/$DDQ^{\bullet-}$ in non-Debye solvents show that their reactions are described most favourably by the relaxation process under the limit of high frequency, $\tau_{L\infty}$. For the DDQ/$DDQ^{\bullet-}$ system, the best results were obtained assuming a weakly diabatic reaction with $\alpha = 0.85$.

Due to the suspicious results obtained from the reactions of TCNE/$TCNE^{\bullet-}$ in DMF and DMA, and DDQ/$DDQ^{\bullet-}$ in DMA and FA, their stability problems are not clear and thus they were omitted from the explanation of the behaviour of the non-Debye solvents on the electron transfer reactions. However, when included, the results from these solvents show an interesting behaviour, much like that reported for several ethereal solvents in the case of TCNE/$TCNE^{\bullet-}$.[4] As seen in figure 40, data points obtained from the solvents DMA and, particularly, DMF for TCNE/$TCNE^{\bullet-}$ fit with those of the ethereal solvents and seem to fall on a second line with a slope of unity. Furthermore, the reactions in PC tend to fit better with this second line than with the first one including the other solvents, as described earlier.

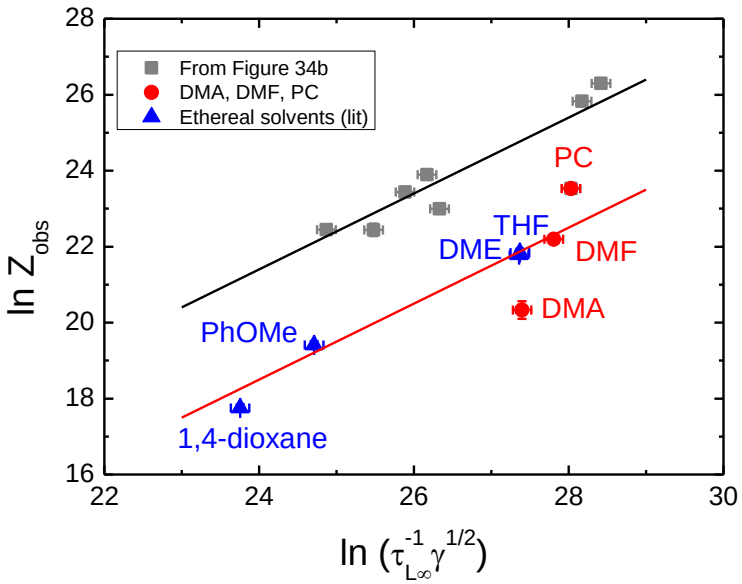

Figure 40. Weaver plot of ln Z_{obs} *vs.* $\ln(\tau_{L\infty}\gamma^{1/2})$ of TCNE/$TCNE^{\bullet-}$ in different solvents at room temperature showing two lines with slope of unity. Literature data is from ref 4.

For the reactions of DDQ/$DDQ^{\bullet-}$, as shown in figure 41, the results from the solvents DMA, PC and FA seem to also generate this second line with the slope of one.

Unfortunately, there is no reported data of DDQ/DDQ$^{\bullet-}$ in the ethereal solvents available to compare with those of the three non-Debye solvents. It may be possible that there is a connection based on the relaxation behaviours characteristic for these solvents, nevertheless, enough information from more experiments would be needed to give any real conclusions.

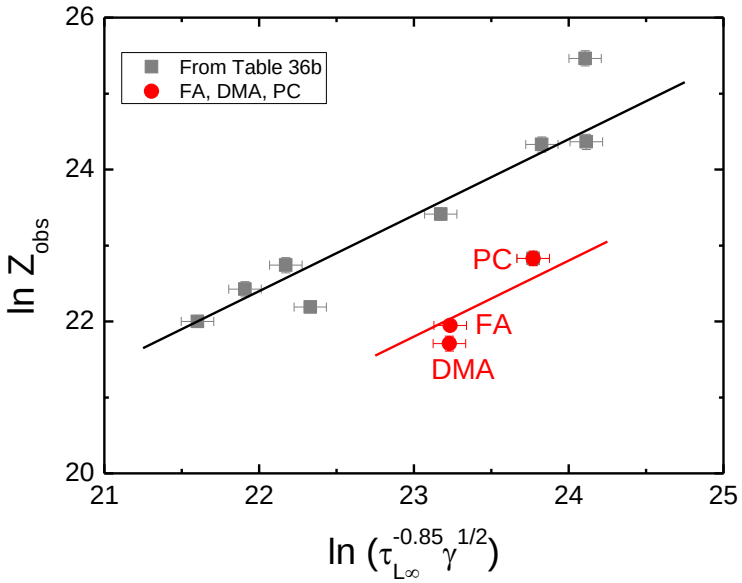

Figure 41. Weaver plot of ln Z_{obs} *vs.* $\ln(\tau_{L\infty}\gamma^{1/2})$ of DDQ/DDQ$^{\bullet-}$ in different solvents at room temperature showing two lines with slope of unity.

6 Results and Discussion: The $Th^{\bullet+}$/Th and $MTh^{\bullet+}$/MTh Couples

The question of whether the large structural difference between thianthrene radical cations and their neutral parent molecules affects their electron transfer reactions, can be investigated by determining the rate constants of thianthrene redox couples in organic solvents. However, since solvent dynamics can also have a large influence on the electron transfer rate constant, this therefore needs to be probed first to properly distinguish between the two effects. Electron transfer reactions have been studied using ESR line broadening experiments at room temperature[17] as well as at various temperatures and these experiments will be a tool to answer the question about the geometric changes. All results from the experiments shall be revealed and discussed below.

6.1 Structural Calculations

Unlike for TCNE and DDQ, information about the structure of the two thianthrenes and the corresponding reorganization energies needed to be determined. Furthermore, due to the geometric differences between the radicals and the neutral molecules, the usual assumption that the two can be represented by the same effective radius is not valid. Thus, the radii of the thianthrenes and their radical cations have been calculated using an ellipsoid model with the mean elliptical radius, $\bar{r}$, as described in equation 2.26. Their semiaxes and r_e were determined and are presented in table 8.

The calculated reaction distances, d'_{calc} estimated from equation 2.27 are 6.9 Å and 8.6 Å for $Th^{\bullet+}$/Th and $MTh^{\bullet+}$/MTh, respectively. The latter couple has larger d'_{calc} because of the bulky $-OCH_3$ groups. Note that using the semiaxes obtained from the individual and the average values of neutral and radical molecules give only very slight differences in d' values. Finally, the outer-sphere reorganization energies, λ_o calculated from the average semiaxes are $151\times\gamma$ kJ mol^{-1} and $120\times\gamma$ kJ mol^{-1} for the $Th^{\bullet+}$/Th and $MTh^{\bullet+}$/MTh systems, respectively.

The inner-sphere reorganization energies, λ_i, have been estimated using the Nelsen Method, as mentioned earlier in the section 2.3.1 From this method, performed with density functional theory (B3LYP/TZVP) using the ORCA package, and taking into account quantum mechanical tunnelling,[20,70,71] λ_i = 36.3 kJ mol^{-1} and 34.8 kJ mol^{-1} for Th$^{\bullet+}$ and MTh$^{\bullet+}$ at 293 K, is obtained. These values are significantly larger than those reported by Heinze[56] with λ_i = 3.9 kJ mol^{-1} for Th$^{\bullet+}$ and 4.6 kJ mol^{-1} for MTh$^{\bullet+}$, using less sophisticated calculations. However, the calculated ionization potentials agree very well with values from more recent reports.[14]

Table 8. The semiaxes and the mean elliptical radius, r_e of thianthrene radical cations and their neutral molecules.

Molecule	Semiaxes* / Å			r_e** / Å
	a	***b***	***c***	
Th	6.15	3.66	2.71	4.12
Th$^{\bullet+}$	6.00	3.76	1.81	3.78
MTh	7.66	4.16	3.24	4.94
MTh$^{\bullet+}$	7.60	4.91	2.52	4.92

*estimated using the ellipsoid model. ** from equation 2.26

6.2 Electron Self-Exchange at Room Temperature

6.2.1 ESR Measurements

ESR spectra of Th$^{\bullet+}$/Th and MTh$^{\bullet+}$/MTh in organic solvents measured on the Varian ESR spectrometer at room temperature are shown in figures 43 and 44, together with their simulations. For Th$^{\bullet+}$ the no-exchange spectra contain five ESR-lines corresponding to 4 hydrogens (figure 42a) with a hfs constant of 1.09-1.27 G and line widths of 0.34-0.46 G. The no-exchange spectra of MTh$^{\bullet+}$ show a more complicated pattern of lines due to the overlap between the splittings from the 4 ring hydrogens and

the 12 hydrogens of the $–OCH_3$ groups (figure 42b) with hfs constants a(4H) = 0.261-0.229 G and a(12H) = 0.47-0.48 G, as well as line widths of 0.16-0.20 G.

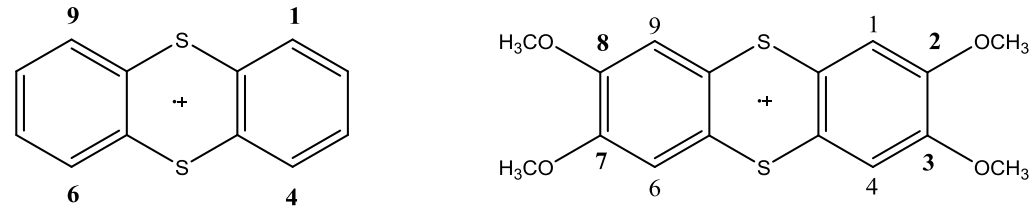

(a) **(b)**

Figure 42. Structures of the radical cations of (a) thianthrene ($Th^{\bullet+}$), (b) 2,3,7,8-tetramethoxythianthrene ($MTh^{\bullet+}$), with numbering hydrogen atoms shown in the ESR spectrum.

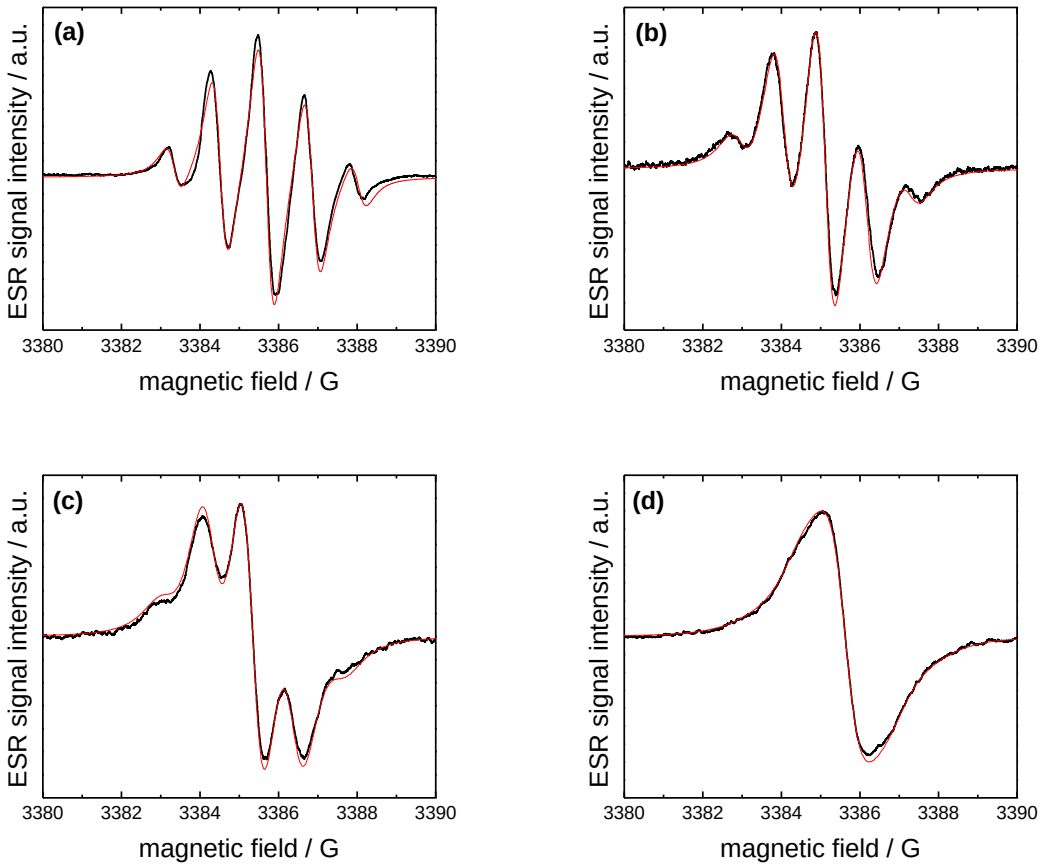

Figure 43. ESR spectra of $Th^{\bullet+}$/Th in DCB at room temperature. [$Th^{\bullet+}$] is kept as 1×10^{-4} M; (a) [Th] = 0 mM, (b) [Th] = 5×10^{-3} M, (c) [Th] = 8×10^{-3} M, (d) [Th] = 1.8×10^{-2} M.

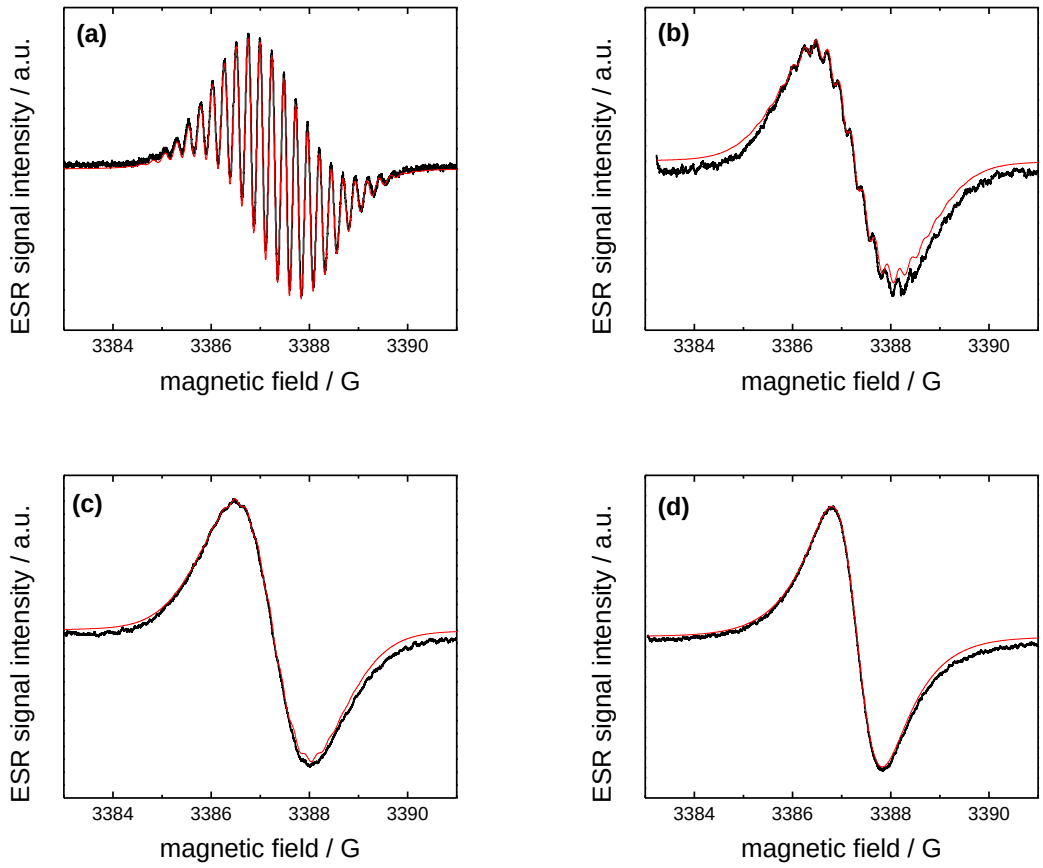

Figure 44. ESR spectra of $MTh^{\bullet+}$/MTh in ACN at room temperature. [$MTh^{\bullet+}$] is kept as 1×10^{-4} M; (a) [MTh] = 0 mM, (b) [MTh] = 1×10^{-3} M, (c) [MTh] = 2×10^{-3} M, (d) [MTh] = 1×10^{-2} M.

6.2.2 ESR Line Broadening

The observed rate constants, k_{obs}, were obtained from ESR line broadening experiments (figures 45 and 46) and these values compare well with those reported by Lu et al.[72] of $3.4\pm0.5 \times 10^9$ $M^{-1}s^{-1}$ (ESR, slow-exchange) and $3.5\pm0.5 \times 10^9$ $M^{-1}s^{-1}$ (NMR), respectively, for the solvent mixture dichloromethane–trifluoroacetic acid (5%). k_{obs} for the $Th^{\bullet+}$/Th and $MTh^{\bullet+}$/MTh redox couples in different solvents are listed in table 9, together with k_d and k_{et}.

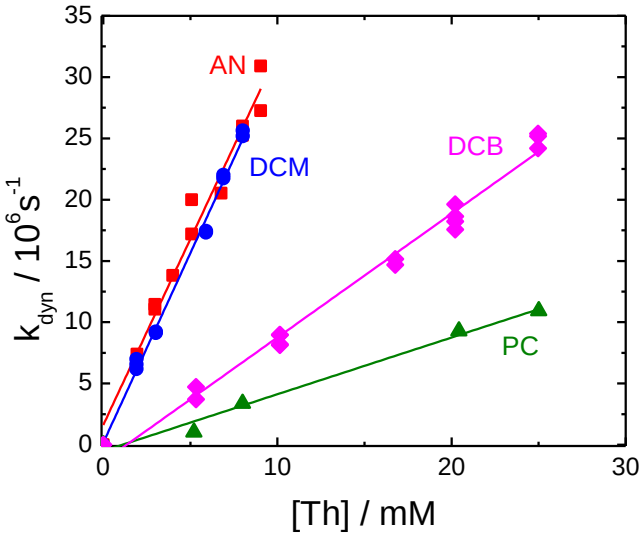

Figure 45. Concentration dependence of the exchange rate of the reaction, k_{dyn}, for $Th^{\bullet+}/Th$ in different solvents (results obtained from the Varian ESR spectrometer).

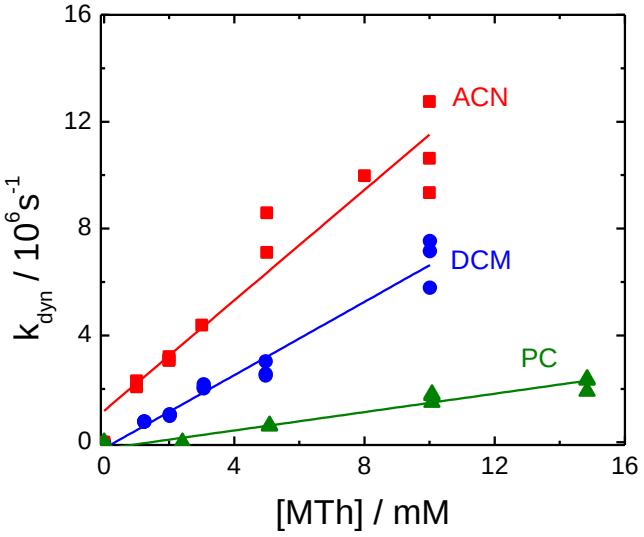

Figure 46. Concentration dependence of the exchange rate of the reaction, k_{dyn}, for $Th^{\bullet+}/Th$ in different solvents (results obtained from the Varian ESR spectrometer).

Table 9. Rate constants of $Th^{\bullet+}$/Th and $MTh^{\bullet+}$/MTh in organic solvents at room temperature (results obtained from the Varian ESR spectrometer).

Solvent	k_d[(a)] (10^8 $M^{-1}s^{-1}$)	k_{obs} (10^8 $M^{-1}s^{-1}$)		k_{et}[(b)] (10^8 $M^{-1}s^{-1}$)	
		$Th^{\bullet+}$/Th	**$MTh^{\bullet+}$/MTh**	**$Th^{\bullet+}$/Th**	**$MTh^{\bullet+}$/MTh**
ACN	191	30±1	10.3±0.7	44±2	11.6±0.8
DCM	151	30.8±0.7	6.9±0.3	52±1	7.5±0.4
PC	23.6	4.5±0.1	1.8±0.1	7.2±0.2	2.0±0.1
DCB	49.2	10.1±0.3	-	17.2±0.5	-

(a) from equation 2.8, (b) from equation 2.15

If the large structural changes of the reactants play a role in the electron transfer reaction, the values of k_{et} are assumed to be relatively small. However, the experiments provide larger k_{et} -values than expected. A comparison between k_{et} of $Th^{\bullet+}$/Th and other organic self-exchange systems show that the rate constants are very similar. For example, TCNE/$TCNE^{\bullet-}$ gives $k_{et} = 22.8 \times 10^8$ M^{-1} s^{-1}, 44.0×10^8 M^{-1} s^{-1} and 2.8×10^8 M^{-1} s^{-1} in ACN, DCM and PC, at 293 K respectively. Also, the values are comparable with the systems presented earlier, which were investigated in various organic solvents, i.e. k_{et} are in the range of $1.2 \times 10^8 – 15.3 \times 10^8$ M^{-1} s^{-1} for TCNE/$TCNE^{\bullet-}$, and $1.8 \times 10^8 – 4.32 \times 10^8$ M^{-1} s^{-1} for DDQ/$DDQ^{\bullet-}$. This suggests that at room temperature the large structural change plays a smaller role than predicted.

6.2.3 Solvent Dynamic Effects

For the $Th^{\bullet+}$/Th and $MTh^{\bullet+}$/MTh systems, an investigation of the solvent dynamic effects based on τ_L has been performed. The Debye solvents ACN and DCB were always treated using τ_{L1}, whereas the value of τ_{L1} was estimated for DCM using the dielectric parameters of the first relaxation time. The small number of non-Debye solvents used does not allow a comparison like the one done above, but it is still possible to examine the correlations with τ_{L0}, $\tau_{L\infty}$ and τ_{L1} for PC. This has been done differently than with the systems of TCNE/$TCNE^{\bullet-}$ and DDQ/$DDQ^{\bullet-}$, where τ_{L1} was not included for PC as it is here.

Table 10. Calculated activation energies ΔG^*_{cal} and the observed pre-exponential factors ln Z_{obs} (results obtained from the Varian ESR spectrometer).

	$Th^{\bullet+}/Th$		$MTh^{\bullet+}/MTh$	
solvent	ΔG^*_{cal} [(a)] (kJ mol^{-1})	ln Z_{obs} [(b)]	ΔG^*_{cal} [(a)] (kJ mol^{-1})	ln Z_{obs} [(b)]
ACN	28.83	34.1	24.43	30.9
DCM	23.30	31.9	20.03	28.7
PC	27.18	31.5	23.11	28.6
DCB	21.08	29.9	-	-

(a) from equation 2.19, (b) from equation 2.34

Values of ln Z_{obs} were determined via ΔG^*_{cal}, which were calculated using the parameters described in section 2.5, and are shown in table 10. Furthermore, the corresponding parameters of solvent properties are listed in table 11.

Table 11. Viscosity and the dielectric parameters of given organic solvents at room temperature.

Solvent	η [(a)] (cP)	γ	n_D^2 [(b)]	ε_{s1}	ε_{s2}	ε_∞	τ_1 (ps)	τ_2 (ps)	τ_L (ps)
ACN	0.341	0.525	1.806	35.84[62]	-	3.51[62]	3.37[62]	-	0.33
DCM	0.43	0.382	2.019	8.83[63]	3.77[63]	2.36[63]	2.17[63]	-	0.98
PC	2.76	0.481	2.015	64.97[49]	4.47[49]	2.42[49]	43[49]	0.57[49]	2.96
DCB	1.324	0.319	2.399	9.93[66]	-	2.34[(c)]	24.8[67]	-	5.84

(a) and (b) from ref 65. (c) No published data; using the approximation $n_D^2 = \varepsilon_\infty$

The plots of ln Z_{obs} vs. ln($\tau_L^{-1}\gamma^{1/2}$) for both thianthrene redox couples are shown in figure 47 which clearly indicates that a solvent dynamic effect controlled by τ_L of the solvents is, in fact, present. The lines using τ_{L1} and τ_{L0} for PC seem to fit well with those of the other solvents. However, linear regression, done like above, shows that the slope of the plot including the former is slightly closer to unity than that which includes the latter. The worst fit is seen in the case of $\tau_{L\infty}$ for PC, which is opposite to the results from the TCNE/TCNE$^{\bullet-}$ and DDQ/DDQ$^{\bullet-}$. This may indicate that the cation systems behave

differently than the anion systems and therefore they may need a different τ_L for the process.

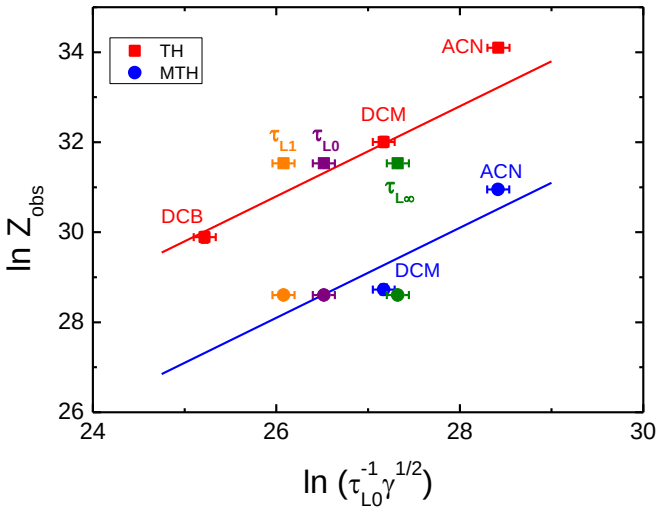

Figure 47. Weaver plot of ln Z_{obs} *vs.* $\ln(\tau_L^{-1}\gamma^{1/2})$, using different τ_{L1}, $\tau_{L\infty}$ and τ_{L0} for the Solvent PC, of $Th^{\bullet+}$/Th and $MTh^{\bullet+}$/MTh in organic solvents at room temperature (results obtained from the Varian ESR spectrometer).

According to the adiabatic solvent dynamical reaction behaviour found above, a plot of ln (k_{et} τ_L $\gamma^{-1/2}$) *vs.* γ for both $Th^{\bullet+}$/Th and $MTh^{\bullet+}$/MTh should provide a straight line as shown in Figure 48. The results using τ_{L0} provide an adequate regression line for further analysis, but as can be seen, those using τ_{L1} produce a significantly better line. The case of $\tau_{L\infty}$ differs from the others, behaving much worse like in the Weaver plot given above. Based on the combined results obtained from figures 47 and 48, it appears that τ_{L1} is the relaxation time which best describes the solvent effect on the systems of the thianthrene redox couples.

Experimental reaction distances, d'_{exp}, determined from the slopes of the regression lines corresponding the τ_{L1} for PC were found to be 5.5 Å and 6.0 Å for $Th^{\bullet+}$/Th and $MTh^{\bullet+}$/MTh, respectively. The large difference between these values and d'_{calc} mentioned above (6.9 Å for $Th^{\bullet+}$/Th and 8.6 Å $MTh^{\bullet+}$/MTh) can be explained by the observation that the ellipsoid model used is not the perfect method for calculation of r_e of complex molecules, especially when these are planar. The difference between d'_{exp}

and d'_{calc} of $MTh^{\bullet+}$/MTh is larger than that of $Th^{\bullet+}$/Th. The bulky $-OCH_3$ groups of $MTh^{\bullet+}$/MTh are the reason that the calculations from the ellipsoid model overestimates d' by more. In contrast, the inter-planar distance of parallel and crossed dimers $(Th_2)^{2+}$ of two radical cations have been calculated using quantum-chemical methods and were reported as 3.00 Å and 3.79 Å, respectively.[14] The crystal structure of trimeric stacks of $(Th)_3^{2+}$, consisting of a central planar Th molecule and two peripheral $Th^{\bullet+}$ with dihedral angles of 164.11°, has been published.[16] The average length of S···S contacts between the three molecules is 0.1 Å larger than found in the dimer $(Th)_2^{2+}$. However, the systems in this work consist of both the radical cations and their neutral molecules. Hence, d'_{exp} of the thianthrene couples should be larger than the values from the literature mentioned above. Possibly, the sum of the shortest semiaxes, c, of the ellipsoids representing the radical cation and the neutral molecule, gives a better estimate of d' than the sum of the r_e's. This quantity illustrates the closest contact between two stacked molecules and for $Th^{\bullet+}$/Th it becomes 4.5 Å, whereas it is 5.8 Å for $MTh^{\bullet+}$/MTh. The reaction distance from the sum of corresponding c-semiaxes is closer to d'_{exp} than to d'_{calc} for both couples. As seen, these calculated values are significantly closer to the experimental ones. This suggests that the two molecules in the precursor complex are, in fact facing each other plane to plane. Nevertheless, the information is not sufficient to decide whether they are parallel or crossed, although the evidence hints towards the latter

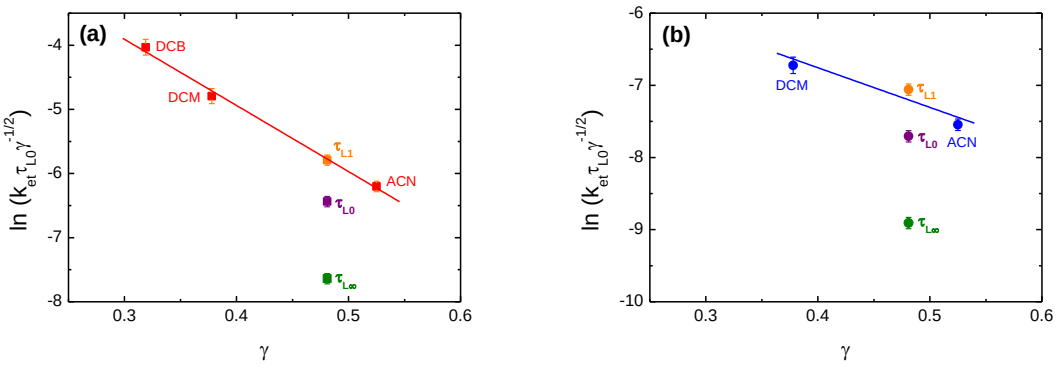

Figure 48. The dependence of ln ($k_{et}\tau_L\gamma^{1/2}$), using different τ_{L1}, $\tau_{L\infty}$ and τ_{L0} for the solvent PC, on the solvent parameter $\gamma = \left(\frac{1}{n^2} - \frac{1}{\varepsilon_s}\right)$ of (a) $Th^{\bullet+}$/Th and (b) $MTh^{\bullet+}$/MTh in different solvents at room temperature (results obtained from the Varian ESR spectrometer).

The term of $(\lambda_o/\gamma)_{exp}$ obtained from the slope of lines in figure 48 are 101 kJ mol^{-1} and 50.5 kJ mol^{-1} for $Th^{\bullet+}$/Th and $MTh^{\bullet+}$/MTh, respectively. The larger value of $(\lambda_o/\gamma)_{exp}$ in $Th^{\bullet+}$/Th corresponds to the smaller r_e and d' of the radical and its parent molecule. Determination of the experimental inner-sphere reorganization energy, λ_i will be possible when the experimental activation energy is known, which shall be described later in the part dealing with the temperature dependent measurements.

6.3 Temperature Dependent Experiments

The results obtained from ESR line broadening of thianthrene redox couples at room temperature, described above, reveal a solvent dynamic effect strongly controlled by the longitudinal relaxation time, τ_L of the solvents. Since the role of the structural change between the redox couples are one of the aim for this study, therefore, the observed activation energy need to be investigated, i.e. temperature dependent experiments are required. The factors controlling the solvent dynamics must be taken into account in the Arrhenius plot in order to investigate the activation energy more precisely, which should provide a better idea of how much the changes in the structure of the reactants affects the reaction.

In order to perform the temperature dependence experiments, the solutions were measured using the Bruker ESR spectrometer, and this obviously generated a second set of data at room temperature. Before the results from the temperature dependence experiments are discussed, that of the 293 K shall be compared with the previous results recorded by the Varian ESR spectrometer.

6.3.1 Measurements on the Bruker ESR Spectrometer at 293 K

The k_{et} values obtained from the Bruker spectrometer are significantly larger than those from the Varian for all systems of thianthrene couples, as can be seen in tables 9 and 12 for $Th^{\bullet+}$/Th and $MTh^{\bullet+}$/MTh, respectively. This may be explained by the observation that the Varian setup possibly has problems with air bubbles in the flow-through system and that the temperature was not controlled unlike on the Bruker which was set to record at 293 K.

Table 12. The rate constants for $Th^{\bullet+}$/Th and $MTh^{\bullet+}$/MTh in different solvents at 293 K (results obtained from the Bruker ESR spectrometer).

Solvent	k_d[a] (10^8 $M^{-1}s^{-1}$)	k_{obs} (10^8 $M^{-1}s^{-1}$)		k_{et}[b] (10^8 $M^{-1}s^{-1}$)	
		$Th^{\bullet+}$/Th	**$MTh^{\bullet+}$/MTh**	**$Th^{\bullet+}$/Th**	**$MTh^{\bullet+}$/MTh**
ACN	191	41±1	20.0±0.6	72±2	25.2±0.8
DCM	151	37±2	9.5±0.6	71±5	10.9±0.7
PC	23.6	5.5±0.2	2.42±0.07	10.1±0.3	3.05±0.09
DCB	49.2	9.0±0.7	-	14±1	-

(a) from equation 2.8, (b) from equation 2.15

The solvent dynamic effect for the systems measured with the Bruker spectrometer have been investigated using the same approach as that of the Varian ESR spectrometer. The plots of ln Z_{obs} *vs* $\ln(\tau_L^{-1}\gamma^{1/2})$ for $Th^{\bullet+}$/Th and $MTh^{\bullet+}$/MTh are provided in figure 49. As above, the slope of unity of the lines based on the τ_{L1}, τ_{L0}, and $\tau_{L\infty}$, together with the regression line in figure 50, confirms the dominance of τ_{L1} on these systems. Therefore, the thianthrene systems will be analysed base on the τ_{L1} for the remaining analysis of temperature dependent data.

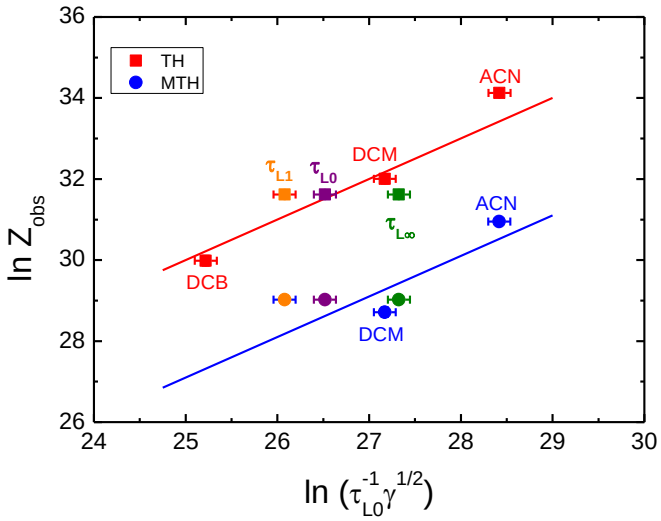

Figure 49. Weaver plot of ln Z_{obs} *vs.* $\ln(\tau_L^{-1}\gamma^{1/2})$, using different τ_{L1}, $\tau_{L\infty}$ and τ_{L0} for the solvent PC, of $Th^{\bullet+}$/Th (red line) and $MTh^{\bullet+}$/MTh (blue line) in organic solvents at 293 K (results obtained from the Bruker ESR spectrometer).

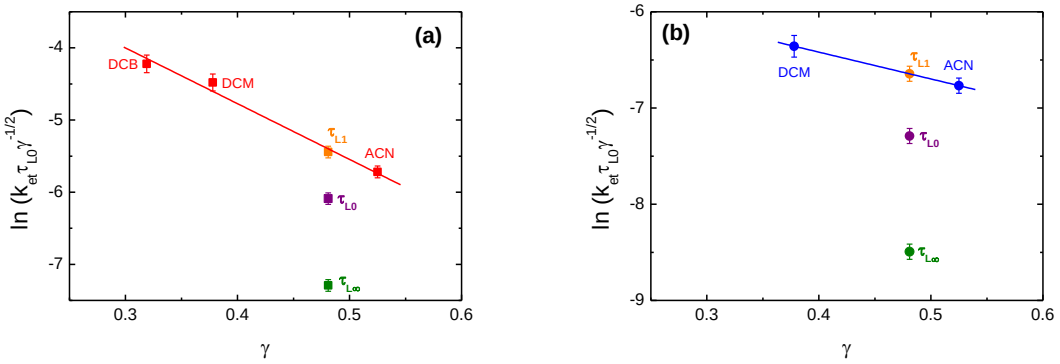

Figure 50. The dependence of ln ($k_{et}\tau_L\gamma^{-1/2}$), using different τ_{L1}, $\tau_{L\infty}$ and τ_{L0} for the solvent PC, on the solvent parameter γ of (a) $Th^{\bullet+}$/Th and (b) $MTh^{\bullet+}$/MTh in different solvents at room temperature (results obtained from the Bruker ESR spectrometer).

The values of d'_{exp} for both couples were determined from plots of ln ($k_{et}\ \tau_L\ \gamma^{-1/2}$) *vs.* γ, and were found to be 5.0 Å for $Th^{\bullet+}$/Th, and 5.6 Å for $MTh^{\bullet+}$/MTh, as shown in figure 50. The d'_{exp} value of $Th^{\bullet+}$/Th is even closer to the reported values described earlier, and the values of both couples are also nearer to the closest contact between two stacked molecules of the radical cations and their parent molecules, which was just mentioned above.

The values of $(\lambda_o/\gamma)_{exp}$ obtained from the Bruker at 293 K were determined as 74.7 kJ mol^{-1} and 27.2 kJ mol^{-1} for $Th^{\bullet+}$/Th and $MTh^{\bullet+}$/MTh, respectively, which are smaller than that from the Varian (101 kJ mol^{-1} for $Th^{\bullet+}$/Th and 50.5 Å kJ mol^{-1} $MTh^{\bullet+}$/MTh). This can be explained by the observation that the larger k_{et} corresponding to the Bruker leads to smaller slopes, meaning the smaller $(\lambda_o/\gamma)_{exp}$.

6.3.2 Temperature Dependent ESR Measurements

The reactions have been measured with the Bruker ESR spectrometer at various temperatures in the range of 213-333 K, depending on the melting and boiling points of the solvents, and also on the stability of the radicals under conditions of low and high temperatures in different solvents. The system of $Th^{\bullet+}$/Th in ACN illustrates the ESR spectra and their line broadening at different temperatures, as seen in figure 51, whereas figure 52 shows that of $MTh^{\bullet+}$/MTh in DCM.

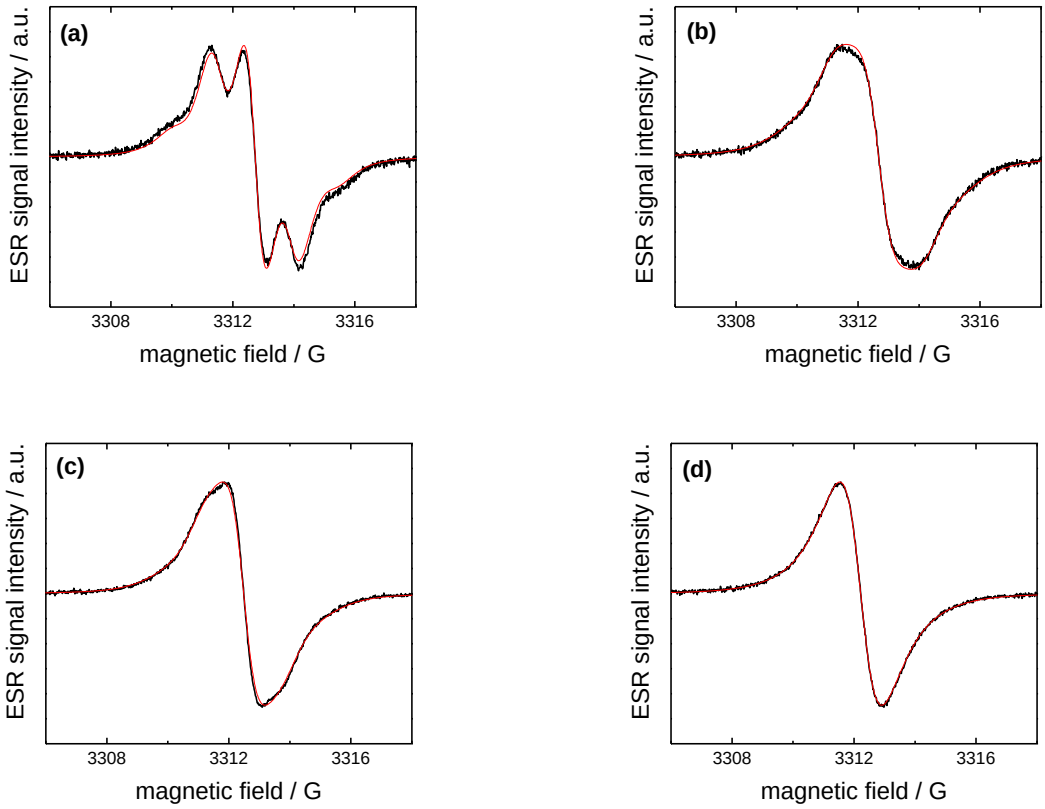

Figure 51. ESR spectra and the simulations of $Th^{\bullet+}/Th$ in the presence of $[Th^{\bullet+}] = 1 \times 10^{-4}$ M and $[Th] = 6 \times 10^{-3}$ M in ACN at (a) 243 K, (b) 268 K, (c) 293 K, (d) 333 K.

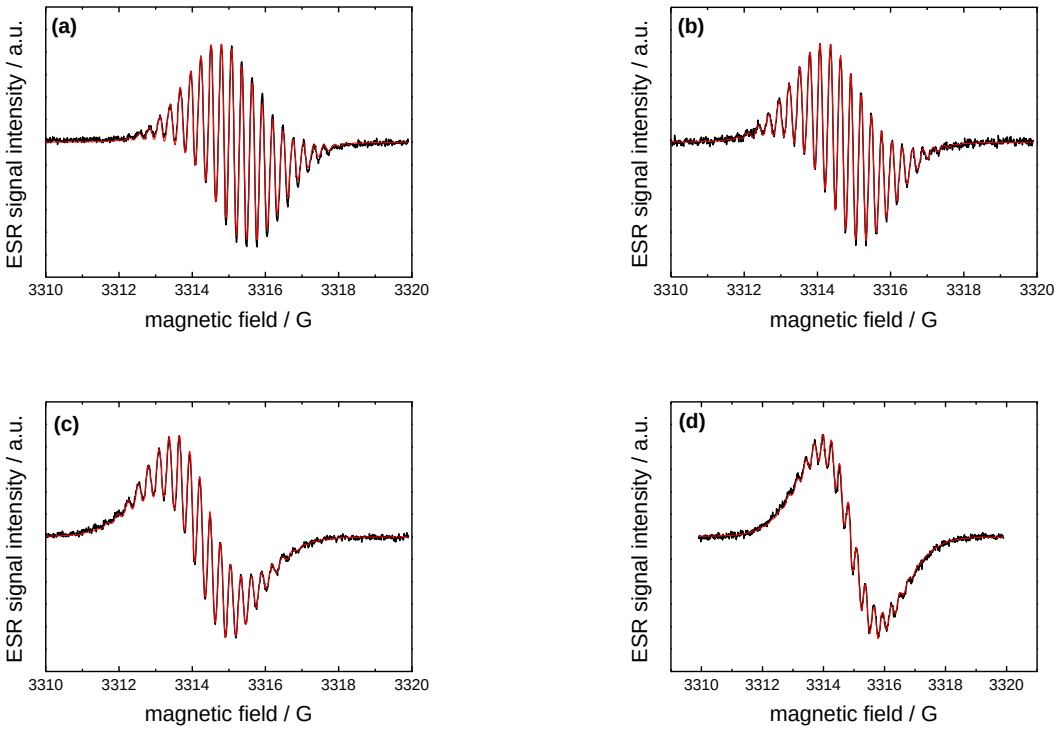

Figure 52. ESR spectra and the simulations of $MTh^{\bullet+}/MTh$ in the presence of $[MTh^{\bullet+}] = 1 \times 10^{-4}$ M and $[MTh] = 2 \times 10^{-3}$ M in DCM at (a) 213 K, (b) 253 K, (c) 273 K, (d) 293 K.

6.3.3 ESR Line Broadening

The concentration dependence of the exchange rate of the reactions k_{dyn} in the range of five temperatures are shown as the ESR line broadening in figure 53 and 54 for $Th^{\bullet+}$/Th and $MTh^{\bullet+}$/MTh, respectively. The rate constants for each system of $Th^{\bullet+}$/Th and $MTh^{\bullet+}$/MTh are listed in table 13 and 14 together with the viscosity η and the Pekar factor γ of the given solvents at each temperature.

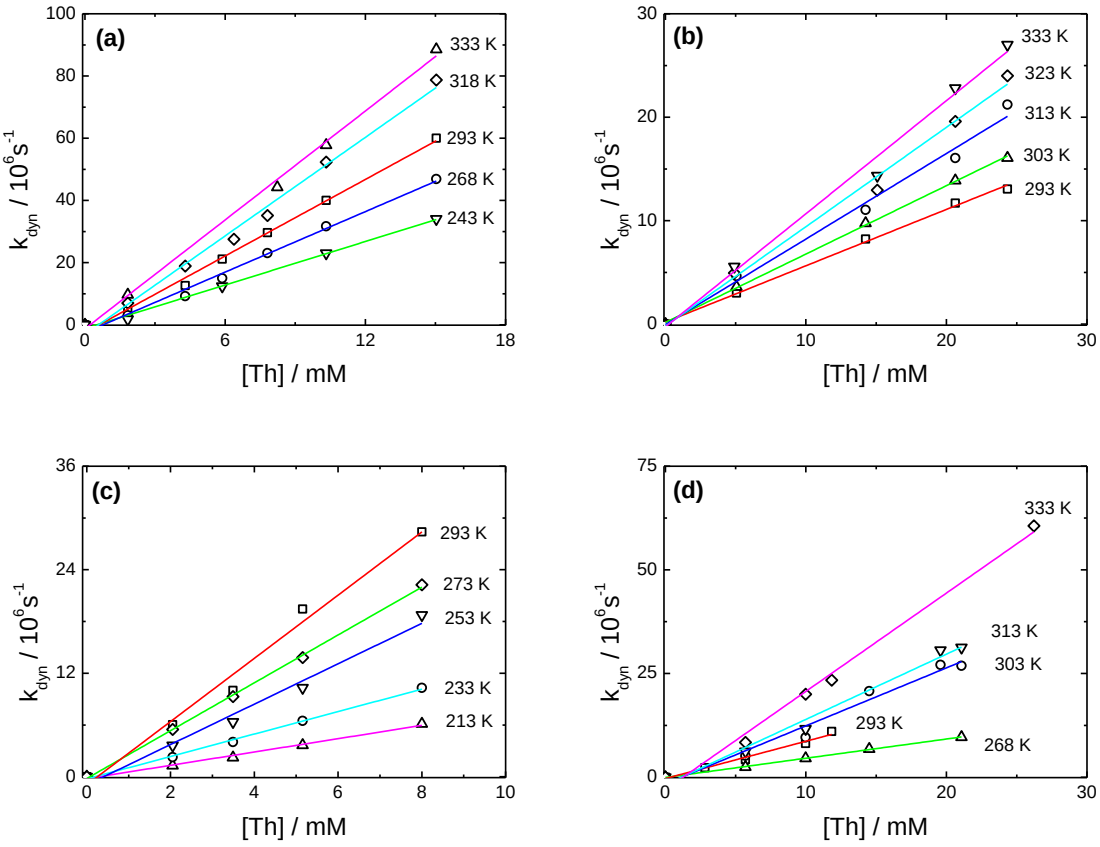

Figure 53. Concentration dependence of the exchange rate of the reactions k_{dyn} of $Th^{\bullet+}$/Th in (a) ACN, (b) PC, (c) DCM, (d) DCB.

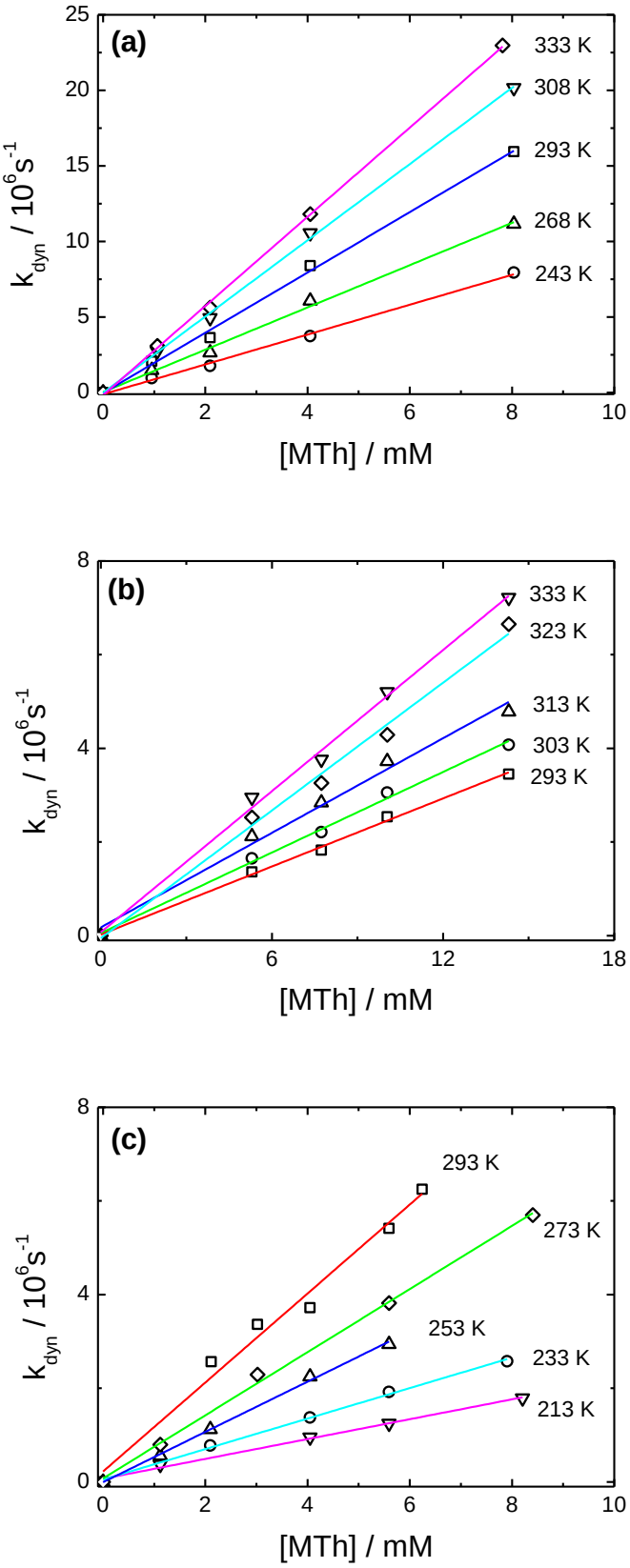

Figure 54. Concentration dependence of the exchange rate of the reactions k_{dyn} of $MTh^{\bullet+}$/MTh in (a) ACN, (b) PC, (c) DCM.

Table 13. Viscosities η and the Pekar factors γ of the used solvents, and rate constants of $Th^{\bullet+}$/Th, at different temperatures.

Temperature (K)	η (cP)	γ	τ_L (ps)	k_{obs} (10^8 $M^{-1}s^{-1}$)	k_d (10^8 $M^{-1}s^{-1}$)	k_{et} (10^8 $M^{-1}s^{-1}$)
			ACN			
243	0.637	0.513	0.916	23.3±0.8	84.6	52±2
268	0.453	0.521	0.478	32±1	131	64±3
293	0.341	0.528	0.279	41±1	190	72±2
318	0.269	0.536	0.177	53±2	263	83±4
333	0.237	0.540	0.139	58±2	312	93±3
			DCM			
213	1.246	0.407	1.90	7.7±0.4	37.9	13.0±0.6
233	0.892	0.400	1.55	13.0±0.4	57.9	23.6±0.7
253	0.673	0.394	1.33	20±2	83.4	39±4
273	0.529	0.387	1.13	27.7±0.5	114	53.8±0.9
293	0.43	0.380	0.991	37±2	151	71±5
			PC			
293	2.76	0.479	3.27	5.5±0.2	23.5	10.1±0.3
303	2.375	0.481	4.27	6.6±0.1	28.3	12.4±0.2
313	2.063	0.484	1.89	8.3±0.5	33.6	16.3±0.9
323	1.808	0.486	1.48	9.6±0.5	39.6	18.7±0.9
333	1.597	0.488	1.17	10.9±0.6	46.2	21±1
			DCB			
268	1.98	0.318	8.76	4.64±0.08	29.9	6.7±0.1
293	1.324	0.316	5.84	9.0±0.7	49.1	14±1
303	1.147	0.315	5.06	14±1	58.6	27±2
313	1.003	0.314	4.42	16±1	69.2	29±2
333	0.785	0.312	3.90	24±1	94.0	48±3

Table 14. Viscosities η and the Pekar factors γ of the used solvents, and rate constants of $MTh^{\bullet+}$/MTh, at different temperatures.

Temperature (K)	η (cP)	γ	τ_L (ps)	k_{obs} (10^8 $M^{-1}s^{-1}$)	k_d (10^8 $M^{-1}s^{-1}$)	k_{et} (10^8 $M^{-1}s^{-1}$)
			ACN			
243	0.637	0.513	0.916	9.9±0.3	84.6	12.9±0.4
268	0.453	0.521	0.478	14.0±0.5	131	17.8±0.6
293	0.341	0.528	0.279	20.0±0.6	190	25.2±0.8
318	0.269	0.536	0.177	25.2±0.5	263	31.2±0.6
333	0.237	0.540	0.139	29.5±0.4	312	36.4±0.5
			DCM			
213	1.246	0.407	1.90	2.12±0.09	37.9	2.4±0.1
233	0.892	0.400	1.55	3.26±0.09	57.9	3.7±0.1
253	0.673	0.394	1.33	5.4±0.1	83.4	6.2±0.2
273	0.529	0.387	1.13	6.4±0.2	11.4	7.6±0.2
293	0.43	0.380	0.991	9.5±0.6	15.1	10.9±0.7
			PC			
293	2.76	0.479	3.27	2.42±0.07	23.5	3.05±0.09
303	2.375	0.481	4.27	2.9±0.1	28.3	3.6±0.1
313	2.063	0.484	1.89	3.4±0.2	33.6	4.2±0.2
323	1.808	0.486	1.48	4.6±0.2	39.6	5.9±0.3
333	1.597	0.488	1.17	5.0±0.2	46.2	6.4±0.2

The temperature dependence of τ_L was calculated using the longitudinal relaxation energy, H_L as given in equation 6.1.[4]

$$\ln \tau_L = \frac{H_L}{RT} + \ln b \qquad (6.1)$$

where ln b is the intercept of the plot between ln τ_L vs $1/T$.

The temperature dependence of η is needed for determining the k_d, and can be calculated following equation 6.2.[4]

$$\eta(T) = \eta_o exp\left(\frac{H_\eta}{RT}\right) \quad (6.2)$$

Here η_o is the hypothetical viscosity at infinite temperature and H_η is the viscosity energy.

For many solvents, the temperature dependence of γ can be described by the empirical equation shown in equation 6.3,[4]

$$\gamma(T) = p + qT \quad (6.3)$$

where q and p is the slope and the intercept of the plots of ln γ *vs* T.

6.3.4 Activation Energies

The traditional Arrhenius plot (ln k_{et} *vs* $1/T$) is commonly used to determine the activation energies (E_a). However, the influence of the adiabatic solvent dynamic effect means that the pre-exponential factor becomes strongly temperature dependent. Therefore, Arrhenius-like plots taking this into account (ln (k_{et} τ_L $T^{1/2}$ $\gamma^{-1/2}$) *vs* $1/T$) have been done as well. The two Arrhenius plots for each system are shown in figures 55 and 56 for $Th^{\bullet+}$/Th and $MTh^{\bullet+}$/MTh, respectively.

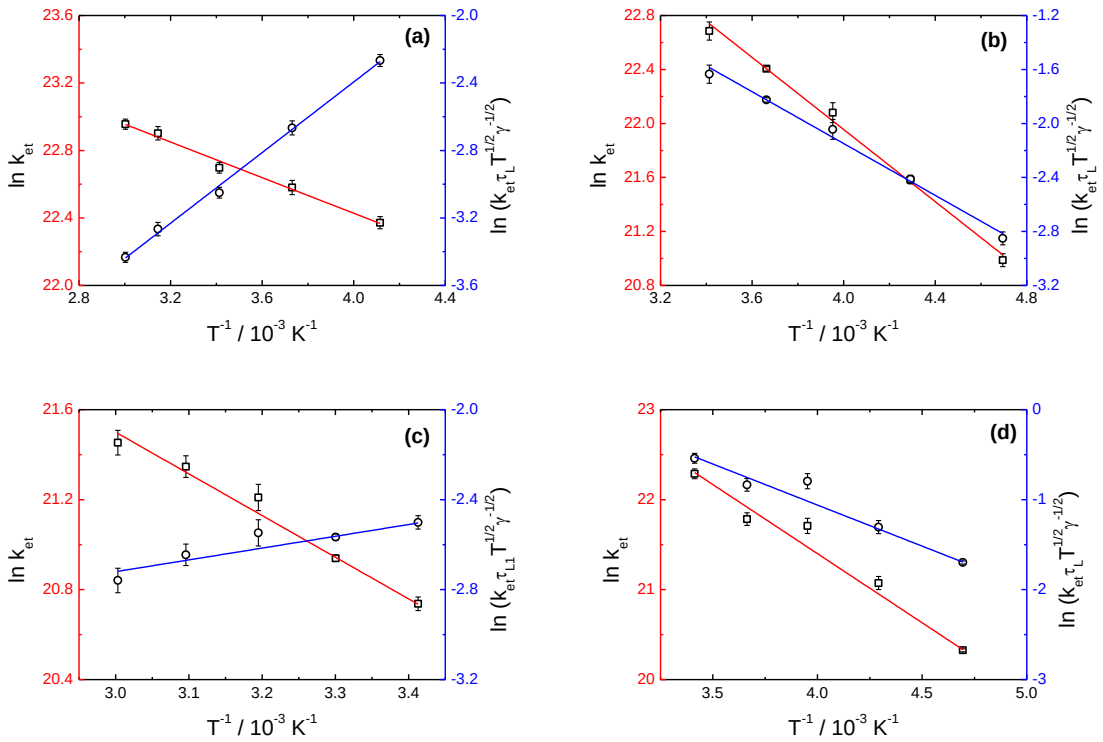

Figure 55. The Arrhenius plots of ln k_{et} *vs* $1/T$ and ln (k_{et} τ_L $T^{1/2}$ $\gamma^{-1/2}$) of $Th^{\bullet+}$/Th in (a) ACN, (b) DCM, (c) PC, (d) DCB.

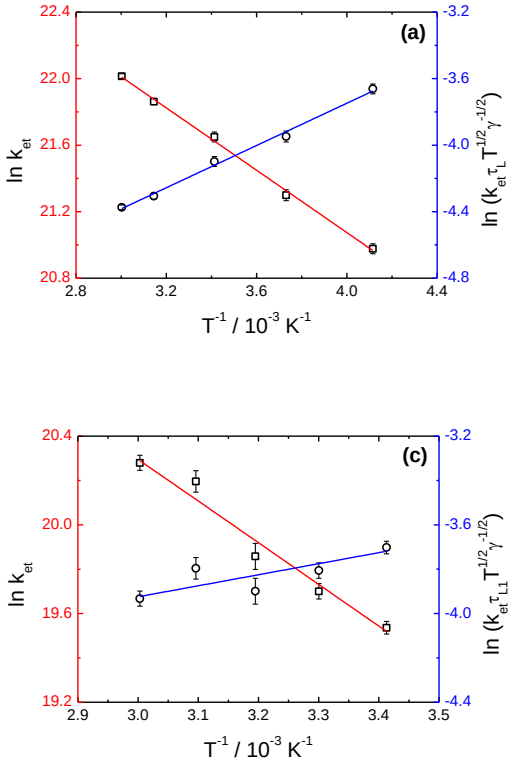

Figure 56. The Arrhenius plots of ln k_{et} *vs* $1/T$ and ln (k_{et} τ_L $T^{1/2}$ $\gamma^{-1/2}$) of $MTh^{\bullet+}$/MTh in (a) ACN, (b) DCM, (c) PC

The activation energies were obtained from the corresponding slopes, providing E_a for the plot of ln k_{et} *vs* $1/T$, and ΔG^* for that of ln (k_{et} τ_L $T^{1/2}$ $\gamma^{-1/2}$) *vs* $1/T$. As seen in table 15, the values of ΔG^* for all systems are significantly smaller than E_a. This confirms the presence of the adiabatic solvent dynamic effect, since $E_a \approx \Delta G^* + H_L$. The small, and sometimes negative, values of ΔG^* suggest that the resonance splitting energy, V_{PS} could be large, and thus cannot be neglected in any further treatment of the energies. Unfortunately, V_{PS} for the thianthrenes have not been reported, and therefore the estimation of the experimental reorganization energies, λ_{exp} is impossible. For this reason, there is no further evidence to prove the influence of the geometric changes between the reactants on the electron transfer reactions. However, the large k_{et} and relatively small ΔG^* tend to suggest that such structural changes do not play a big role for the thianthrene systems.

Table 15. The experimental activation energies of thianthrene redox couples in different solvents, and the relevant longitudinal relaxation energies, H_L.

Solvent	H_L	$Th^{\bullet+}/Th$		$MTh^{\bullet+}/MTh$	
		E_a [(a)]	ΔG^{*} [(b)]	E_a [(a)]	ΔG^{*} [(b)]
	(kJ mol^{-1})	(kJ mol^{-1})	(kJ mol^{-1})	(kJ mol^{-1})	(kJ mol^{-1})
ACN	14[73]	4.0±0.3	-8.7±0.3	7.8±0.2	-5.3±0.2
	(1)[74]				
DCM	4.23[63]	11.1±0.4	7.9±0.4	9.8±0.5	6.8±0.5
	(0.7)[75]				
PC	20.88[49]	15±1	-5±1	16±2	-4±2
	(24.6)[76]				
	(15.8)[77]				
DCB	10.8[(c)]	28±2	13±2	-	-

(a) obtained from the traditional Arrhenius plots (ln k_{et} *vs* 1/*T*)
(b) obtained from the traditional Arrhenius plots corresponding to the adiabatic reaction
(c) using H_η instead of H_L

Another important factor in the discussion of ΔG^* concerns the values of H_L and their reliabilities. The negative values of ΔG^* for the reactions in the PC and ACN are partly caused by the relatively large values of H_L for these solvents. Therefore it is important to know much the values can be trusted. For three of the four solvents used, alternative sources of temperature dependent data exists and the corresponding values of H_L have been included in table 15. In all cases, the references have been assessed and the H_L of the most reliable report chosen, based on e.g. the frequency range used to determine the relaxation parameters and the range of temperatures used. For PC and DCM, particularly trustworthy data has been reported whereas the data for ACN is more questionable. For DCB, the information of temperature dependent measurements of ε and τ_D is not available, therefore it is impossible to determine the τ_L values at other

temperatures by using H_L. Nevertheless, under the approximation that the τ_D is inversely proportional to the viscosity, the viscosity energy, H_η of DCB can be used instead.

6.3.5 Solvent Dynamic Effects at 333 K

It is clear that adiabatic solvent dynamics is presence at room temperature for the thianthrene self-exchange redox couples. However, this behaviour may possibly change when the solutions have higher or lower temperature. The temperature ranges used for different solvent were chosen based on their melting and boiling points and the only temperatures which coincide for most solvents are 293 K and 333 K. The former has already been described above and the latter shall be discussed here.

Figure 57 shows the Weaver plots based on the adiabatic dynamics of $Th^{\bullet+}$/Th and $MTh^{\bullet+}$/MTh at 333 K for AN, PC and DCB. As seen, both systems provide results which are close to the slope of unity. This clearly indicates that the reactions of thianthrene redox couples at higher temperature are still strongly controlled by τ_L.

The experimental reaction distances, d'_{exp} of the thianthrene couples at 333 K were investigated from plots like those in figure 58, and were found to be 6.1 Å and 7.0 Å for $Th^{\bullet+}$/Th and $MTh^{\bullet+}$/MTh, respectively. Even though the plot corresponding to the $MTh^{\bullet+}$/MTh consists of only two data points, its slope of one has not been omitted. The values of d'_{exp} obtained at 293 K and 333 K are compared, which suggests that the d' is larger when the temperature is higher. Unfortunately, there is not enough data to compare for that from lower temperatures, which may help understand how the reactants behave during the reaction under those conditions.

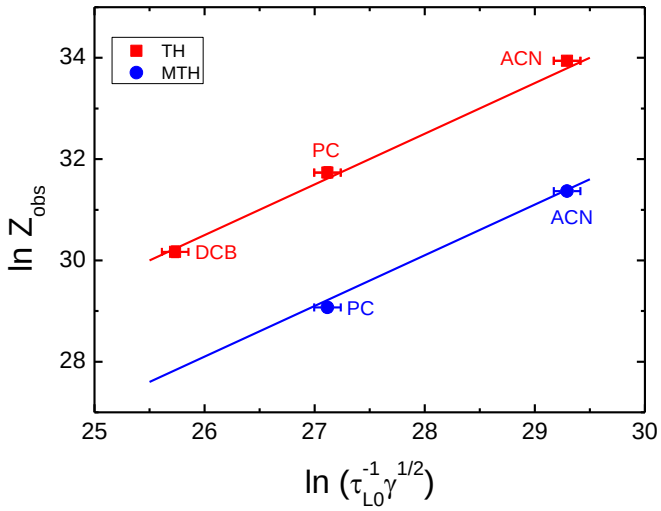

Figure 57. Weaver plot of ln Z_{obs} *vs.* $\ln\left(\tau_L^{-1}\gamma^{1/2}\right)$, of $Th^{\bullet+}$/Th (red line) and $MTh^{\bullet+}$/MTh (blue line) in organic solvents at 333 K.

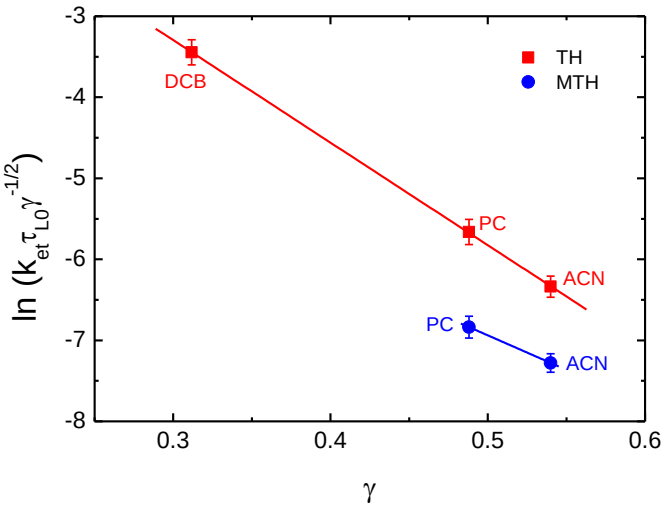

Figure 58. The dependence of ln $(k_{et}\tau_L\gamma^{1/2})$ on the solvent parameter γ of $Th^{\bullet+}$/Th (red line) and $MTh^{\bullet+}$/MTh (blue line) in organic solvents at 333 K.

7 Conclusions

In terms of the Marcus theory of electron transfer, solvent dynamics are present and can significantly influence the rate of reactions. The relaxation process of solvents corresponding to the longitudinal relaxation time, τ_L can strongly govern the electron transfer, resulting in the so-called adiabatic solvent dynamic effect. Various organic systems exhibiting such adiabatic dynamics have been reported, and most of them were studied in Debye solvents which show only a single relaxation process. For non-Debye solvents, longitudinal relaxation may originate from different processes, and it is not straightforward to decide which τ_L has the most influence on the electron transfer reactions. In order to understand more about the influence of these multiple relaxation processes on the electron transfer reactions, the well-known redox couples of TCNE/TCNE$^{\bullet-}$ and DDQ/DDQ$^{\bullet-}$ have been investigated in non-Debye solvents.

Apart from the systems above, the solvent dynamic effect has been studied in two thianthrene redox couples, i.e. Th$^{\bullet+}$/Th and MTh$^{\bullet+}$/MTh, in organic solvents. The main interest in these particular couples is that the difference in structures of the neutral thianthrenes and their radical cations is quite large, the former is angled and the latter planar. This leads to the question of, to what extent this large change in geometry has an effect on the electron transfer reactions. Therefore, small rate constants of reactions and relatively large activation energies would be expected. However, in order to answer this question, the influence of solvent dynamics on the reactions must first be investigated to properly distinguish between the two types of effects.

Returning to the systems of TCNE/TCNE$^{\bullet-}$ and DDQ/DDQ$^{\bullet-}$, adiabatic solvent dynamic effects have been revealed in the literature. In the present work, different non-Debye solvents were used, in which the electron transfer reactions of the two systems have not been studied before. The rate constants of the reactions at room temperature were obtained by ESR line broadening experiments, and they are in good agreement with those which were already published. The adiabatic solvent dynamic effect was probed using Weaver plots based on the different limiting cases of τ_L in terms of the low and high frequency limits, which are denoted as τ_{L0} and $\tau_{L\infty}$, respectively. From such plots it was found that the studied systems fit well with those of both Debye and non-Debye solvents from literature, and the results based on the $\tau_{L\infty}$ provided the best fit.

Furthermore, values of the reaction distances, determined corresponding to the adiabatic reaction of both systems, were found to be similar to the literature data. In summary, the experiments for both TCNE/TCNE$^{\bullet-}$ and DDQ/DDQ$^{\bullet-}$ redox couples in different non-Debye solvents have successfully shown that $\tau_{L\infty}$ is the relaxation time which best describes the solvent dynamic effect on the electron transfer processes.

The Weaver plots of TCNE/TCNE$^{\bullet-}$ systems led to surprising results. A second trend line with slope of unity could be seen when data from DMA and DMF were included, and they seem to fit well with those of PC and also a number of ethereal solvents taken from the literature. For the DDQ/DDQ$^{\bullet-}$ couple, Weaver plots taking into account the data of DMA and FA also generate this second trend line with a slope of one, which looks even more convincing when the data of PC is included. This suggests that the ethereal and amide solvents may influence the reactions in a different manner than the remaining ones. However, there is not enough information to explain this phenomenon in greater detail, more experiments are needed.

For the thianthrene redox couples, the measurement of samples only succeed in a few organic solvents, which are the only ones where the thianthrene radicals are reasonably stable and soluble. This makes it impossible to perform the same kind of detailed analysis as for TCNE/TCNE$^{\bullet-}$ and DDQ/DDQ$^{\bullet-}$, nevertheless, an attempt was made using the available data. τ_{L1} was used for the Debye solvents ACN and DCB. For DCM, the relaxation processes are rather more complex than in the other non-Debye solvents, and information about the second Debye relaxation time τ_2 only results in an estimated value. For this reason, τ_{L1} obtained from the dielectric parameters of the first relaxation time were used for DCM, similarly to ACN and DCB. For the analysis of the systems in the non-Debye solvent PC, the correlation of the results using τ_{L1}, τ_{L0} and $\tau_{L\infty}$ with those of the other solvents using τ_{L1}. The unit slope of the Weaver plots from both redox couples at 293 K reveals adiabatic solvent dynamic effects. Considering the Weaver plots together with the dependence of ln ($k_{et}\tau_L\gamma^{-1/2}$) on γ shows that the best fit was found when using τ_{L1} for PC.

The experimental reaction distances of the two thianthrene couples, obtained from the slope of plots of $\ln\left(k_{et}\tau_L\gamma^{-1/2}\right)$ *vs.* γ, suggest that the reactant molecules in the precursor complex are stacked, corresponding to other findings in literature. The large structural changes have a surprisingly small effect on the electron transfer rate constants

at 293 K, and thus temperature dependent measurements needed to be done in order to determine the experimental activation energies.

From these temperature dependences, the determined activation energies are provided as E_a and ΔG^*. The former were obtained from traditional Arrhenius plots, while the adiabatic solvent dynamics were taken into account for the latter. Both experimental values of activation energies are very small and the ΔG^* values are significantly smaller than those of E_a. This is due to the solvent dynamics causing the longitudinal relaxation energies, H_L of the solvents to have a strong influence on such plots and therefore affect the activation energies. For instance, the large H_L of the solvent PC results in negative values of ΔG^*, which were found to be -5±1 kJ mol^{-1} for Th$^{\bullet+}$/Th and -4±1 kJ mol^{-1} for MTh$^{\bullet+}$/MTh. This suggests that the resonance splitting energy, V_{PS} must be relatively large. However, it must also be taken into account that experimental values of H_L are somewhat uncommon and in several cases conflicting values have been published.

It is therefore impossible to determine the experimental reorganization energies, λ for both thianthrene couples. For this reason, it cannot be completely ruled out that the structural changes between the reactants has a pronounced influence on the electron transfer reactions. Nevertheless, the large k_{et} and relatively small ΔG^* tend to suggest that the structural changes do not play a significant role in the self-exchange of the thianthrene redox couples.

To check the influence of the adiabatic behaviour on the self-exchange reactions of the thianthrene couples at higher temperature, Weaver plots have been made for both systems at 333 K. The results clearly show that the reactions are still strongly controlled by the τ_L of the solvents. Similarly to the systems at room temperature, d'_{exp} of the thianthrene couples at 333 K have been investigated, and it was found that their d'_{exp} values are somewhat larger than those of 293 K. This suggests that d' is larger at higher temperature. However, there is not enough information for a similar comparison at lower temperatures, and it is therefore impossible to conclude how the reactants behave during the reaction under those conditions.

From the outcome mentioned above, there are several interesting ways to gain more insight in the role of non-Debye solvents. The studied systems of TCNE/TCNE$^{\bullet-}$ and DDQ/DDQ$^{\bullet-}$ led to a different behaviour of the electron transfer reaction in the ethereal solvent PC and the amide solvents DMF, DMA and FA, as compared to the remaining

solvents. Investigating both systems in other ethereal and amide non-Debye solvents would provide a very interesting future study.

For the thianthrenes, the problem concerning the small selection of solvents seems to be the primary concern. Finding either more suitable solvents or possibly different thianthrenes could help answer some of the remaining questions regarding the influence of the structural changes.

References

1 R. A. Marcus, *J. Chem. Phys.*, 1965, **43**, 679.

2 R. A. Marcus, *J. Chem. Phys.*, 1956, **24**, 966.

3 R. A. Marcus and N. Sutin, *Biochim. Biophys. Acta BBA - Rev. Bioenerg.*, 1985, **811**, 265–322.

4 G. Grampp and W. Jaenicke, *Berichte Bunsenges. Für Phys. Chem.*, 1991, **95**, 904–927.

5 C. C. Moser and P. L. Dutton, in *Photosystem I*, ed. J. H. Golbeck, Springer Netherlands, Dordrecht, 2006, vol. 24, pp. 583–594.

6 G. Grampp and K. Rasmusse, in *Nitroxides - Theory, Experiment and Applications*, ed. A. Kokorin, InTech, 2012.

7 R. L. Ward and S. I. Weissman, *J. Am. Chem. Soc.*, 1957, **79**, 2086–2090.

8 T. Layloff, T. Miller, R. N. Adams, H. FäH, A. Horsfield and W. Proctor, *Nature*, 1965, **205**, 382–383.

9 M. J. Weaver, *Chem. Rev.*, 1992, **92**, 463–480.

10 G. Grampp and K. Rasmussen, *Phys. Chem. Chem. Phys.*, 2002, **4**, 5546–5549.

11 G. Grampp, S. Landgraf and K. Rasmussen, *J. Chem. Soc. Perkin Trans. 2*, 1999, 1897–1899.

12 W. R. Fawcett, *Liquids, solutions, and interfaces: from classical macroscopic descriptions to modern microscopic details*, Oxford University Press, Oxford ; New York, 2004.

13 S. B. Larson, S. H. Simonsen, G. E. Martin, K. Smith and S. Puig-Torres, *Acta Crystallogr. C*, 1984, **40**, 103–106.

14 M. F. Peintinger, J. Beck and T. Bredow, *Phys. Chem. Chem. Phys.*, 2013, **15**, 18702.

15 G. Grampp, B. Großmann, J. Heinze, S. Landgraf and K. Rasmussen, *ChemPhysChem*, 2008, **9**, 854–860.

16 R. T. Tjahjanto, M. F. Peintinger, T. Bredow and J. Beck, *Eur. J. Inorg. Chem.*, 2012, **2012**, 3625–3635.

17 P. Choto, K. Rasmussen and G. Grampp, *Phys Chem Chem Phys*, 2015, **17**, 3415–3420.

18 R. M. Fuoss, *J. Am. Chem. Soc.*, 1958, **80**, 5059–5061.

19 D. R. Rosseinsky, *Comments Inorg. Chem.*, 1984, **3**, 153–170.
20 N. Sutin, in *Progress in Inorganic Chemistry*, ed. S. J. Lippard, John Wiley & Sons, Inc., Hoboken, NJ, USA, 1983, vol. 30, pp. 441–498.
21 L. Landau, *Phys. Z. Sowjetunion*, 1932, **2**, 46–51.
22 L. Landau, *Phys. Z. Sowjetunion*, 1932, **1**, 88–98.
23 C. Zener, *Proc. R. Soc. Math. Phys. Eng. Sci.*, 1932, **137**, 696–702.
24 T. Holstein, *Philos. Mag. Part B*, 1978, **37**, 49–62.
25 M. Bixon and J. Jortner, *Chem. Phys.*, 1993, **176**, 467–481.
26 J. Jortner and M. Bixon, *J. Chem. Phys.*, 1988, **88**, 167. (-171)
27 S. F. Nelsen, S. C. Blackstock and Y. Kim, *J. Am. Chem. Soc.*, 1987, **109**, 677–682.
28 A.-M. Kelterer, S. Landgraf and G. Grampp, *Spectrochim. Acta. A. Mol. Biomol. Spectrosc.*, 2001, **57**, 1959–1969.
29 Y. I. Kharkats, *Elektrokhimiya*, 1976, **12**, 1284–91.
30 Y. I. Kharkats, *Elektrokhimiya*, 1974, **10**, 1137–41.
31 G. I. Likhtenshteĭn, *Solar energy conversion: chemical aspects*, Wiley-VCH, Weinheim, 2012.
32 D. Rehm and A. Weller, *Berichte Bunsenges. Für Phys. Chem.*, 1969, **73**, 834–839.
33 R. A. Marcus and P. Siders, *J. Phys. Chem.*, 1982, **86**, 622–630.
34 I. R. Gould, J. E. Moser, B. Armitage, S. Farid, J. L. Goodman and M. S. Herman, *J. Am. Chem. Soc.*, 1989, **111**, 1917–1919.
35 I. R. Gould, J. E. Moser, D. Ege, R. Moody, B. Armitage and S. Farid, *J. Imaging Sci.*, 1989, **33**, 44–6.
36 J. R. Miller, L. T. Calcaterra and G. L. Closs, *J. Am. Chem. Soc.*, 1984, **106**, 3047–3049.
37 G. Grampp and G. Hetz, *Berichte Bunsenges. Für Phys. Chem.*, 1992, **96**, 198–200.
38 L. D. Zusman, *Chem. Phys.*, 1980, **49**, 295–304.
39 H. L. Friedman, *J. Chem. Soc. Faraday Trans. 2*, 1983, **79**, 1465.
40 D. Kivelson and H. Friedman, *J. Phys. Chem.*, 1989, **93**, 7026–7031.
41 L. D. Zusman, *Chem. Phys.*, 1988, **119**, 51–61.
42 H. Sumi and R. A. Marcus, *J. Chem. Phys.*, 1986, **84**, 4894.
43 W. R. Fawcett and L. Blum, *Chem. Phys. Lett.*, 1991, **187**, 173–179.
44 W. R. Fawcett, *Chem. Phys. Lett.*, 1990, **174**, 167–175.
45 J. M. G. Barthel and R. Buchner, *Pure Appl. Chem.*, 1991, **63**.

46 J. Barthel, H. Hetzenauer and R. Buchner, *Berichte Bunsenges. Für Phys. Chem.*, 1992, **96**, 988–997.

47 J. T. Hynes, *J. Phys. Chem.*, 1986, **90**, 3701–3706.

48 W. R. Fawcett, *Chem. Phys. Lett.*, 1992, **199**, 153–160.

49 J. Barthel, R. Buchner, C. G. Hölzl and M. Münsterer, *Z. Für Phys. Chem.*, 2000, **214**.

50 J. Barthel, K. Bachhuber, R. Buchner and H. Hetzenauer, *Chem. Phys. Lett.*, 1990, **165**, 369 – 373.

51 T. Sato and R. Buchner, *J. Phys. Chem. A*, 2004, **108**, 5007–5015.

52 T. Sato and R. Buchner, *J. Chem. Phys.*, 2003, **118**, 4606.

53 F. Gerson, *Electron spin resonance spectroscopy of organic radicals*, Wiley-VCH, Weinheim, 2003.

54 J. A. Weil and J. R. Bolton, *Electron Paramagnetic Resonance*, John Wiley & Sons, Inc., Hoboken, NJ, USA, 2006.

55 S. Hünig, K. Sinzger, R. Bau, T. Metzenthin and J. Salbeck, *Chem. Ber.*, 1993, **126**, 465–471.

56 P. Hübler and J. Heinze, *Berichte Bunsenges. Für Phys. Chem.*, 1998, **102**, 1506–1509.

57 B. Boduszek and H. J. Shine, *J. Org. Chem.*, 1988, **53**, 5142–5143.

58 G. Grampp and G. Stiegler, *J. Magn. Reson. 1969*, 1986, **70**, 1–10.

59 J.-M. Lü, S. V. Rosokha and J. K. Kochi, *J. Am. Chem. Soc.*, 2003, **125**, 12161–12171.

60 V. Ganesan, S. V. Rosokha and J. K. Kochi, *J. Am. Chem. Soc.*, 2003, **125**, 2559–2571.

61 S.-H. Ma, X.-D. Zhang, H. Xu, L.-L. Shen, X.-K. Zhang and Q.-Y. Zhang, *J. Photochem. Photobiol. Chem.*, 2001, **139**, 97–104.

62 J. Barthel, M. Kleebauer and R. Buchner, *J. Solut. Chem.*, 1995, **24**, 1–17.

63 J. Hunger, A. Stoppa, A. Thoman, M. Walther and R. Buchner, *Chem. Phys. Lett.*, 2009, **471**, 85–91.

64 J. Barthel, K. Bachhuber, R. Buchner, J. B. Gill and M. Kleebauer, *Chem. Phys. Lett.*, 1990, **167**, 62 – 66.

65 Y. Marcus, *The properties of solvents*, Wiley, Chichester ; New York, 1998.

66 J. A. Riddick, *Organic solvents: physical properties and methods of purification*, Wiley, New York, 4th ed., 1986.

67 E. M. Turner, D. W. Anderson, L. A. Reich and W. E. Vaughan, *J. Phys. Chem.*, 1970, **74**, 1275–1280.

68 K. Rasmussen, PhD thesis, Graz University of Technology, 2006.69 W. R. Fawcett and C. A. Foss, *J. Electroanal. Chem. Interfacial Electrochem.*, 1991, **306**, 71–85.

70 T. Holstein, *Philos. Mag. Part B*, 1978, **37**, 499–526.

71 F. Neese, *Wiley Interdiscip. Rev. Comput. Mol. Sci.*, 2012, **2**, 73–78.

72 J. Lu, L. Yang, P. Chen, Y. Liu and Z. Liu, Chin. J. Magn. Reson., 1995, **12**, 1.

73 S. N. Helambe, A. Chaudhari and S. C. Mehrotra, *J. Mol. Liq.*, 2000, **84**, 235–244.

74 K. Mansingh and A. Mansingh, *Indian J. Pure Appl. Phys.*, 1964, **2**, 176–8.

75 V. P. Pawar and S. C. Mehrotra, *J. Mol. Liq.*, 2003, **108**, 95–105.

76 E. A. S. Cavell, *J. Chem. Soc. Faraday Trans. 2 Mol. Chem. Phys.*, 1974, **70**, 7884.

77 A. Declemy and C. Rulliere, *Chem. Phys. Lett.*, 1988, **146**, 1–6.